MODELING OF IN-PLANE CRUSHED HONEYCOMB CORES WITH APPLICATIONS TO RAMPDOWN SANDWHICH STRUCTURE CLOSURES

_____

A Thesis

Presented to the

Faculty of

San Diego State University

_____

In Partial Fulfillment

of the Requirements for the Degree

Master of Science

in

Aerospace Engineering

_____

by

Jeremy D. Stromsoe

Spring 2011

SAN DIEGO STATE UNIVERSITY

The Undersigned Faculty Committee Approves the

Thesis of Jeremy D. Stromsoe:

Modeling of In-Plane Crushed Honeycomb Cores with Applications to Rampdown Sandwich Structure Closures

Satchi Venkataraman, Chair
Department of Aerospace Engineering

Luciano Demasi
Department of Aerospace Engineering

Sam Kassegne
Department of Mechanical Engineering

March 30, 2011.
Approval Date

DEDICATION

This work is dedicated to my father, Wayne. Thanks for everything.

"I believe every human has a finite number of heartbeats. I don't intend to waste any of mine."
-Neil Armstrong

ABSTRACT OF THE THESIS

Modeling of In-Plane Crushed Honeycomb Cores with
Applications to Rampdown Sandwich Structure Closures
by
Jeremy D. Stromsoe
Master of Science in Aerospace Engineering
San Diego State University, 2011

Sandwich laminates are often ramped down to a solid composite laminate at its end to enable the use of mechanical fasteners to connect them to support structures. The rampdown regions are often the site of fatigue damage initiation and delamination failure. This thesis investigates the effectiveness of using a functionally graded sandwich core material in the rampdown closure region of a sandwich panel to mitigate the large shear stresses induced by the stiffness and geometry changes, and the mismatch in facesheet and core stiffness properties. It further investigates methods to create functionally graded materials by densifying commercially available metallic honeycomb core materials. The thesis presents the finite element analysis of sandwich beam with end rampdown closure subjected to in-plane, transverse and bending loads. The effect of different functional grading on core-facesheet interface normal and shear stresses and the variation of bending stresses in the factsheet in the rampdown structures are presented. Investigations show that the exponential variation of core stiffness at the taper region provides the best solution.

The main contribution of this thesis is the development and demonstration of a finite element model for rolling of honeycomb core to create edge wise graded properties. The commercially available Aluminum 5052-H39 foil Hexweb™ honeycomb core material is used as the initial material in the densification simulations. Finite element simulation of honeycomb core crushing (including effects of large nonlinear deformations, plasticity, and contact between cell walls) was performed using ABAQUS for uniform in-plane crushing (as a validation case) and for edge rolling induced crushing (to create functionally graded cores). The results indicate that a multistage rolling operation with careful selection of roller diameter and crushing depth for each pass can achieve desired densification gradient in the honeycomb core.

TABLE OF CONTENTS

PAGE

LIST OF TABLES

PAGE

LIST OF FIGURES

PAGE

ACKNOWLEDGEMENTS

I would like to thank my thesis advisor Professor Satchi Venkataraman for his support on this effort as well as my fellow graduate students. I would also like to thank my mother, brothers, sister, and wife to be, for all of their love and patience throughout all of my educational endeavors.

CHAPTER 1

INTRODUCTION

Sandwich laminates use thin and stiff outer material for the facesheets to resist bending, while using a lightweight inner material for core that provides the spacing to increase bending stiffness and carries the transverse shear stress. The layers have to be bonded together using an adhesive or brazing to prevent them from relative sliding of the layers in the sandwich. An example of the components of a typical sandwich laminate is shown in Figure 1.1 [1].

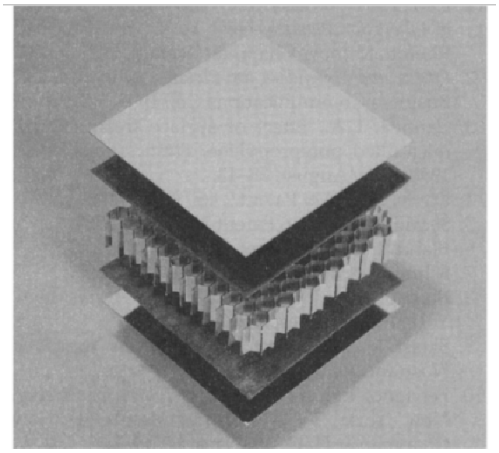

Figure 1.1. The elements of a sandwich structure, in this case 2 facesheets on either side, and a metal honeycomb type core material. Source: Peters. S. T., Handbook of Composites, 2nd ed., Chapman & Hall, New York, 1998, Chap. 12.

Many materials have been investigated for the construction of structural sandwich laminates. For facesheets, wood, metals, and high stiffness and high strength materials such as fiber reinforced materials (e.g. carbon-epoxy, glass-epoxy) have been used. Using orthotropic or anisotropic materials for the facesheets provide freedom to tailor the direction of bending stiffness and bending-extension or bending-twist couplings as desired. For core materials, a low relative density material is desired to separate the facesheets and increase the cross-sectional area moment of inertia. Materials used for core include corrugated paper,

honeycomb, polymer or metallic foam, and lightweight wood like balsa. While core materials are lightweight they must be sufficient in strength to carry shear loads.

The facesheets and core interface is usually an area of high shear stress concentration due to the mismatch in the in-plane stiffness properties of the two materials that can initiate delamination failures. A large body of work exists on ways to mitigate problems that arise due to the stiffness mismatch of facesheets and core materials in a sandwich laminate. One particular solution investigated in recent years is to develop materials designs for sandwich construction that exhibit a smooth and continuous variation in stiffness between the facesheets and core layers. Such material designs are referred to as "functionally graded materials" (FGM). The use of FGM can mitigate sharp discontinuity caused by large density and stiffness gradients in the mating of dissimilar materials.

While sandwich laminates have significantly high bending stiffness, they also exhibit very low transverse strength in compression (due to core crushing). This is particularly a problem when one has to attach sandwich laminates to other support structures using fasteners (e.g. fuselage or wing skin attachments to ring frames or ribs frames). To increase the compressive strength of sandwich laminates, designers incorporated various inserts at the fastener hole location or taper the sandwich to a solid laminate at the ends where the sandwich laminate has to be attached to the support structure with mechanical fasteners. Additional plies are introduced into the laminate at such location to improve the bearing strength and to compensate for the loss of bending stiffness as a result of tapering the core from its original thickness to zero thickness. These transition layers have complex load distributions and often exhibit a buildup of shear stresses. This thesis investigates the development of a functionally graded material for use in such tapered rampdown region of sandwich panels.

The thesis is organized as follows: Chapter two presents a review of some basic literature on sandwich laminates and use of functionally graded materials in sandwich construction. This is followed by the presentation of the problem of sandwich rampdowns and the survey of current published literature on the analysis, testing and design of sandwich rampdown structures. Chapter three presents the results of a finite element analysis investigation on using a linearly graded sandwich core in the tapered closure region of a sandwich beam. The change in the stress field as a result of using the FGM material is

discussed. The investigation in chapter 3 is based on a mathematical model having a material with continually varying modulus. In reality such a material has to be produced. In this thesis we investigate the use of graded cores obtained by crushing metallic honeycomb cores. Chapter 4 presents the modeling of crushing of honeycomb cores. The results of uniform edge crushing of honeycomb cores used to validate the finite element modeling are presented here. Chapter 5 presents the results of the simulations of core crushing using multi-stage edgewise compressive rolling operations to develop a graded core material. The control variables identified and the density grading obtained are presented and discussed. Chapter 6 presents the summary and conclusions.

CHAPTER 2

LITERATURE RESEARCH

Before attempting to find ways to improve upon sandwich structures, in particular the core materials, a literature review on the matter must be conducted. Here we look at what these types of structures are being used for, why they are used and what are the pros and cons of such structures. Our aim is to determine what can be done to improve sandwich structures in a cost effective manner.

First, different types of sandwich structures are considered. Sandwich structures are widely used in the aerospace community due to their high strength and low weight. A representative of the use of sandwich structures in the aerospace industry is presented in Figure 2.1 [2, 3].

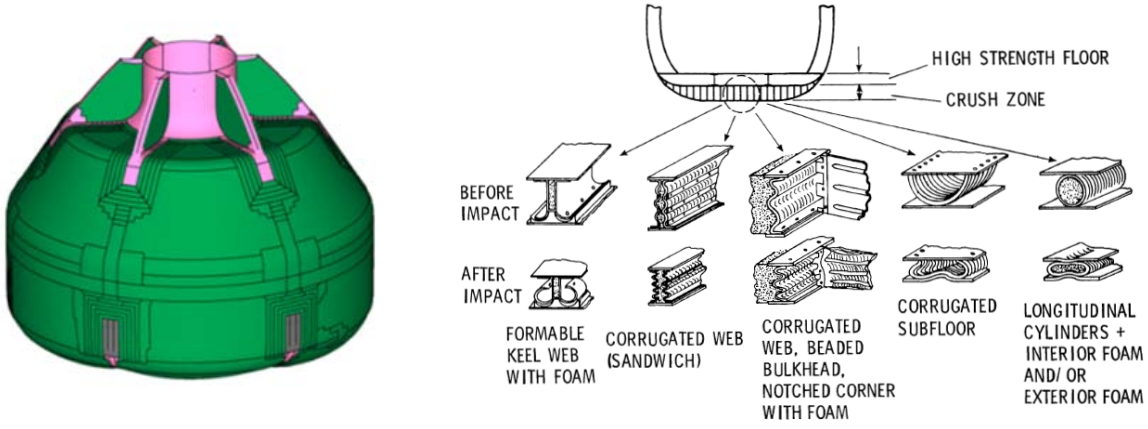

(a) (b)

Figure 2.1. Examples of sandwich structure use, (a) Design of NASA composite crew module (CCM) (green is sandwich material), (b) Design of impact absorbing helicopter subfloor. Sources: Collier, C., Yarrington, P., and Pickenheim, M., "Analysis Methods used on the NASA Composite Crew Module (CCM)," 49th AIAA/ASME/ASCE/AHS/ASC Structures, Structural Dynamics and Materials Conference, AIAA Hampton, VA, 2008, pp. 2008-2251; Cronkhite, J. D., and Berry,V .L., "Crashworthy Airframe Design Concepts Fabrication and Testing," NASA Contractor Report, No. 3603, Fort Worth, TX, 1982.

Sandwich structures are useful in various scenarios. These include energy absorption [4], heat transfer [5, 6] and a variety of other applications that range from launch vehicles [2] and fixed wing aircraft [7, 8] to helicopter subfloors [9]. There are also many types of facesheets and core materials which are used to make sandwich panels.

2.1 SANDWICH CORE MATERIALS

Selection of core materials are used in sandwich structures, selection of depends on the application. Often core materials are cellular structures constructed from materials shown in Figure 2.2 [9, 10]. One must consider mechanical properties such as weight, water absorption, damage tolerance and surface quality of the final product [6] to select the best core material.

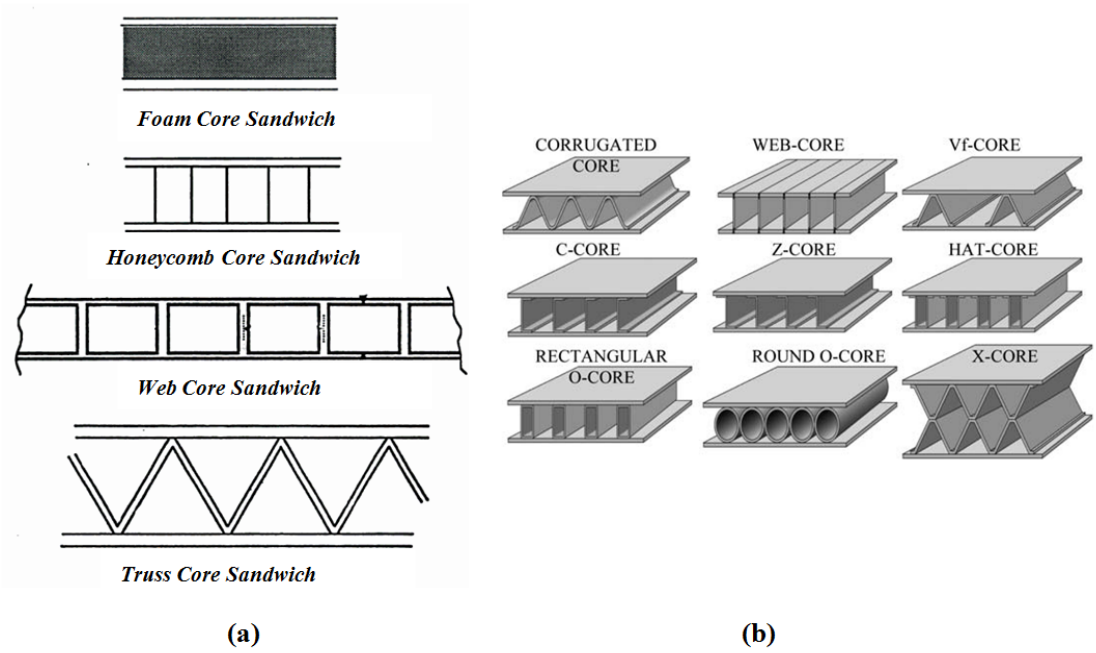

Figure 2.2. (a) *Top to bottom* foam, honeycomb, web core, and truss core sandwich structures, (b) various metallic core materials. Sources: Vinson, J. R., *The Behavior of Sandwich Structures of Isotropic and Composite Materials*, Technomic Publishing Company, Lancaster, PA, 1999, Chap. 1; Romanoff, J., and Varsta, P., "Bending Response of Web-Core Sandwich Beams," *Composite Structures*, Vol. 73, 2006, pp. 478-48.

The cores materials are not homogeneous rather; they themselves are structures on a smaller scale. Foam material can be tailored to the desired density, absorptive, mechanical and thermal properties. The random cell nucleation makes foams essentially isotropic in

terms of its mechanical properties. Foams are easy to produce and are low in cost. A handbook of composite materials [6] points out foams can be produced as open cell or closed cell type.

Another type of core material that can be used is a truss type structure. Sikorsky Aircraft [1] developed a carbon fiber truss style foam sandwich panel which has undergone material testing. These have been proven to reduce structural weight by 10-15% over honeycomb panels of the same thickness while maintaining the same shear and compression properties (see Figure 2.3 [11]). Since foam is used in conjunction with the truss, water absorption may be an issue in some applications. Also associated costs may be higher since the pultruded carbon used for the truss structure requires specialized techniques to make and it is a more expensive material than a simple foam or metallic truss structure.

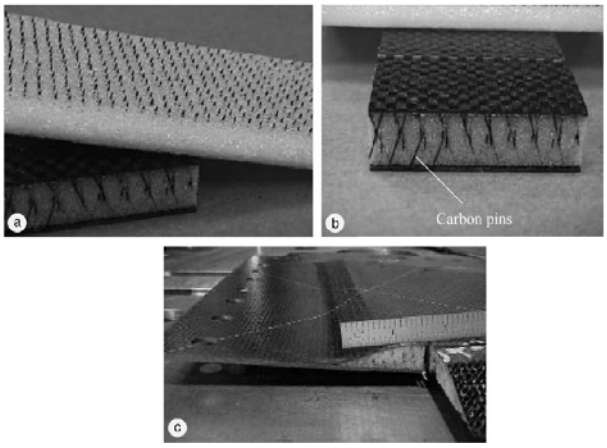

Figure 2.3. Material testing of carbon pin truss sandwiches. Source: O'Brien, T. K., and Paris, I. L., "Exploratory Investigation of Failure Mechanisms in Transition Regions between Solid Laminates and X-cor® Truss Sandwich," *Composite Structures*, Vol. 57, 2002, pp. 189-204.

One of the most widely used sandwich core materials of the aerospace industry as well as others including in terms of structural sandwiches is hexagonal cell cores, referred to commonly as honeycomb core. Honeycomb type core, due to its high damage tolerance, heat transfer, and low relative density, is used in commercial and military aircraft cabin floors, ceilings, and walls (see Figure 2.4 [1]) as well as in ailerons, doors, and flaps [12], and also in civil engineering in the form of bridge panels [13]. In fact aluminum and titanium

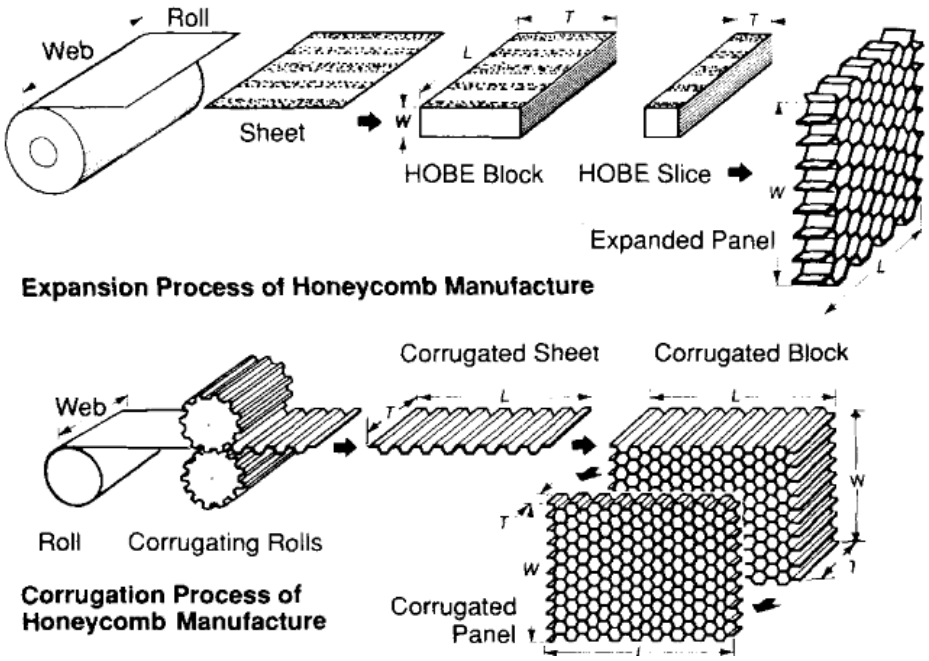

Figure 2.4. Honeycomb core and its manufacturing processes. Source: Peters. S. T., *Handbook of Composites*, 2nd ed., Chapman & Hall, New York, 1998, Chap. 12.

honeycombs comprise 1.6% of the total weight of the F-15E [12], despite its low density. However, care must be taken to ensure that if this type of core is used with a bonded fibrous laminate facesheet that the laminate does not dip into the cells during cure [6], which is not an issue with cellular foams.

Certain mechanical properties of honeycomb cores are dependent upon density, and can even depend linearly if specific metallic alloys are utilized. This is shown in Figure 2.5 [1].

The mechanical behavior of regular hexagonal honeycombs are well understood and many studies including analytical, FEA, and physical [14 - 18] have been conducted. A schematic example of honeycomb is shown in Figure 2.6 [15]. The overall properties of honeycomb cores and associated metallic foils will be discussed later in this chapter.

2.2 Previous Analyses with Various Core Materials

In order to understand the strengths and weaknesses of sandwich panels and how one might go about improving core materials, research was conducted on previous works

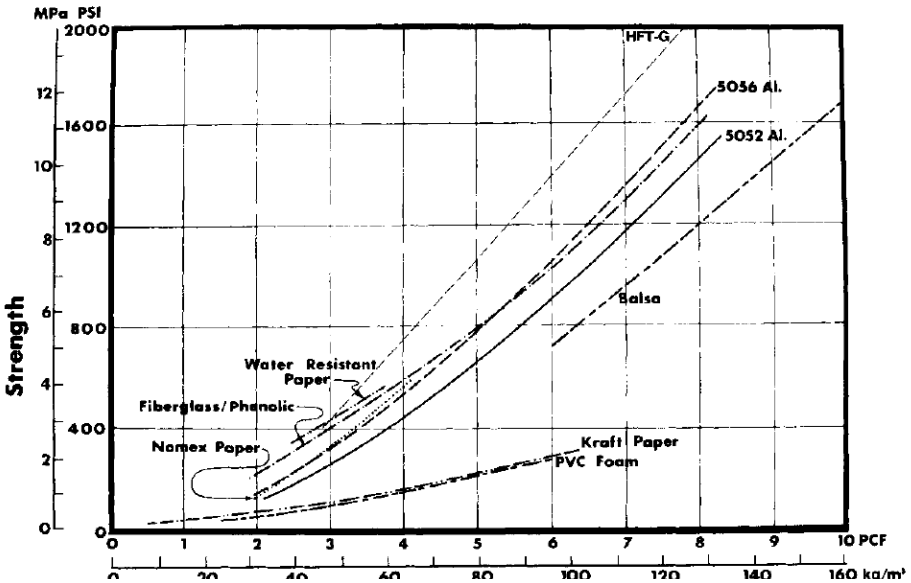

Figure 2.5. In-plane variation of honeycomb strength vs. honeycomb density. Source: Peters. S. T., *Handbook of Composites*, 2nd ed., Chapman & Hall, New York, 1998, Chap. 12.

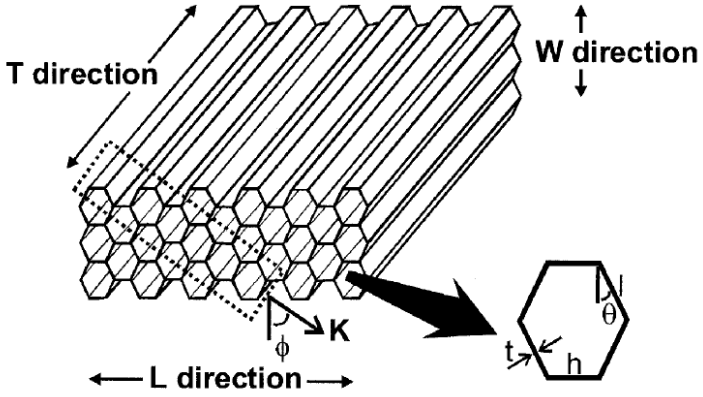

Figure 2.6. Schematic example of a honeycomb structure, including industry accepted standard dimensional parameters. Source: Doyoyo, M., and Mohr, D., "Microstructural Response of Aluminum Honeycomb to Combined Out-of-Plane Loading," *Mechanics of Materials*, Vol. 35, 2003, pp. 865-876.

associated with this topic. The following sections will explain some of the work that has already done including analytical and finite element analysis modeling as well as physical testing.

2.2.1 Sandwich Analytical and FEA Modeling

Sandwich laminates experience different modes of failure: facesheet yielding (tension), facesheet buckling (compression), core yielding, core shear, core crushing, (due to differential curvature of the facesheets), core crushing under applied transverse load, and facesheet wrinkling or dimpling [19, 20]. Analytical models are not accurate for some other modes of failure in sandwich laminates. One such mode is the delamination failure along the facesheet-core interface. This requires fracture mechanics principles [21]. Finite element analysis models coupled with virtual crack closure technique have been employed to perform delamination analysis of sandwich laminates under static and cyclic loading (fatigue).

Analytical models have been developed to predict modes of failure of sandwich structures including a fatigue model by [22] as well as [23] and [24]. Clark et al. [22] determined that fatigue caused a decrease in stiffness of the foam of the sandwich. Core shear failure in various repetitive loading conditions was also shown. The model agreed well with further experimentation.

Sandwich laminates are very prone to low velocity impact [25]. Models of low velocity impact tests have been conducted which show that initial damage caused by an indenter had localized core crushing which leads to the main mode of failure, thus reiterating the low compressive strength of aluminum honeycomb core material as a cause of failure. These were confirmed by physical testing.

FEA models of aluminum honeycomb core sandwiches beams under classic four point bending were made in order to produce and solve three dimensional governing equations [26]. This particular test modeled the honeycomb core as a solid homogenous material of equivalent properties where numerical and analytical work was done to characterize the equivalent properties. From this Abbadi et al. [26] determined that higher order theories had a much higher accuracy than classical lamination theory for these types of sandwiches.

Work has been done to understand the interfacial stresses between the honeycomb core and skin material of the sandwich in a computational model [27]. This can then be used to detect critical sections of a structure where the interfacial stresses are high and thus delamination imminent. Thus far it appears that the low compression strength, core shear [28], and high interfacial stresses between the core and skin are key issues in sandwich testing and use. Physical testing has also been done using various core materials to determine the failure modes of sandwich structures.

2.2.2 Sandwich Physical Testing

Fatigue tests have been done and static tests have been reviewed [29] on foam sandwich beams where it was determined that core shear and face compression were the most common modes of failure in foam cores. The relationship and transition between the two modes was identified as:

$$\frac{L}{h_f} = C\frac{F_f}{F_{cs}} \tag{2.1}$$

where L is the length of simply supported cantilever beam, h_f is the facesheets thickness, F_f is the facing strength in compression, F_{cs} is the core shear strength and C is based on the boundary conditions and loading. It appears that problems can arise in foam cores due to low compression strength of the core and core shearing. Foam core indentation was studied in detail by [30] due the sensitivity of sandwich panel to indentation damage.

Fiberglass skins with Nomex honeycomb core sandwiches were also tested in [29] using 3 point bending tests per ASTM C393-62. During this testing it was found that once the out of plane stress caused by the roller equaled the out of plane compression strength of the honeycomb, failure occurred from local indentation. Another mode of failure in the core included global core deformation once the mean shear stress in the core equaled the shear strength, unlike foam cores where a crack first initiates and grows.

Nomex and aluminum honeycomb were tested for shear and compressive strength in [31]. For the aluminum cores the compressive mode of failure was plastic yielding. Also, the gaps between honeycomb core cells and low out of plane core compressive strength. This lead to sandwich buckling failure by symmetric or mixed mode facesheet wrinkling at a characteristic half cell size wavelength, discussed in detail in [32].

So far we have discussed physical experimentation and modeling of sandwiches in general. We must however, also look at how these structures are integrated into supporting structure to get an idea on the type of stresses imposed.

2.3 REGIONS OF ATTACHMENT

Sandwich structures, while very efficient in bending, are weak in carrying transverse shear and compression loads. This poses a problem when sandwich laminates have to be mechanically fastened to support structures. Due to the low compressive strength of core materials, using a standard fastener is nearly impossible; damage caused by indentation from a bolt or washer on either standard foam or honeycomb core sandwiches can lead to permanent losses in fatigue strength and subsequent global shear deformation or core shear. To overcome this difficulty the sandwich laminate is tapered down to a solid composite laminate (other methods studied in [33, 34]) at the end regions where attachments using mechanical fasteners are required. The transition region from the sandwich laminate is referred to as the rampdown region, or end closure region in practice. This is illustrated by Collier, Yarrington and Pickenheim [2] in Figure 2.7.

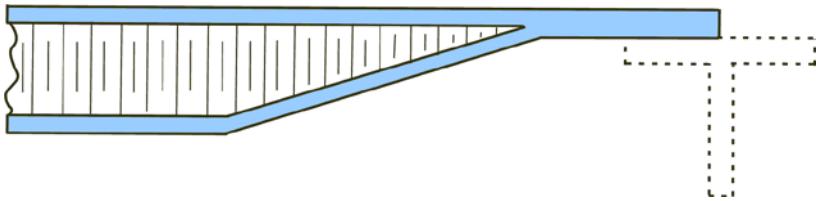

Figure 2.7. Rampdown structure with honeycomb core and composite facesheet for NASA composite crew module (CCM). Source: Collier, C., Yarrington, P., and Pickenheim, M., "Analysis Methods used on the NASA Composite Crew Module (CCM)," *49th AIAA/ASME/ASCE/AHS/ASC Structures, Structural Dynamics and Materials Conference,* AIAA Hampton, VA, 2008, pp. 2008-2251.

2.4 RAMPDOWN ATTACHMENT

Tapering the skin and core material down to a thick region requires no new material and typically the compressive strength of the joined solid facesheets are vastly superior to the compressive strength of a honeycomb or other core material. This technique allows the use of standard types of fasteners without the associated risk of damaging the core material,

which could lead to premature failure. Rampdown closures require a ply buildup [35] to increase the thickness to compensate for the reduction in bending stiffness and to increase the bearing strength of the laminate. These additional plies at the rampdown region require detailed analysis models where attachments will be made.

2.4.1 Existing Research in Rampdown Regions

Rampdown regions have been the topic of research interest in recent years. Castanié [36] et al. have analytically studied asymmetrical sandwich structures with composite laminate skins and Nomex honeycomb cores. They discovered that while the asymmetrical design is promising and efficient, further improvement must be made in the design of the ramp type closure [37]. This topic was also considered by Evertz [38].

Frostig et al. [39] studied bending of a generalized tapered sandwich beams in the transverse direction analytically. In a subsequent paper [40] they also present different types of adhesive joints in sandwich structures. This including spew fillets (fillet joint caused as a consequence of bonding two flat panels) and square ends (joint of flat panels without fillet). Analyses attempted to find correct spew fillet joint radii analytically for various applications.

Thomsen [41] also analyzed tapered sandwich beams analytically, and found that due to geometric and boundary conditions, localized bending was severe in the tapered region and that this must be considered further. His works showed that the normal transverse stresses in the region of the taper were very high and could crush the low compressive strength core and "may endanger the structural integrity of the sandwich panels in consideration" ([41], pp 1875).

Hirose et al. (Figure 2.8) [21] attempted to reduce the possibility of delamination at the facesheet junction by using finite element modeling of a rampdown region with included filler joint. This was tested by the same group to stave off delamination to a higher tension load on the asymmetric panel using this method.

2.4.2 Rampdown Physical Testing

Several experimental studies have been conducted on sandwiches with ramp regions, Figure 2.9 [21], to understand the failure mechanisms. Failure of this type of panel was also studied by [42].

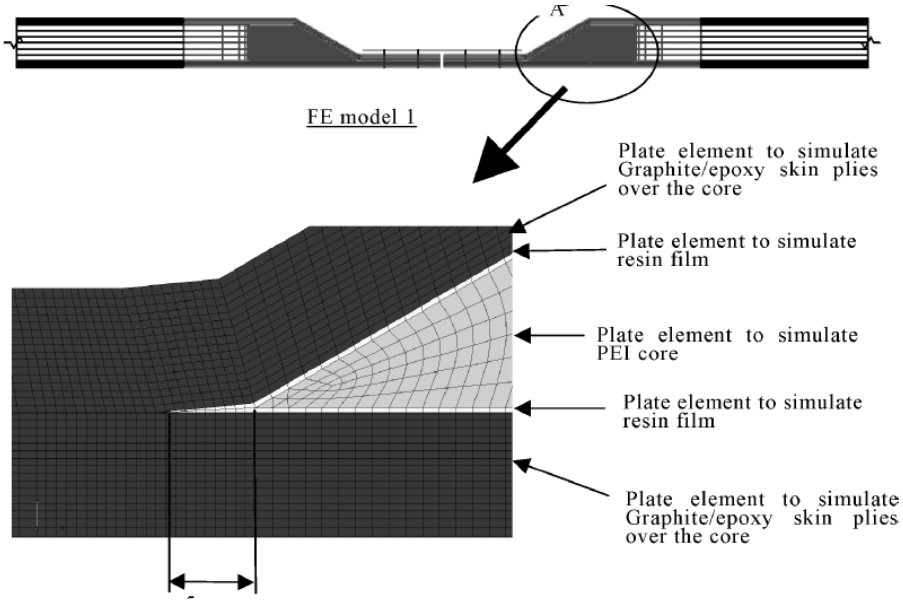

Figure 2.8 Filler joint modeled by Hirose et al. Source: Hirose, Y., Nishitani, M., Ochi, S., Fukumoto, K., Kawasaki T., and Hojo, M., "Proposal of Suppression of Delamination for the Foam Core Sandwich Panel Joint with Filler," *Advanced Composite Materials*, Vol. 15, No. 3, 2006, pp. 319-339.

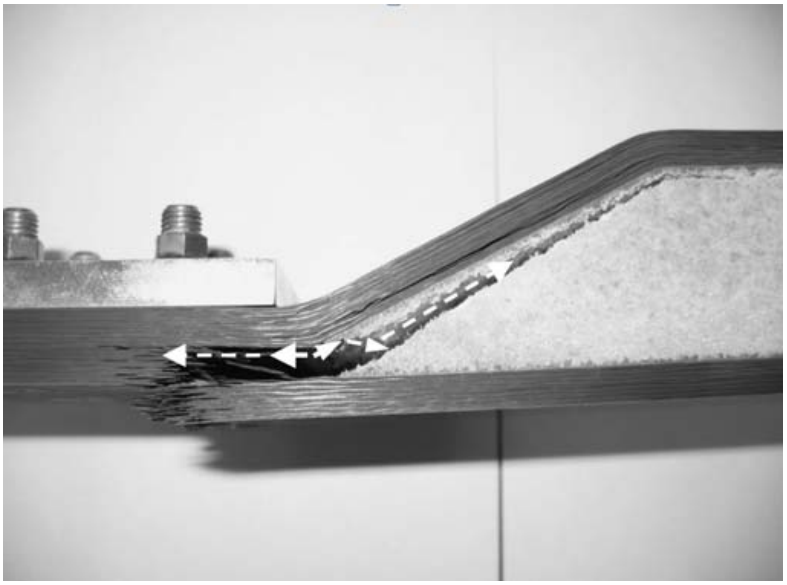

Figure 2.9. Tension testing on carbon fiber reinforced sandwich ramp region with foam core, with crack growth along upper facesheet. Source: Hirose, Y., Nishitani, M., Ochi, S., Fukumoto, K., Kawasaki T., and Hojo, M., "Proposal of Suppression of Delamination for the Foam Core Sandwich Panel Joint with Filler," *Advanced Composite Materials*, Vol. 15, No. 3, 2006, pp. 319-339.

Hirose [21] did the structural testing shown in Figure 2.9 prior to attempting an FEA model. He proved first physically and then using FEA that a resin impregnation filler joint in the ramp region could reduce energy release rates and suppress initiation of delamination.

2.5 FUNCTIONALLY GRADED (FGM) CORE MATERIALS

Functionally graded materials are used in sandwich structures to lessen stress concentrations caused by a discontinuous material interface. A functionally graded material has a continuously and gradually varying elastic modulus or strength properties that have been tailored to its load distribution. One interesting use of FGMs is to reduce the thermal stress gradients in the joining of two materials which have largely different coefficients of thermal expansion (CTE mismatch) [43]. However, there also have been extensive studies on the use of FGMs to mitigate structural fatigue and stress concentrations. Those will be discussed in the next section.

2.5.1 Examples of Uses: Modeling

Functionally grading the core material in the through the thickness direction of the sandwich has been investigated by many researchers to mitigate the large shear stresses in the facesheet-core interface. Sankar [44] developed an elasticity solution for a beam having experimentally varying elastic moduli along the thickness direction. Sankar also found an elasticity solution for an exponentially varying elastic modulus while the Poisson ratio was constant. The beams were simply supported and subjected to a uniform sinusoidal load. Stress concentrations were found to be less when the beam was loaded on the softer side.

Venkataraman and Sankar extended the elasticity solution to sandwich beams [45]. They also noted that the large discontinuity in elastic moduli at the skin/core interface caused a large increase in shear stresses. The result was similar to what was found in [44].

Etemadi [46] investigated FGMs using 3D FEA on low velocity impact by a cylindrical projectile on a FGM sandwich panel which has through the thickness variation of elastic modulus. It was found that contact stresses increased.

2.5.2 Examples of Uses: Experimental Work

FGM has also been utilized in other sandwich applications for example, [47] studied dynamic fracture toughness for feasibility of foam core with a bilinear gradient of

epoxy/microballoons. These were compared to a standard core of a single density of foam. It was shown that the bilinear graded core sandwich was able to resist delamination when compared to the standard core results in dynamic fracture testing.

Jakobsen studied the junctions of two core materials of differing elastic moduli [48], and found that a “peel stopper” glass composite laminate insert can suppress delamination at the junction between foams of different densities. This is shown in Figure 2.10 [48].

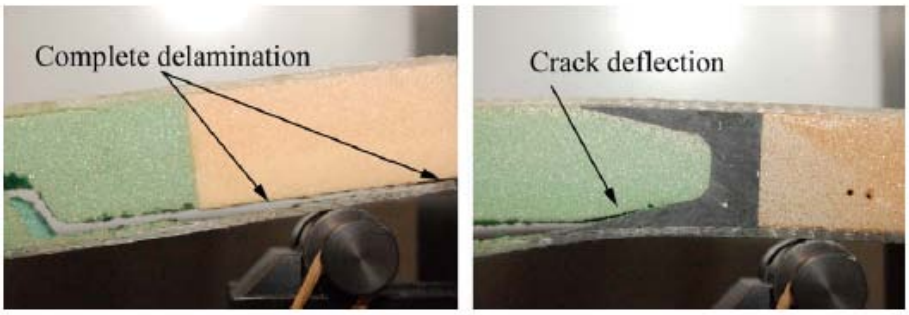

Figure 2.10. Crack deflection using "peel stopper" laminate insert. Source: Jakobsen, J., Andreasen, J. H., and Thomsen, O. T., “Crack Deflection by Core Junctions in Sandwich Structures,” *Engineering Fracture Mechanics*, Vol. 76, 2009, pp. 2135-2146.

Similar studies were done by Bozhevolnaya and Thomsen [49] where “scarf” junctions and other types of core material interfaces are tested. It was found that during physical bending tests that mismatch of local core stresses due to material interfaces was the cause of most failures.

It has thus far been shown that FGM can help mitigate material mismatches. One material which has been studied to a high degree but not for use in an FGM structural sandwich is honeycomb.

2.5.3 Honeycomb Core Deformation and Properties

Honeycomb core deformation has been studied extensively in literature for properties and behavior in all types of loading conditions both in [14, 28, 50, 51] and out [15, 31] of plane, linear[18] and non linear[4, 18, 52, 53] as well as low[31, 51] and high[4, 52] global strain rates. Also, numerical modeling has been done by [15] and [16], and bending tests have been done in [10]. This anisotropic material was covered briefly in section 2.1, and more detail will follow here on the deformation and mechanical behavior of aluminum honeycomb.

Zhang and Ashby [31] have studied the out of plane properties of honeycombs in both physical and analytical testing. They discovered the out of plane shear and compression strengths of the honeycomb cores they tested were independent of the height of the core as well as the cell wall angle. However, the strengths were highly dependent upon cell density and thus cell size.

Analyses have been done on the in-plane crushing response of honeycomb cores and the overall constitutive relations of these crushed cores have been computed. Atli-Veltin [4, 52] wrote investigated the crushing of honeycomb cores for use in helicopter subfloors and has done extensive modeling both 2D and 3D of single and multiple cell arrangements. A 2D beam element model on uniform in-plane crushing was built with ABAQUS finite element software and was verified against the work of Papka and Kyriakides [53]. Work in [53] was verified via experimental results.

Overall in-plane properties of honeycombs have been studied by Ajdari [18] for uniform loading conditions however the more fundamental aspects of linear, plastic, and buckling deformation of honeycombs is also considered. Functionally graded Voronoi structures are also explored to represent free cell nucleation in foam materials. Varying the cell size and thus the apparent density of honeycombs and its effect on elastic properties was explored, which was shown to have a nearly linear relationship.

Whitty et al. [50] have done some numerical work in determining the overall in-plane properties of honeycomb core when the wall parameters are varied. He has found that when the vertical walls of a honeycomb core are reduced in length compared to the inclined walls reduced the vertical elastic stiffness.

2.6 Discussion of Literature

After completion of the literature review, a few questions were raised that seemed left unanswered, especially in terms of FGM applied to sandwich closures.

The first matter of concern in the taper region of a sandwich structure is when it comes to delamination due to local bending and high shear stresses caused by material mismatch. While it is simple to ramp the facesheets together to close the sandwich and fasten it to support structure, the type of global deformation that could result is a serious

drawback to the use of this design. A real concern is that no core material design has been developed specifically for this type of sandwich closure, while it remains widely used.

The second matter of concern is that while studies have been done in grading of sandwich core materials, there have been few studies which grade the core in the in-plane direction and zero studies which have graded the core in the ramp region of sandwich structures in their in-plane direction. If one is to deal with high gradients of mechanical properties in the ramp region of a sandwich closure, in-plane core material grading must be investigated.

The final problem is what material to use for this core grading, and is it possible to obtain a desired gradient. Because aluminum honeycomb have been the material of choice for sandwich structures in the aerospace business, and because much of the way they deform in relation to their material properties is known and studied in high detail, this is the material of interest for this work. Also important are studies like [37] which show that the shear strength of a sandwich increases with the number and quality of fillets created. This gives rise to the idea that perhaps densified honeycomb could be the solution to delamination issues in the ramp region.

In order to address each of these concerns, we start with a two dimensional model in ABAQUS of a sandwich beam with a discretely graded core along the ramp region to determine the benefit or consequence. Next a geometrically and materially non-linear beam element FEA model consisting of a 5x6 honeycomb core is assembled and validated against Papka and Kyriakides [53] as well as Atli-Veltin and Gandhi's [4, 52] findings under uniform in-plane deformation. Then, since it has been shown that the material properties of honeycombs vary with density, a novel approach to crushing these types of cores to obtain a desired core density is presented and a method to calculate the apparent density of the resulting honeycombs is developed.

CHAPTER 3

BEAMS WITH ANALYSIS OF SANDWICH RAMPDOWN REGIONS WITH FUNCTIONALLY GRADED CORES

A 2D cantilever beam model of a rampdown sandwich structure closure was created using ABAQUS/Standard. This will become the basis for further research in using a modified core in the rampdown region. The following results will show that by increasing the elastic modulus along the length of the ramp from the parallel facesheet region to the tip location where the facesheets join that specific facesheet stresses can be alleviated. This is factor of key importance when discussing the failure modes of these panels.

3.1 SANDWICH CANTILEVER BEAM WITH RAMPDOWN END CLOSURE

In this section the effect of varying elastic modulus of the core in the taper region of a sandwich beam is investigated. The objective was to understand how the in-plane variation in elastic modulus affects the facesheet-core interface normal and shear stress and facesheet stress in the taper region.

3.1.1 Plane Strain 2D Sandwich Model

A plane strain model of a sandwich structure was used in our current investigation. The rampdown region of the model was constructed such that each section defined in Figure 3.1 had a discrete elastic modulus.

These are shown in the magnified view and numbered 1 through 10 as shown. The properties for each of the parameters in Figure 3.1 are shown in Table 3.1. Because this model was built purely for comparison of the elastic modulus variation and the model stresses, L_1 and t were chosen arbitrarily. Once they were fixed L_2 was chosen such that there was at least six times the core thickness (t) between the boundary conditions at the left edge and the start of the ramp. This was to minimize local effects from the start of the ramp

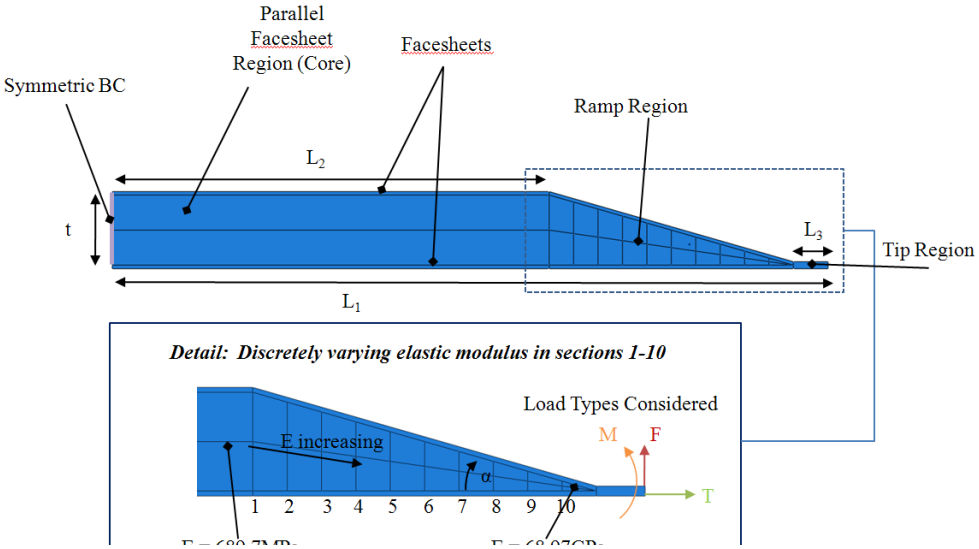

Figure 3.1. 2D ABAQUS model shown with boundary conditions, dimensions and associate coordinate system.

Table 3.1. 2D ABAQUS Model Parameter Definitions

2D Model Parameters	*Value*	*Description*
L_1	0.164 m	length upper facesheet
L_2	0.1m	length lower facesheet
L_3	0.008m	length facesheet tip
α	15°	ramp angle
t	0.016m	core thickness
F	10kN	transverse load
T	10kN	tension load
M	24N·m	moment load

to the root of the cantilever. Also, L_3 was then chosen to be at least 3 times the facesheet thickness in the tip region, to minimize localized effects of the applied loading. The ramp angle chosen is a typical ramp angle used in the composite sandwich industry. Jakobsen et al. [48] ran previous ABAQUS simulations on ramp angles from 10^o to 90^o. It is discussed in [32] that ramp angles larger than 15^o are considered large and therefore 15^o was chosen in this experiment

3.1.2 2D Sandwich Model Setup and Boundary Conditions

The top of the beam was loaded under F, T, and M as shown in Figure 3.1. These were applied individually in separate cases. They were chosen such that material yielding is

prevented, maintaining the assumption of a completely linear model. Because linear elements were used to mesh this model the translational degrees of freedom at each node (1 in the *x*-direction and 1 in *y*-direction), the moment load case was approximated using a force couple. The facesheet thickness is 7.9375 x 10^{-4}m (double at the tip junction along L_3) and one unit depth in the *z*-direction is set nominally. Also note that the left edge of the beam is given symmetric boundary conditions where one node was fixed in both directions to prevent rigid body motion, and the others along that edge were fixed only in the *x*-direction.

3.1.3 2D Sandwich Model Meshing and Constraints

Figure 3.2 shows the finite element mesh of the plane strain sandwich beam model. The finite element model uses combined four node quadrilateral and some three node triangular elements. Triangular elements were used in the region of the taper because quad elements will be severely distorted in such regions leading to lower accuracy. The model was continuously meshed with several seed biases applied to increase the number of elements in regions with extremely high stress gradients, for example, at the tip of the model and at material transitions.

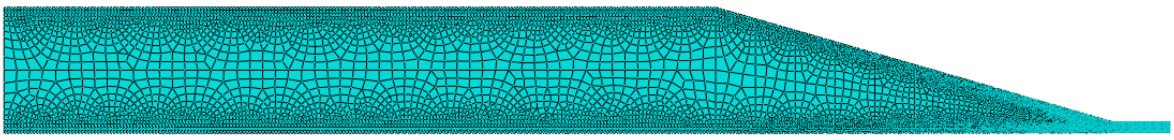

Figure 3.2. Final mesh of 2D sandwich structure model.

The final mesh contained 13,654 elements which were a combination of ABAQUS CPS4R 4 node bi-linear plane stress quad elements with hourglass control and CPS3 3 node bi-linear plane stress tri elements. The combination was used in order to make meshing more efficient given the mix of rectangular geometry (parallel facesheet region) and triangular geometry, (rampdown region). This final model had 28,212 degrees of freedom and 14,106 nodes.

3.1.4 Mesh Convergence for 2D Model

A mesh convergence study was undertaken in the transverse load case to ensure the deflection values were not affected due to the discrete nature of the model. The model was

seeded with an increasing number of elements and subsequently meshed. The results are shown in Table 3.2. The percent change in tip deflection was noted between each model.

Table 3.2. Convergence Testing of a 2D ABAQUS Sandwich Structure

2D Model Convergence Test				
CPS3/CPS4 Elements	***Nodes***	***DOFs***	***Tip Deflection (m)***	***%Change***
108	268	804	0.028725	n/a
564	1280	3840	0.0310108	7.96%
703	1583	4749	0.0310535	0.14%
1480	3212	9636	0.0314979	1.43%
13654	*14106*	*28212*	*0.0316509*	*0.49%*

The convergence criteria were met once the tip deflection stabilized (based on the percent change from the previous simulation versus number of DOFs). The final model chosen has average element edge lengths 3.167×10^{-3}m in the parallel core region (legs of triangular elements) and 1.109×10^{-3}m in the ramp region.

3.1.5 Materials used in 2D Model

Aluminum, alloy 5052 temper H39, was in this research since its properties are well understood [17, 54, and 55]. The upper and lower facesheets were identical and constructed of this alloy as well using the properties in Table , which include the very tip of the model where the facesheets unite to double their original thickness (see right side of Figure 3.1).

The parallel region of the core before the ramp closure is assigned a material which has 1% of the elastic modulus of aluminum, or 689.7MPa. This value is typical of foam cores. The main assumption of this work is that while the elastic modulus varies throughout the rampdown region, the Poisson ratio is constant ($\nu = 0.33$). This assumption will not affect to a great degree the overall change in stress distribution for the core and facesheets. At first the entire model including the core in the rampdown closure is given an elastic modulus of 689.7 MPa (un-graded) and converged, then it is compared to graded cores.

Each of 10 discrete regions of the model near the rampdown region are given a discrete but increasing elastic modulus until finally the last region at the tip of the structure has a modulus equivalent to that of the facesheets. Figure 3.3, shows an idealized variation of

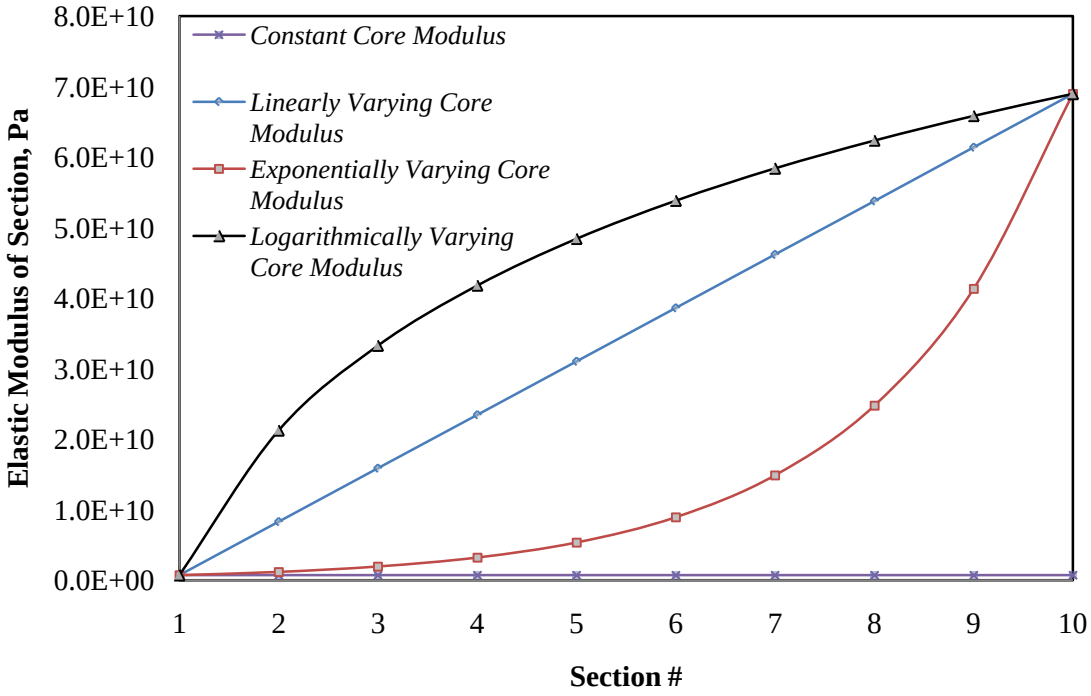

Figure 3.3. Ideal continuous variation of elastic modulus; section 1 is at beginning of taper region, section 10 is at the tip.

core elastic modulus, while Figure 3.4 demonstrates the actual variation applied to the discrete regions of the model. The variation of the discrete regions (Figure 3.1) is the key experimental parameter. In addition to a non-graded (baseline) case, a linearly varying modulus, an exponentially varying modulus, and a logarithmically varying modulus designs are considered.

3.2 Comparison of Global Stiffness of Sandwich Rampdown Region with Different Material Grading Schemes

The following results were obtained from a static linear analysis of the 2D sandwich beam structure model with rampdown closure. The main goal was to understand the effect of varying the elastic modulus of the core material in the ramp region on the overall bending stiffness of the model and its role in stress distribution in the rampdown region. The global bending stiffness is characterized the tip deflection of the beam under transverse load.

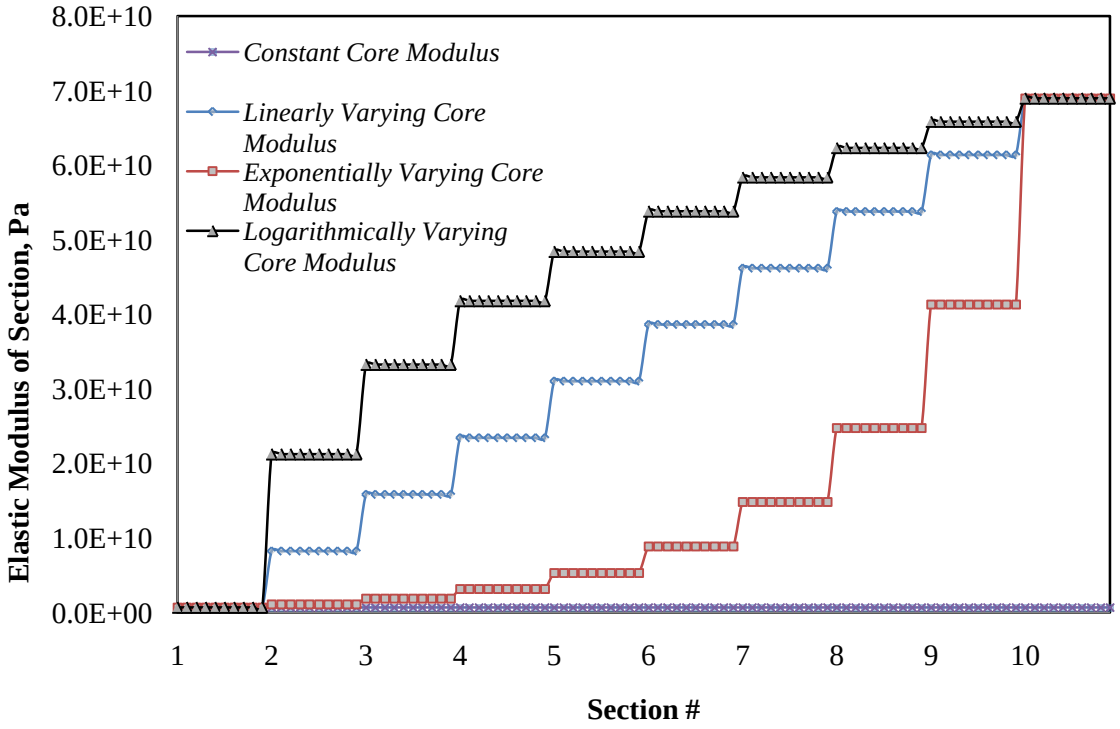

Figure 3.4. Actual modulus values assigned to the model in each discrete rampdown region.

In all cases the most stressed regions are the facesheets and the apex at which the sandwich rampdown transitions to the solid laminate. This allows a more clean visualization of the stress field in the sandwich rampdown region.

There is a concern that the gradation leads to an increase in core stresses in this region. Typically increasing the moduli of a core (foam or honeycomb) by densification also leads to an increase in material strength values. If the material strength increases at a rate faster than the increase in stresses due to densification (functional grading) then the design will have positive stress failure margins.

Table 3.3 shows the result of a transversely loaded ramp region von mises stress distribution with a non-graded core material. The green in the plot shows that most of the core is under an approximately 5 MPa constant stress. In plotting stress distribution the maximum fringe value was limited to 30MPa. This allows a more clean visualization of the stress field in the sandwich rampdown region.

Table 3.3 Contour Plot of Cantilever Beam Ramp Region Under a Transverse Load at the Tip

Rampdown Region with Varying Core Material Elastic Modulus, Transverse Case
Resulting Stress (deformation scaled +1x)
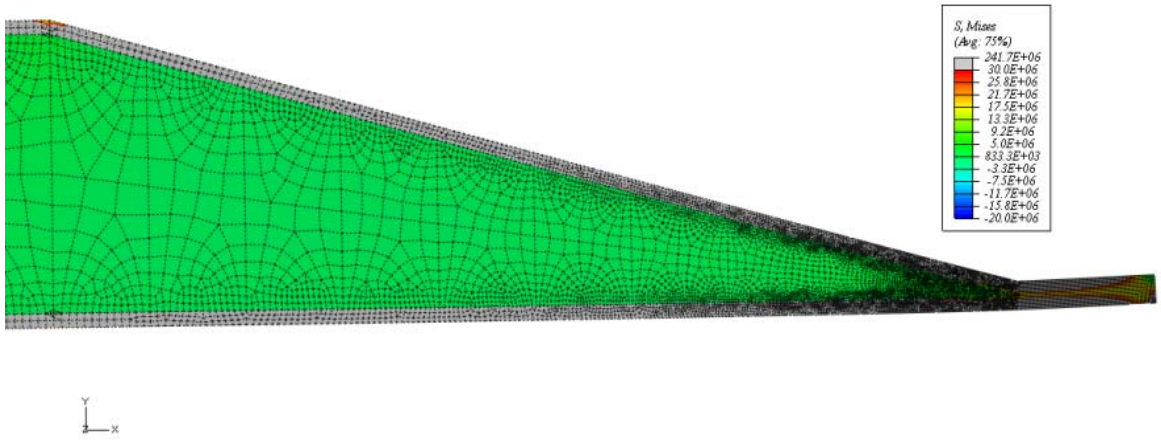 ***Constant Elastic Modulus*** E_{core} ***= 689.7 MPa***
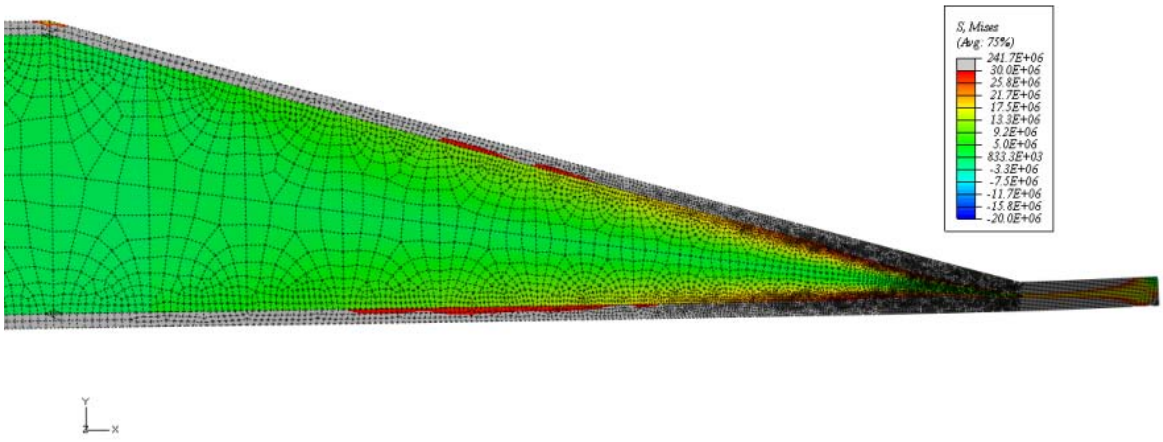 ***Linearly Varying Elastic Modulus***

(table continues)

Table 3.3. (continued)

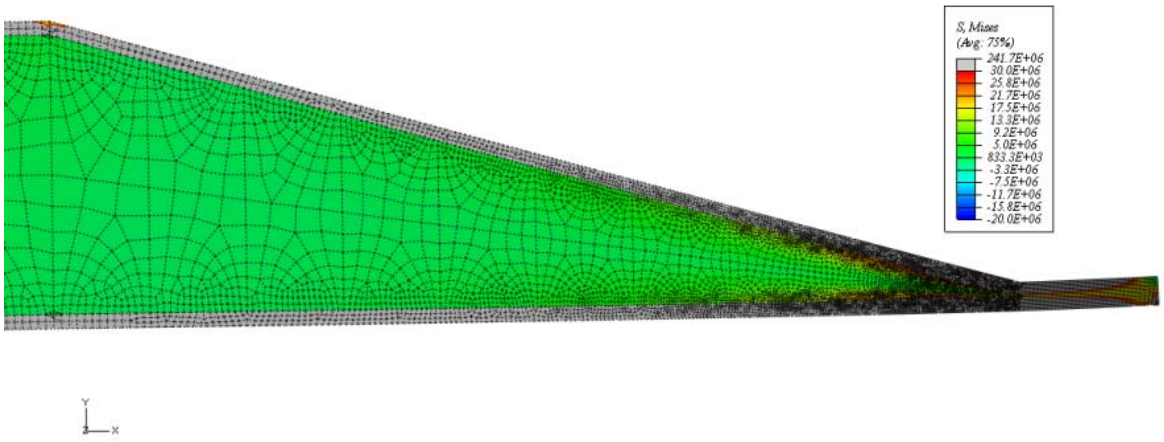

Exponentially Varying Elastic Modulus

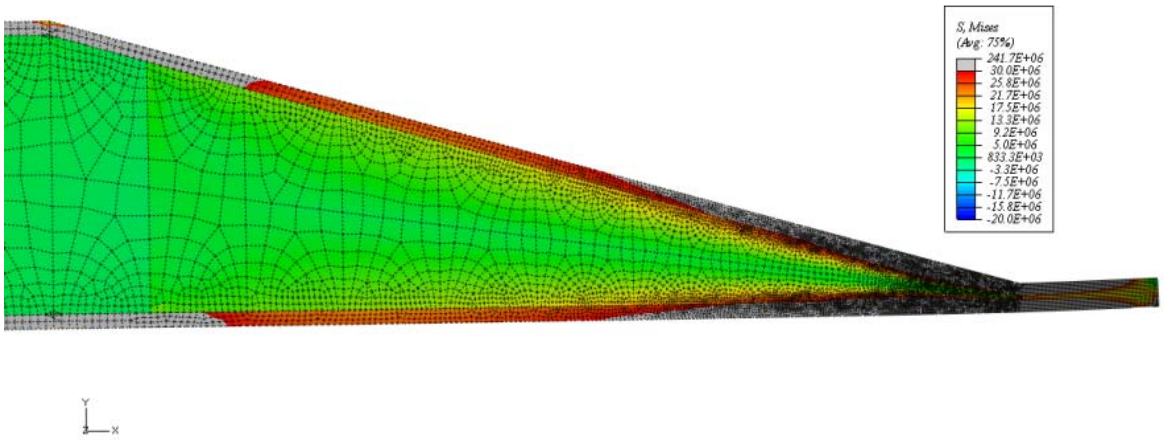

Logarithmically Varying Elastic Modulus

In the second, third and fourth plot in Table 3.3, the variation of core stress shows that by increasing the elastic modulus along the ramp from the parallel facesheet region to the tip where the facesheets unite, the von mises stresses increase slightly near the core. For example in the logarithmically varying core material (plot 3 in Table 3.3), the stresses near the upper facesheet at the tip are 2-3 times higher than in the constant core.

In all cases the most stressed regions are the facesheets and the apex at which the sandwich rampdown transitions to the solid laminate.

The contour plots of the von mises stresses indicate that rampdown regions with linearly and logarithmically graded core show increased stresses at the transition region. The increased stiffness of the core leads to more bending stresses in the core region. However since the core can carry more bending stress the facesheet bending stress should decrease. This offsets to some degree the increase in facesheet bending stresses due to the tapering of the sandwich. A more even variation of bending stresses along the facesheet can lead to decreased shear stresses.

Table 3.3 suggests that the facesheet stresses are being mitigated; the extent of this will be discussed later. It is also important to keep in mind that while the core is increasingly becoming stiffer toward the tip, the material strength must also increase, and is equal to that of aluminum in the last discrete region of the core (section 10 in Figure 3.1).

The case where a tension T is applied to model is presented in Table 3.4. In the tension case the deformation has been scaled up 20 times to more effectively visualize the deformation. In this case the lower facesheet and core is under much more stress due to the asymmetrical geometry of the ramp and the load location shown in Figure 3.1. Stress variations observed under different loadings are similar for example, when the core has is not graded in the transversely loaded beam case, a much larger portion of the load is carried in the facesheets, with a sharp increase at the rampdown junction at the tip. Here the green contours represent a stress of 2MPa, and the maximum specified (before grey out occurs) is 5MPa. As the core elastic modulus is varied under the same loading stresses increase up to a factor of 2 larger than the constant case. In the tension case, the facesheets begin to take load differently when the core material is graded than when it is not.

In Table 3.5 a pure moment load at the tip of the model is considered, and is visually displayed at 40 times the actual deformation. Here the stress distribution is clearly more symmetrical than the tension case due to the nature of the load. The portion in blue is -0.9MPa, green is 0MPa and the red is 0.9MPa, and anything out of bounds is grayed out. In the constant case (first plot) much of the stress is concentrated at the tip of the model. When the core is graded (subsequent plots) the stress in the core is greater, but much more evenly distributed away from the tip of the ramp region. Also, consider that the graded core material

Table 3.4. Contour Plot of Cantilever Beam Ramp Region Under a Tension Load at the Tip

Rampdown Region with Varying Core Material Elastic Modulus, Tension Case
Resulting Stress (deformation scaled +20x)
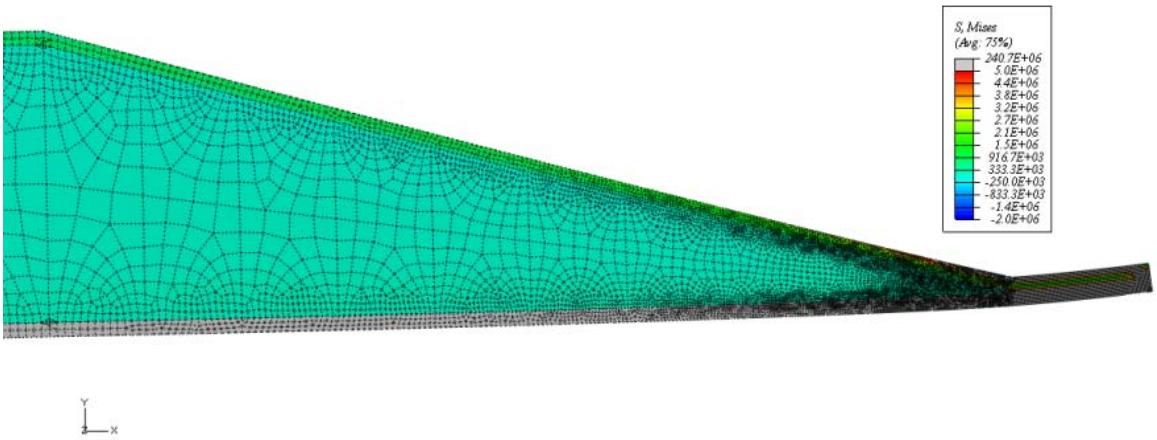 ***Constant Elastic Modulus*** ***E_{core} = 689.7 MPa***
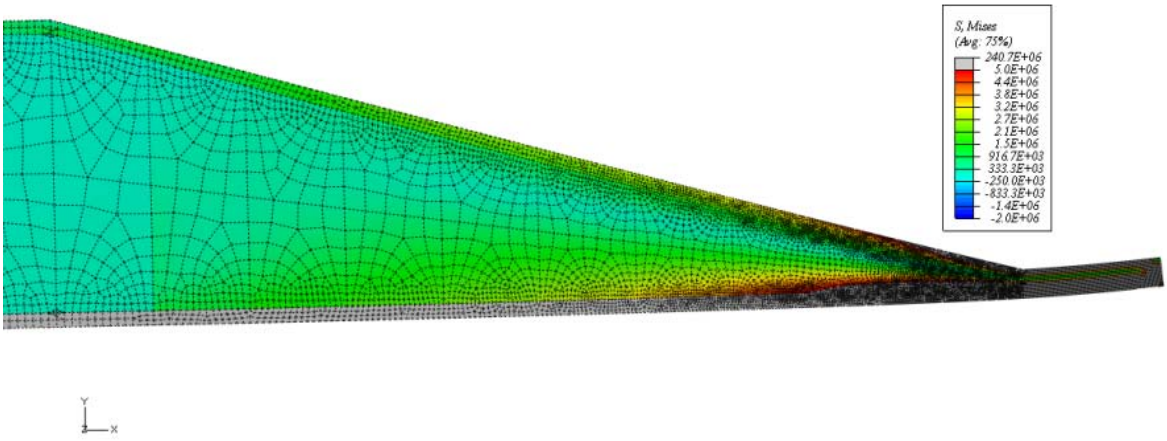 ***Linearly Varying Elastic Modulus***

(table continues)

Table 3.4. (continued)

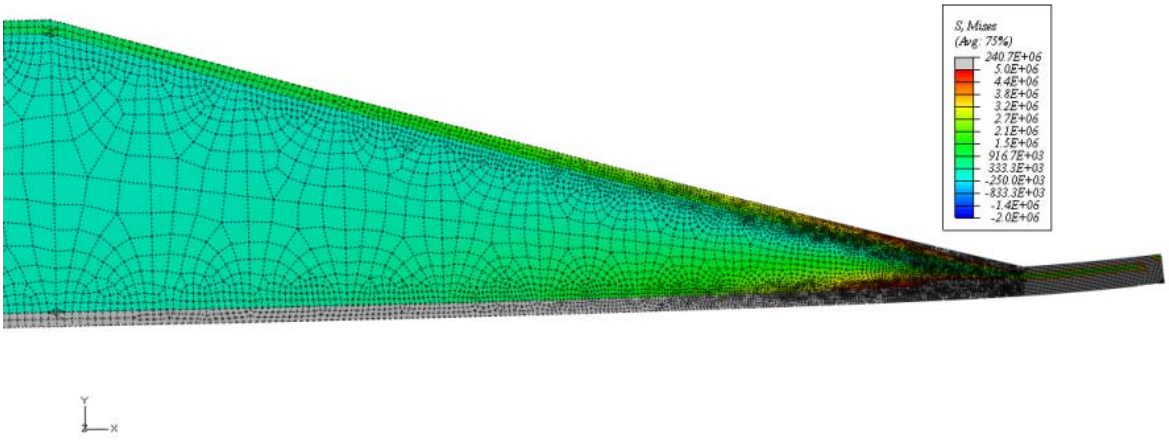

Exponentially Varying Elastic Modulus

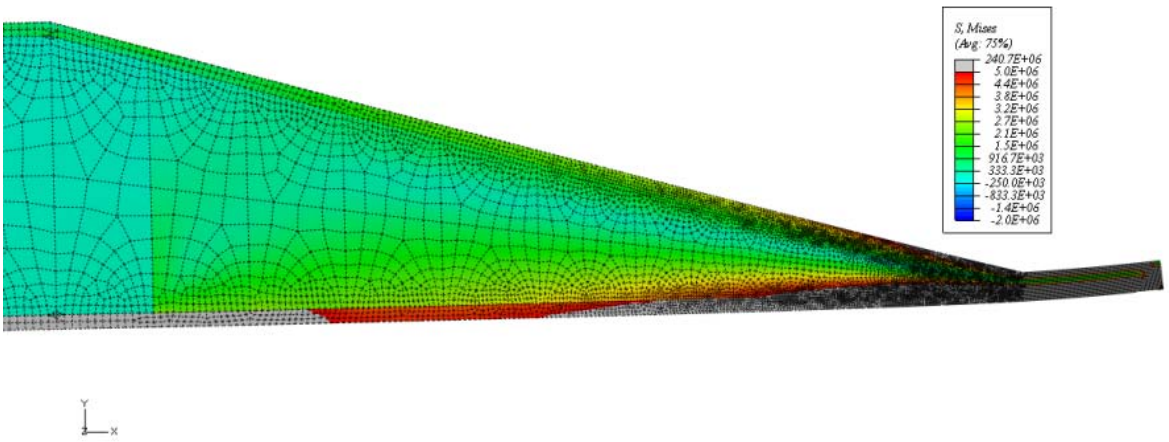

Logarithmically Varying Elastic Modulus

Table 3.5. Contour Plot of Cantilever Beam Ramp Region Under a Moment Load at the Tip

Rampdown Region with Varying Core Material Elastic Modulus, Moment Case
Resulting Stress (deformation scaled +40x)
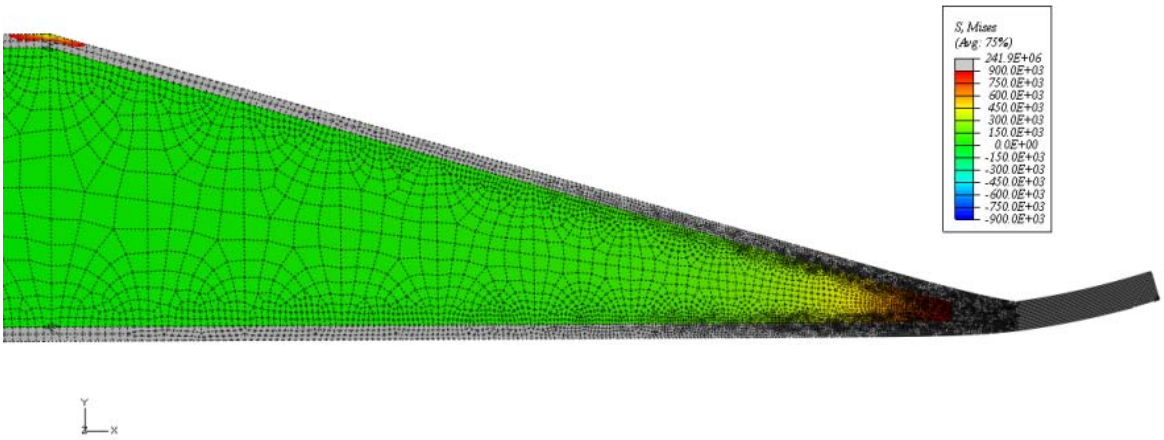 ***Constant Elastic Modulus*** ***E_{core} = 689.7 MPa***
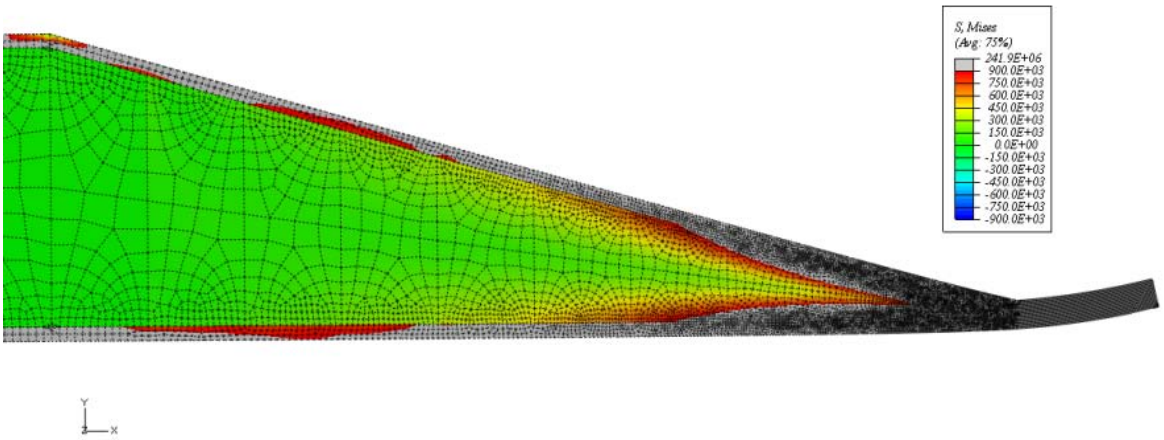 ***Linearly Varying Elastic Modulus***

(table continues)

Table 3.5. (continued)

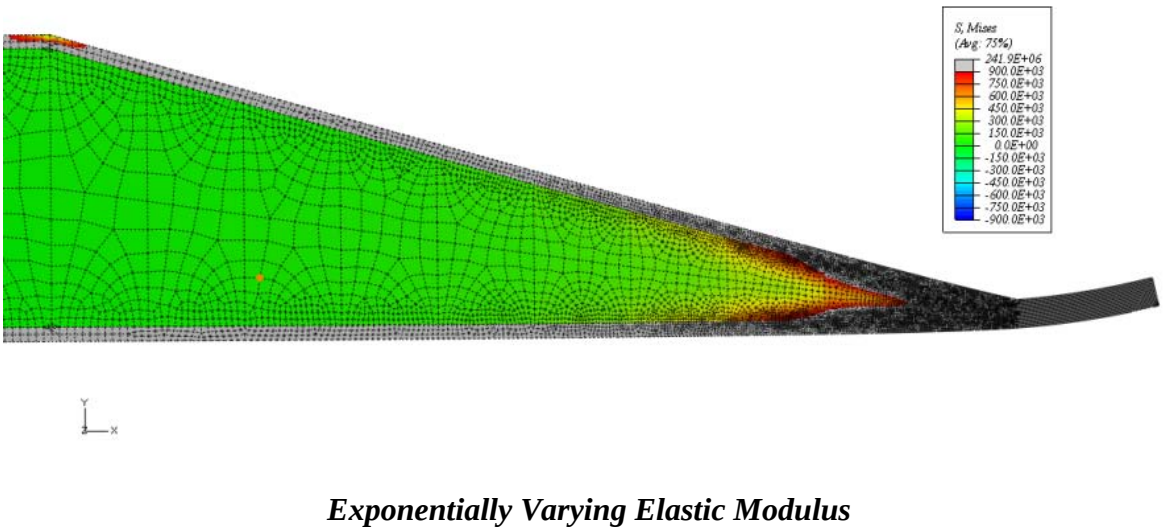

Exponentially Varying Elastic Modulus

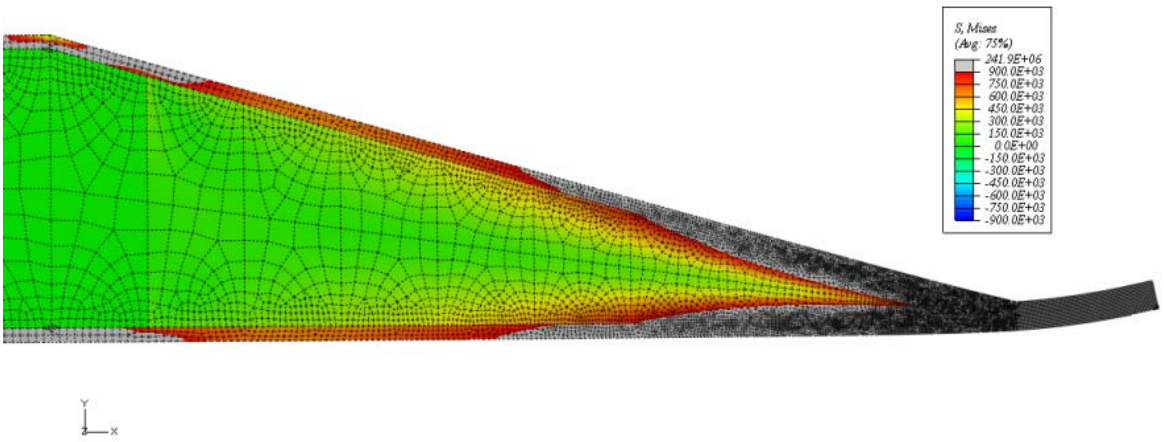

Logarithmically Varying Elastic Modulus

in the tip of the ramp region is now much stronger than the tip of the non-graded constant modulus case (100x stiffer), and thus while the stresses may be higher, the yield stress of the new material should also be considered. For example, typical yield stresses suggested by Hazrati [31] indicated Rohacell WF51 foam has a yield stress around 1MPa. In the non-graded core, this might be a typical material used to demonstrate 1% of the facesheet

material elastic modulus. In contrast to the yield strength of the foam, aluminum (which in the graded cases is what the 10^{th} section (tip) is made of) has a yield stress of 292MPa, around 300 times greater than the foam.

While our core stresses have increased only perhaps 3 fold as we grade the core in all load cases after grading the core material to a higher elastic modulus gradually, the material strength at the tip has increased by a factor of 100 at a conservative estimate.

3.4 Comparison of Tip Deflections due to Various Load Cases of a Functionally Graded Sandwich Beam Model

Before this is done, the deflections of each load case and core grading are also considered in Figure 3.5 and Table 3.6. By considering Table 3.6 one can deduce the best core gradation for each load case based on the percent difference from the non-graded elastic modulus core case. If it is negative, the deflection has been reduced. If it is positive, the deflection has increased.

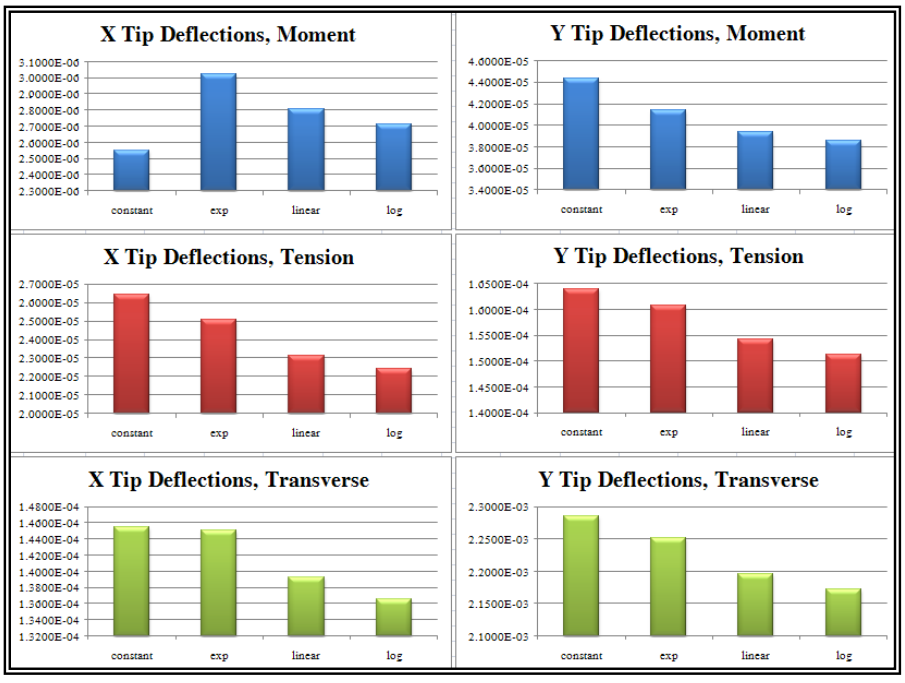

Figure 3.5. Comparison of tip deflections for the 2D cantilever beam model with varying elastic modulus.

It is interesting that the y direction tip deflection of the model was improved in a logarithmically varied core modulus by nearly 13% compared to the constant core in the same (moment) loading condition. If the y direction tip deflection was the greatest concern,

Table 3.6. Tabulated Tip Deflections of the Varying Load Cases and Elastic Modulus

Tip Deflection(m)	*Moment*				*Tension*				*Transverse*			
	X	***% Δ***	***Y***	***% Δ***	***X***	***% Δ***	***Y***	***% Δ***	***X***	***% Δ***	***Y***	***% Δ***
constant	2.5E-06	0.0 %	4.4E-05	0.0%	2.6E-05	0.0%	1.6E-04	0.0 %	1.5E-04	0.0 %	2.3E-03	0.0 %
exp	3.0E-06	18.6 %	4.1E-05	-6.6%	2.5E-05	-5.2%	1.6E-04	-2.0 %	1.5E-04	-0.3 %	2.3E-03	-1.5 %
linear	2.8E-06	10.1 %	3.9E-05	-11.3 %	2.3E-05	-12.5 %	1.5E-04	-6.0 %	1.4E-04	-4.3 %	2.2E-03	-3.9 %
log	2.7E-06	6.6 %	3.9E-05	-13.1 %	2.2E-05	-15.1 %	1.5E-04	-7.7 %	1.4E-04	-6.1 %	2.2E-03	-4.9 %

logarithmically varying the core elastic modulus produced the highest percent reduction of displacement from the constant core case.

If it were the *x*-direction deflection (while around 10 times less than the *y*-direction in all cases) was the main concern, if an applied moment load were considered the best choice would be an exponentially graded core. If a tension or transverse load were given, the best choice would be a logarithmically graded core.

3.5 Comparison of Facesheet-Core Interface Normal and Shear Stresses in Sandwich Rampdown Region with Different Material Grading Schemes

The following plots show the distribution of stress along the ramp in each the lower core and the upper core, not the facesheets. Note that the coordinate system orientation is such that the *x*-direction is aligned with the section of the ramp in consideration. Therefore the upper core has the coordinate system rotated clockwise 15^{o} (same as ramp angle), and follows it where X is normalized such that it is 0 at the parallel region to ramp transition and equal 1 at the tip of the core region where the facesheets join. This is illustrated in Figure 3.6.

For a transversely loaded sandwich beam structure, Figure 3.7 shows the constant and exponential core gradations while Figure 3.8 shows the logarithmic and linear core gradations. Similarly Figure 3.9 and Figure 3.10 show the same for a tension loaded sandwich, and Figure 3.11 and Figure 3.12 show the same for a moment load case.

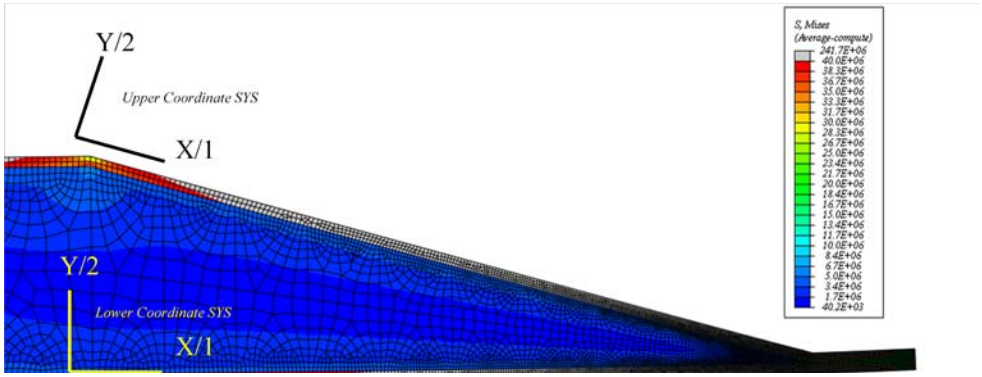

Figure 3.6. Coordinate system orientations for upper and lower core region.

With a constant elastic modulus in the core region throughout the ramp under a transverse load (Figure 3.7, top) the upper core peel stress (S22) have a value of around 2 MPa near the start of the ramp which reduced to 1 MPa near the tip. In comparison with the other core grading, the core stresses were the lowest for the constant core modulus design. However, the core material has constant strength and therefore an increased stress locally which could indicate failure initiation at that location.

In the exponential, logarithmic, or linear graded cores, the peak component stresses reach much higher values than in the constant core case. The max shear stress was higher at the core-facesheet interface by as much as 5 times in the exponentially graded upper core shear stress. We see this at X equal 0.9 **(**Figure 3.7, bottom). Also note the discontinuities with the graded cores at multiples of X equal 0.1 due to the discrete material transitions. A continuously graded core material in the X direction would likely further reduce these stress variations. However, the results from the discrete designs are still useful to understand how interface stresses are affected by the material gradation in the rampdown region.

Figure 3.9 and Figure 3.10 present the interface stresses for the four designs under an axial load. The stresses overall are much smaller than the transverse load of the same magnitude (10kN) because more of the load is taken by the facesheets.

Due to the geometry of the model, and the location of the load application as shown in Figure 3.1, the shear stresses in the lower core facesheet interface in the tension case will inevitably be higher than the upper core facesheet interface.

In addition to the transverse and tension loading conditions, a pure moment case where 24 N·m is applied is also studied. This negates the asymmetrical geometry in the

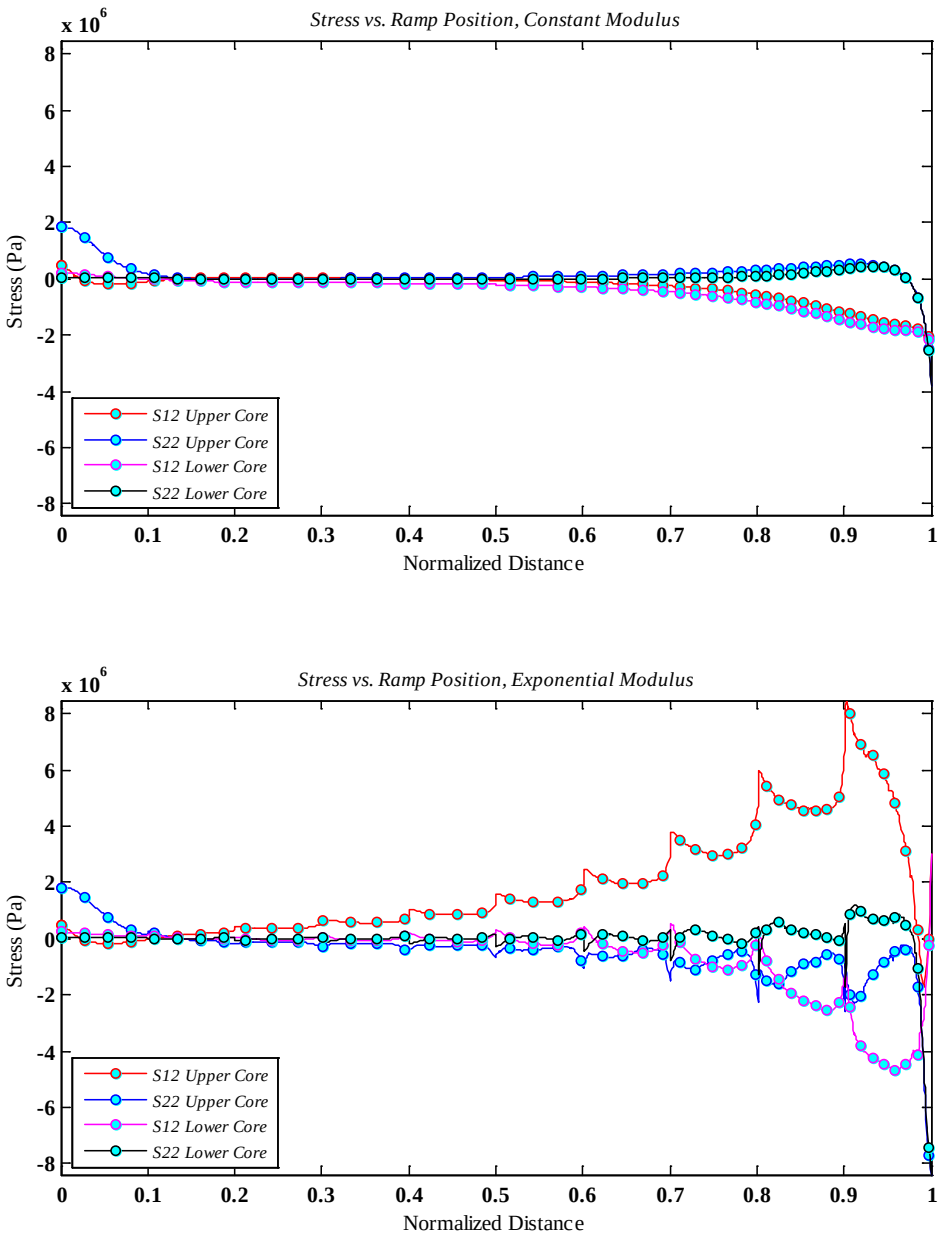

Figure 3.7. Ramp component stresses of transverse loaded model at facesheet-core interface, constant and exponential core grading.

model as the cause of any stress resultant variation. The interface stresses due to a tip moment load is shown in Figure 3.11 and Figure 3.12. Similar to the tension case the stresses are on the order of tenths of MPa. In the moment case the peak stresses are much closer to the tip (X equal 1) than in the preceding cases. In this case the core grading because upper and lower core stresses which are only 2 times (1.6 MPa to 0.8 MPa) compared to the non- graded case. Again it must be emphasized that despite these much

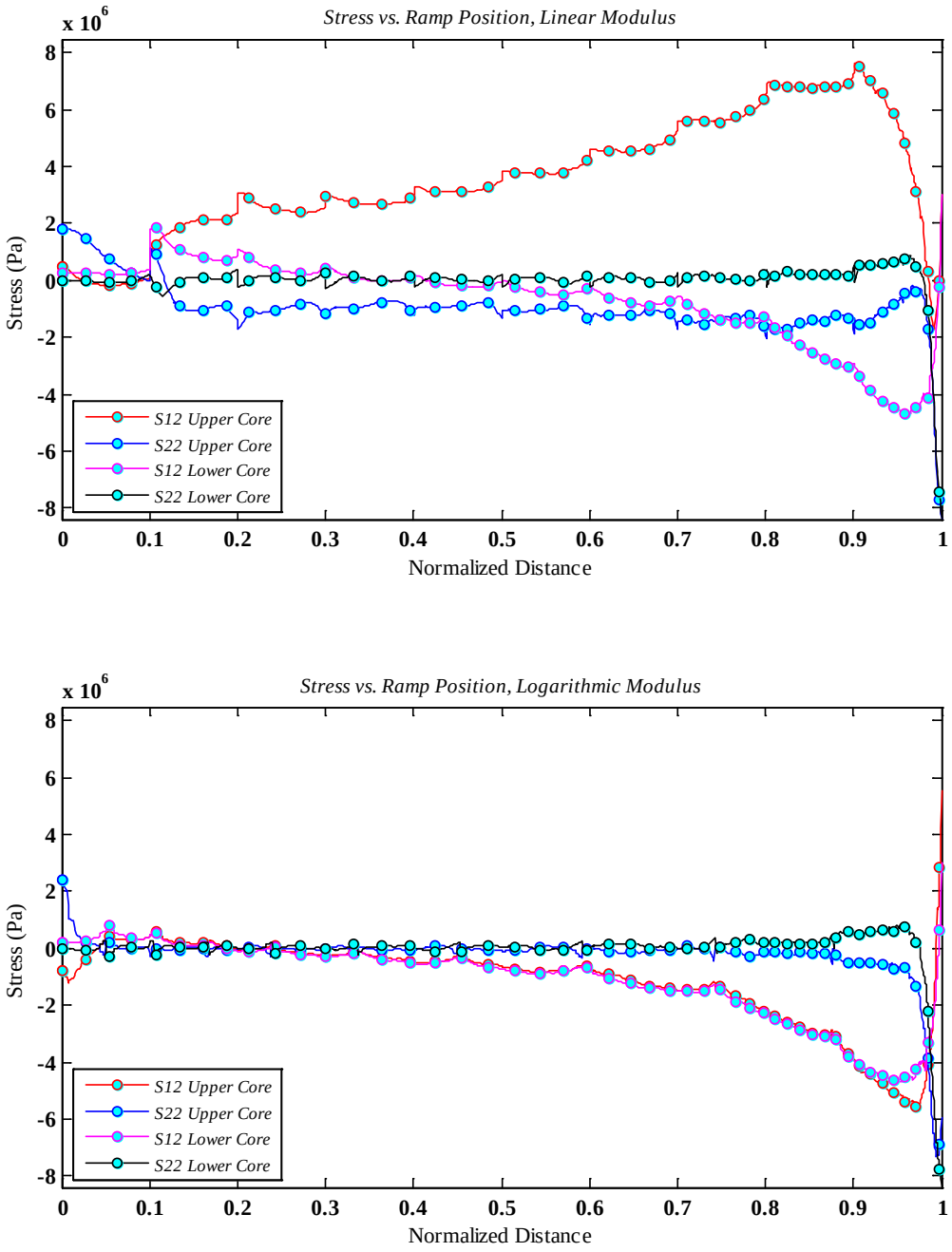

Figure 3.8. Ramp component stresses of transverse loaded model at facesheet-core interface, linear and logarithmic core grading.

higher stresses in the core, the location and material must be considered. Keep in mind that where these new higher peak stresses are occurring is where the material would be much stronger in than in the non-graded case. Neither core material nor the material strength is strictly identified; only the elastic modulus is specified. However in each of the core graded

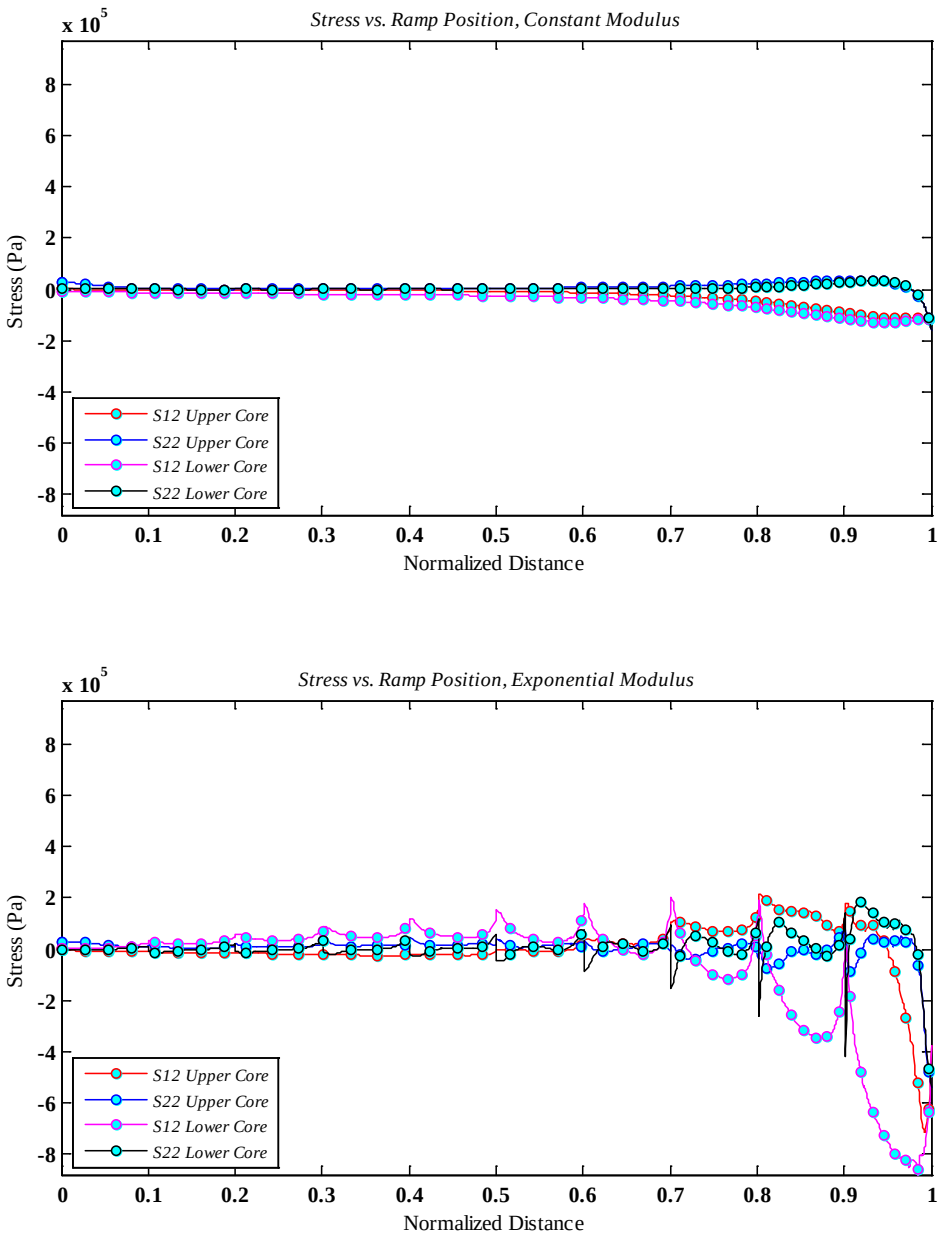

Figure 3.9. Ramp component stresses of tension loaded model at facesheet-core interface, constant and exponential core grading.

cases the elastic modulus at section 10 (between X equal 0.9 and 1.0) is the same as that of the non-graded case.

Figure 3.13 and Figure 3.14 shows the positive impact of the coregrading on the stress at the facesheet junction (X equal 1) of the sandwich model. In the constant graded core case (Figure 3.1.3, top) there are extremely high von mises stresses in the lower facesheet at X equal 0 and in the upper facesheet at X equal 1. These are mainly due to the

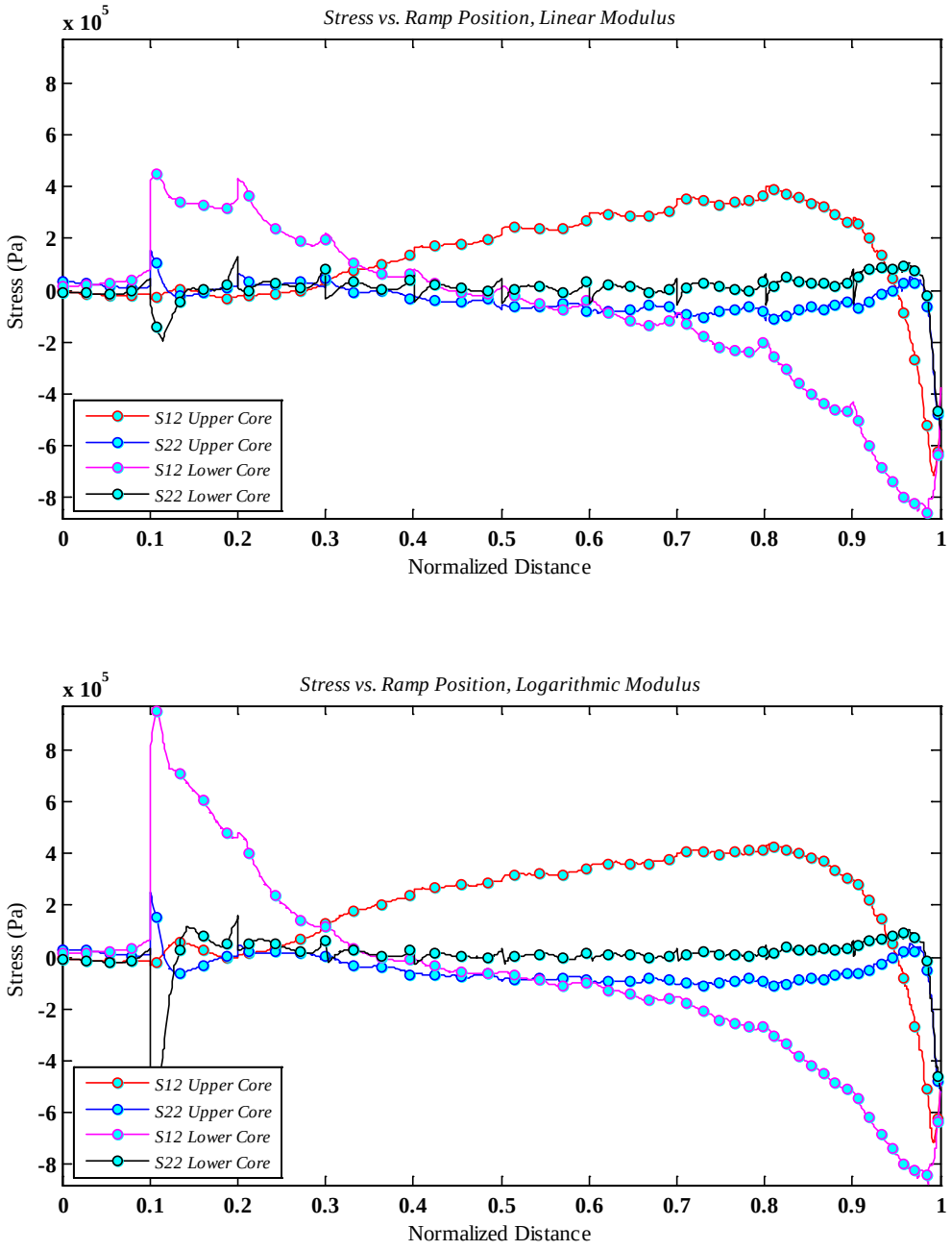

Figure 3.10. Ramp component stresses of tension loaded model at facesheet-core interface, linear and logarithmic core grading.

compression in the upper facesheet and tension in the lower facesheet and are on the order of 30 MPa. In any of the subsequent cases which all have core grading, the stress concentration in the facesheets at both ends (X equal zero and X equal 1) is reduced by 6 times, to around 5 MPa. Also important to note is that the gradient of stress as one approaches the point where the facesheets join (X equal 1) is significantly reduced, and for even the worst case of core

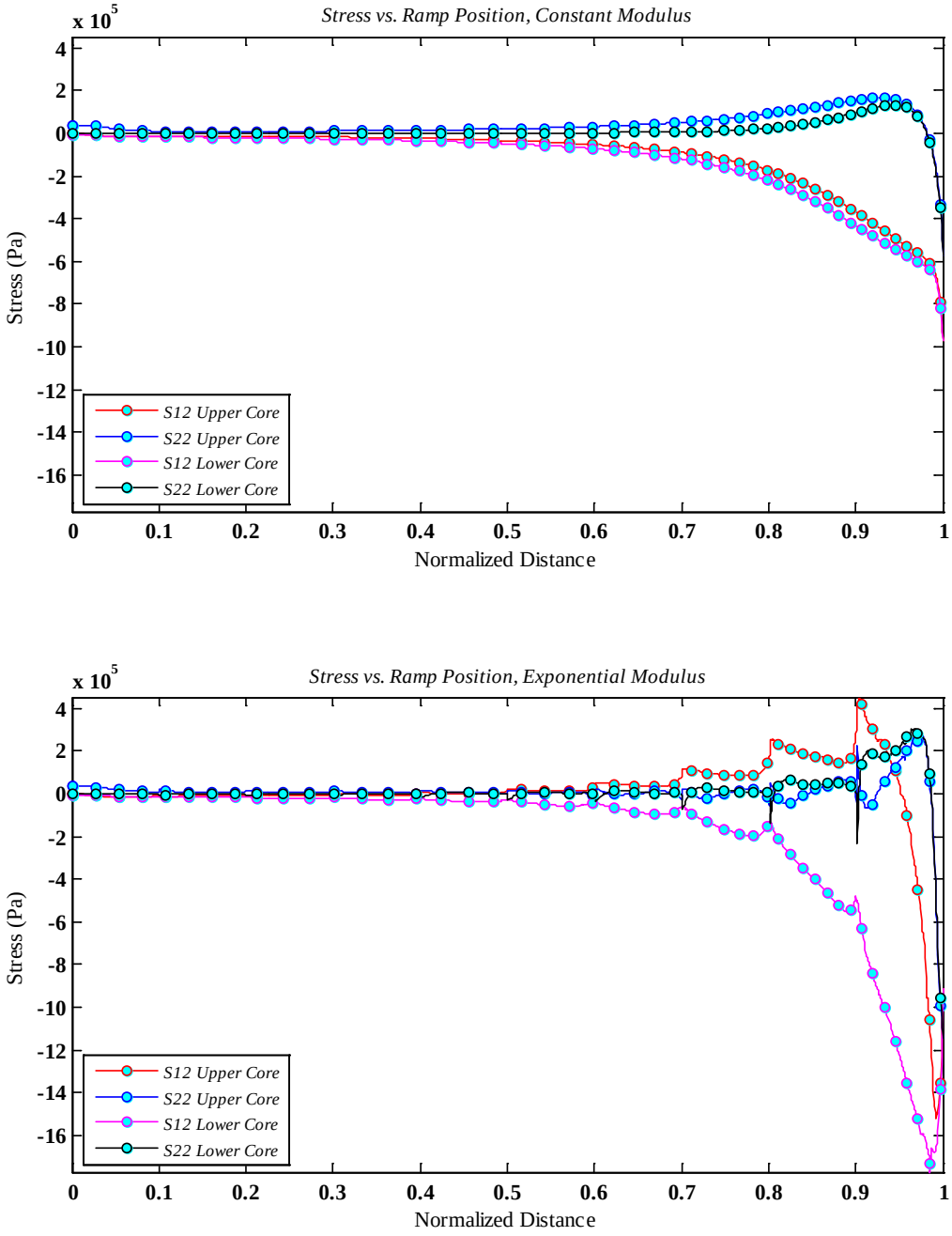

Figure 3.11. Ramp component stresses of moment loaded model at facesheet-core interface, constant and exponential core grading.

gradation (linear elastic modulus case in Figure 3.14,top) where the stress nearing the facesheet junction is nearly made to be zero. This is the advantage of having a functionally graded core and this stress mitigation occurs primarily due to the matching of material between the core and facesheet at the facesheet junction.

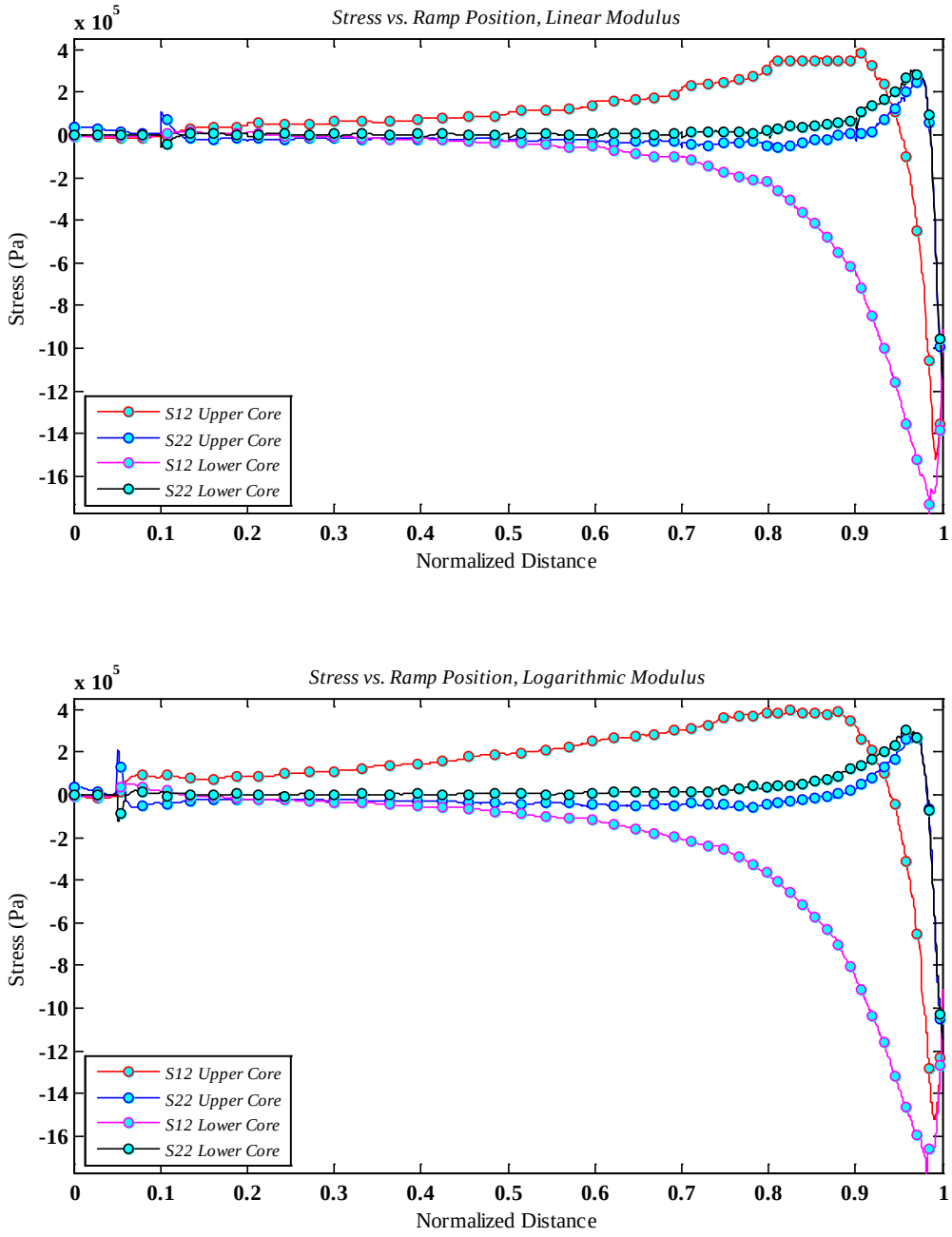

Figure 3.12. Ramp component stresses of moment loaded model at facesheet-core interface, constant and exponential core grading.

Even though the core stresses increase by a factor of 2 by grading the core in the moment loading case, the material strength would potentially increase by a factor of 100. This would have a significant effect on reducing the stress gradient between the core and facesheets. In this effort, this is not further investigated. This is simply shown for emphasis that the functionally grading the core is beneficial in the design of sandwich beams. Clearly

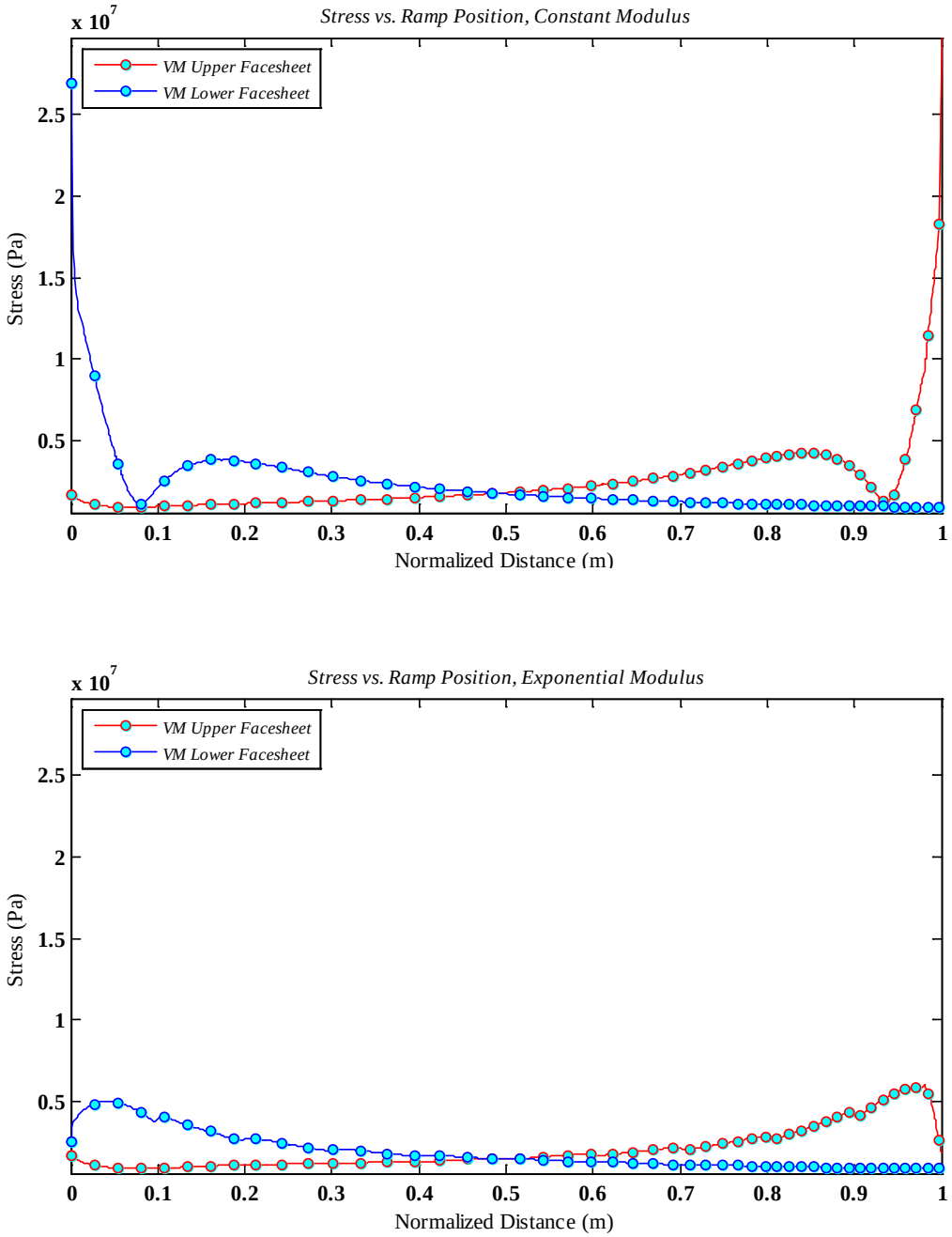

Figure 3.13. Ramp von mises stresses of moment loaded model at facesheet-core interface, constant and exponential core grading.

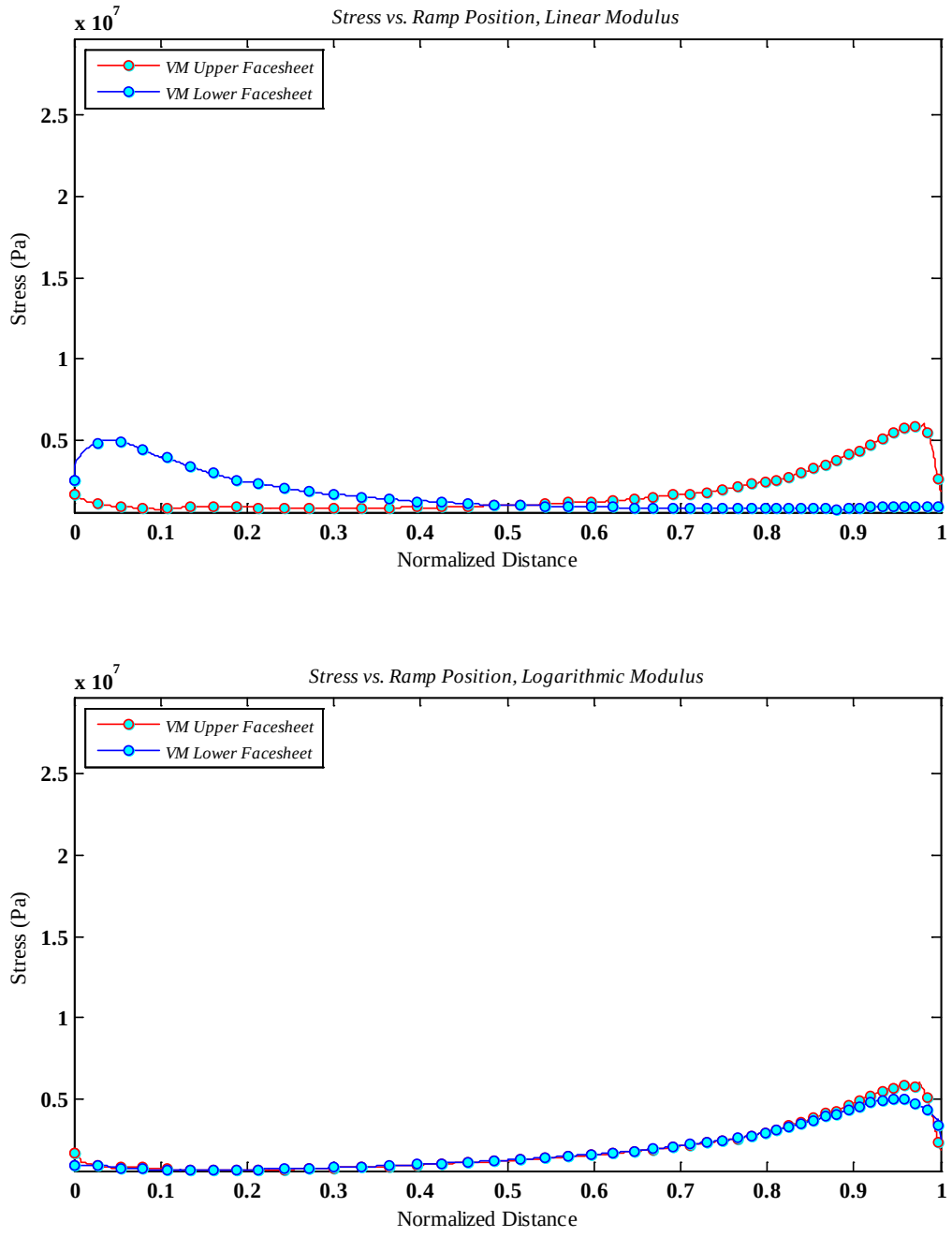

Figure 3.14. Ramp von mises stresses of moment loaded model, linear and logarithmic core grading.

this is the case from the above result, however the true question lies in whether or not this type of grading can be accomplished with a commercially available and already in use material. For that we turn to honeycomb core.

Anisotropic honeycomb cores, aluminum in particular, can be deformed from the standard density into a desired one, but more work must be done to determine whether or not and how graded honeycombs can be fabricated.

CHAPTER 4

FINITE ELEMENT MODELING OF IN-PLANE CRUSHING OF METALLIC HONEYCOMBS

A generic two dimensional cellular structure is a high volume, lightweight, unified material made up of solid faces that are extended in one dimension, but vary in the other two dimensions. The word "cell" comes from the Latin *cella*: A small compartment, an enclosed space [56]. Figure 4.1 [56] presents several types and geometries of cellular structures used as sandwich core material.

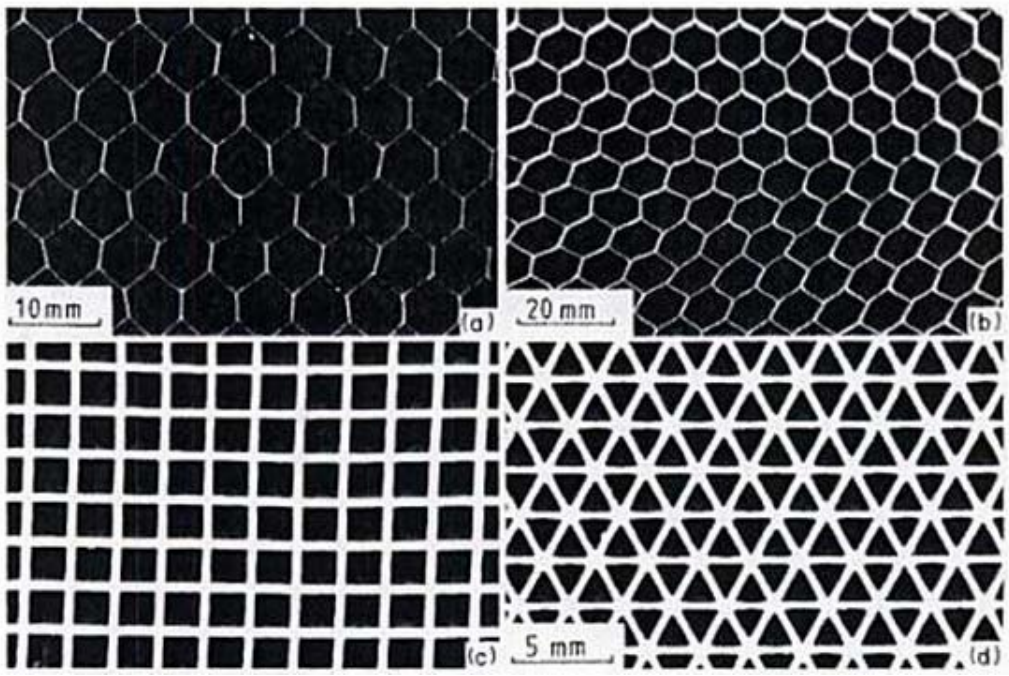

Figure 4.1. Several types of 2D cellular structures, (a) Hexagonal Aluminum, (b) hexagonal paper-phenolic, (c) square ceramic, (d) triangular ceramic. Source: Gibson, L. J., and Ashby, M. F., *Cellular Solids: Structure and Properties*, Pergamon Press, Oxford, 1988.

Foams, honeycombs, cellular solids, and other aerospace structural materials can be used to improve the stiffness to weight performance, impact energy absorption and heat transfer in aircraft and launch vehicles. In many structural applications, honeycombs are used to increase the moment of inertia of beam and plate structures in order to withstand

shear loading due to bending, but incur the smallest weight penalty possible. Functionally graded materials (FGM) are materials which can have unique properties such as thermal, acoustic, electrical, or structural characteristics that vary over a specified dimension of the material. In this work an FGM material is shown to have structural benefit in the case of rampdown sandwiches. However with regular repeating patterns for honeycombs as seen in Figure 4.1 it is difficult to tailor the material such that its overall density and material properties differ in a single dimension.

Honeycombs as pictured above have a regular repeating pattern. However, foam type materials exhibit irregular Voronoi cell patterns (Figure 4.2 [56]). Computer simulations using Voronoi patterns have been shown to reproduce the behavior of closed cell foams [57]. Biner [58] used Voronoi cells to investigate functionally graded materials, as did Ajdari [18] by gradually changing the relative density in one direction. However, manufacturing such functionally graded foam to specified density has not been reported.

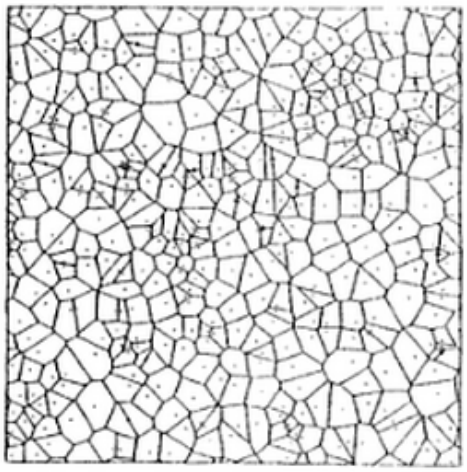

Figure 4.2. Voronoi structure. Source: Gibson, L. J., and Ashby, M. F., *Cellular Solids: Structure and Properties*, Pergamon Press, Oxford, 1988.

In this work we investigate methods to densify aluminum hexagonal honeycomb material which is commercially available to achieve a material property gradation for use in the rampdown region of sandwich structures.

4.1 Mechanical Behavior of Hexagonal Honeycombs and Rampdown Sandwiches

Commercial honeycomb in this work is loaded in-plane only and therefore this type of mechanical behavior is studied here. This refers to the L direction in Figure 2.6.

4.1.1 Honeycomb Uniform In-plane Mechanical Behavior, Linear Elastic

When hexagonal regular aluminum cellular honeycombs are loaded in-plane in the *y*-direction, they exhibit first linear elastic response, then after a certain strain value the honeycomb cells experience buckling. Buckling leads to plastic deformation after which the cell begins to densify and stiffen dramatically. The elastic response of the honeycomb can be described using simple analytical models [59].

When under a uniform in-plane load, as shown in Figure 4.3, the cellular structure can be treated as if the side walls are perfectly vertical columns with minimal deformation (only translation) and the inclined walls act as cantilever beams with the components and parameters shown in Figure 4.3. The force F_x is equal to zero (crushing acts only in y direction) and F_y can be calculated as:

$$F_y = d\sigma_y l \cos\theta \tag{4.1}$$

here d is the out of plane cell depth, taken for this and all subsequent cases as one unit. Using this force one can calculate the associated moment acting on the inclined cell wall that produces zero net force in the transverse direction to be:

$$M = \frac{F_y l \cos\theta}{2} \tag{4.2}$$

Using the above calculated force and moment the deflection of the cell wall δ, assuming a linearly elastic Euler-Bernoulli beam model is calculated as:

$$\delta = \frac{F_y l^3 \cos\theta}{12 E_s I} \tag{4.3}$$

where E_s is the material elastic modulus of the cell wall and I is the area moment of inertia ($dt^3/12$). Then, global strain is found by taking the vertical component of the deflection δ divided by the original height of the vertical column (h) added to the height component of the inclined cell wall ($l\sin\theta$):

$$\varepsilon_y = \frac{\delta \cos\theta}{h + l \sin\theta} \tag{4.4}$$

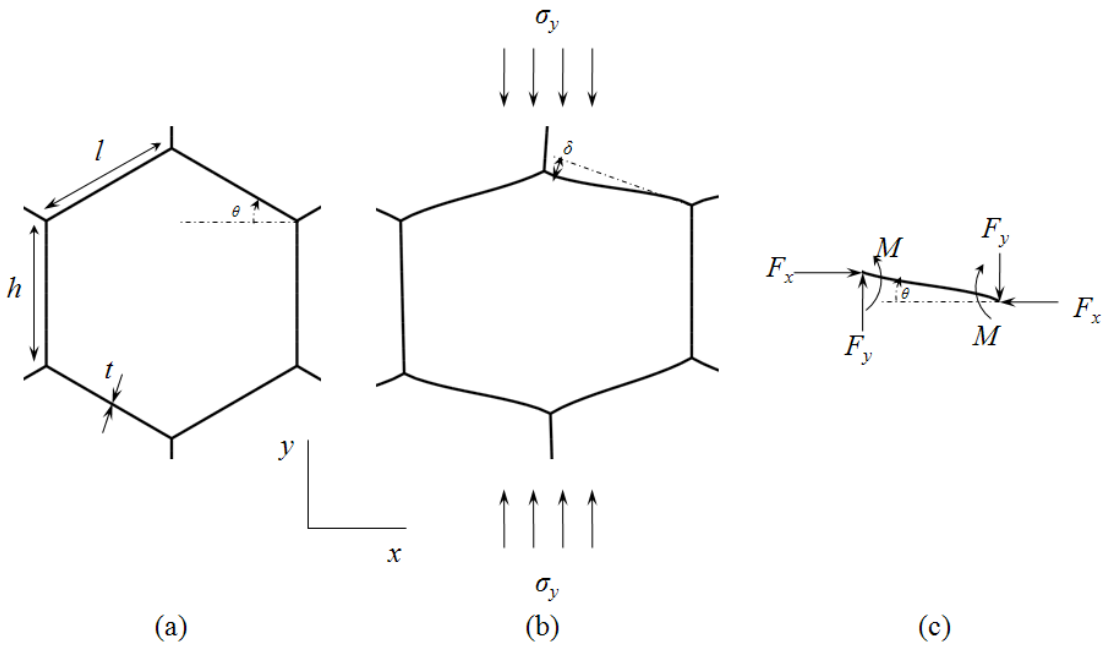

Figure 4.3. In-plane linear elastic regime of honeycomb deformation, (a) undeformed honeycomb cell (b) cell under uniform load, (c) inclined cell wall free body diagram.

Since we know the stress σ_y the value of $E_y = \sigma_y/\varepsilon_y$ can be computed and leads to the expression for E_y/E_s as follows:

$$\frac{E_y}{E_s} = \frac{t^3(\frac{h}{l}+\sin\theta)}{l^3(\cos^3\theta)} \tag{4.5}$$

The E_y/E_s gives a dimensionless ratio of the elastic modulus of the honeycomb to the elastic modulus of the material that comprises the honeycomb cell walls. In this work, θ will always equal 30^o, and h is equal to l, therefore equation 4.5 reduces to:

$$\frac{E_y}{E_s} = \frac{t^3}{l^3}2.309 \tag{4.6}$$

4.1.2 Honeycomb Uniform In-plane Mechanical Behavior, Euler Buckling

The vertical walls of the honeycomb begin to buckle like columns once past a critical load P_{cr}. From classical column buckling theory [60] pioneered by Leonhard Euler in the 1700s we can determine this.

The pinned ended column in Figure 4.4 shows how the vertical members of the hexagonal honeycomb can be represented as they begin to buckle under the deformation

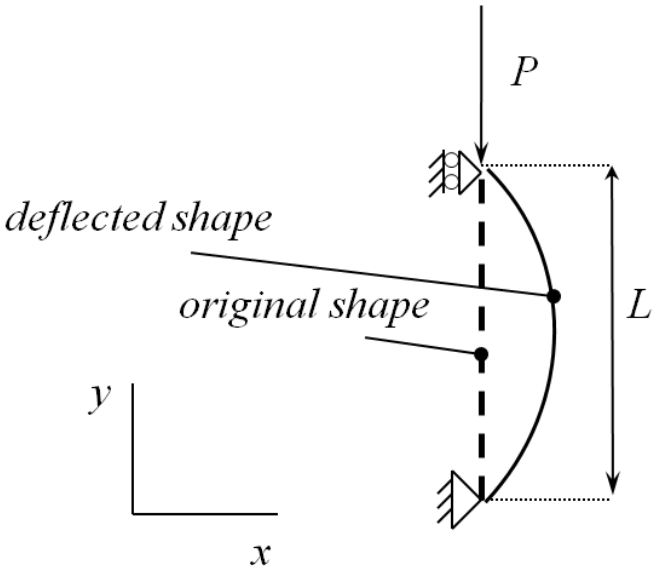

Figure 4.4. Pinned ended column represents vertical members of the hexagonal honeycomb for buckling.

shown in Figure 4.3. The displacement in the *x*-direction can be represented by a second order linear homogeneous differential equation with constant coefficients as:

$$\frac{d^2x}{dy^2} + \sqrt{P/E_sI}\frac{dx}{dy} = 0 \tag{4.7}$$

Where P is the load, where E_s and I have been discussed previously. The general solution is of the form

$$x = A\sin(y\sqrt{P/E_sI}) + B\cos(y\sqrt{P/E_sI}) \tag{4.8}$$

The boundary conditions are x(0) = 0, x(L) = 0, which yields B = 0 and therefore to obtain a non-trivial solution

$$\sin(L\sqrt{P/E_sI}) = 0 \text{ or } L\sqrt{P/E_sI} = n\pi, n = 1,2,3 \ldots \tag{4.9}$$

If we solve for P, we then obtain:

$$P = \frac{n^2\pi^2EI}{L^2} \tag{4.10}$$

The critical buckling load for the classical case is the smallest value of P which corresponds to the smallest value of n (n=1), or

$$P_{cr} = \frac{\pi^2EI}{L^2} \tag{4.11}$$

The value of n is related however in the real case of a hexagonal honeycomb to the degree to which the pinned end is elastically restrained (i.e. the boundary condition at the pinned end).

The value determined for regular hexagonal cells by [56] is n=0.69 in the case where h=l for the cell walls. The buckling load is highly sensitive to imperfections in the cell geometry and thus only represents an approximate critical load.

4.1.3 Honeycomb Uniform In-plane Mechanical Behavior, Plasticity

After the critical load is reached, the deformation and plastic yielding characteristics are shown in [39] to depend on the rotation φ (Figure 4.5). The dot-dash lines in the figure represent the original (undeformed) geometry of the cell.

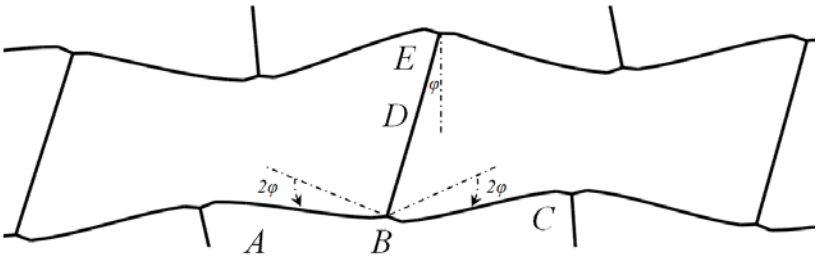

Figure 4.5. Plastic regime deformation of a honeycomb cell during uniform in-plane loading, characterized by angle φ.

Plastic displacements in the model will be looked at it more detail later in this work with a finite element model using beam elements to represent the cell wall structures.

4.2 5X6 HONEYCOMB CORE UNIFORM CRUSHING FINITE ELEMENT MODEL TO SIMULATE CRUSHING OF A METALLIC HONEYCOMB CORE

One objective of this research is to show that it is possible to functionally grade commercially available aluminum honeycomb material to increase its stiffness and interface fracture toughness when used in sandwich structures at rampdown facesheet junctions. Based on literature research conducted prior to the modeling and subsequent experimentation especially in [52], Atli-Veltin and Gandhi's work, ABAQUS™ finite element software was chosen to perform the simulations. This was because the crushing of honeycomb cores requires a software package that can accommodate large plastic deformations and non-linear analysis as well as the contact conditions required. Since ABAQUS had been used successfully [52], it was decided to first try to replicate the results available to develop confidence in the model set up and analysis parameters.

4.2.1 Finite Element Model Geometry

A multi-cellular core was selected for uniform in-plane crushing in order to validate the model using densification results [4, 52, and 53] that exist in literature. Once a validated core model is available, it can be used for studying other in-plane densification methods. Figure 4.6 shows the various geometric parameters needed to describe cell geometry. For this study, a 1 square meter of sample was procured from Hexcel Composites [61] and thus the geometry for this specific type of honeycomb was used in the model so that it may be validated during future physical testing. The *x*- and *y*- axis shown above correspond to global coordinates of the finite element model. The geometric parameters (Figure 4.6 [52]) for the honeycomb studied here are given in Table 4.1.

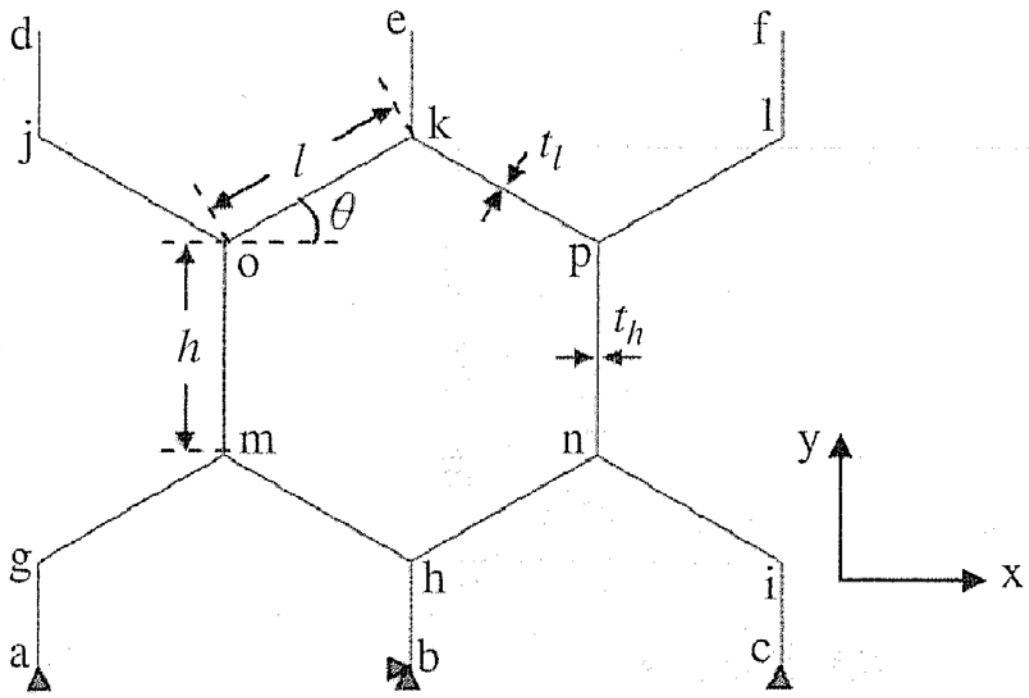

Figure 4.6. Typical parameters for a single honeycomb cell. Source: Atli-Veltin, B., and Gandhi, F., "Effect of Cell Geometry on Energy Absorption of Honeycombs Under In-Plane Compression," *AIAA Journal*, Vol. 48, No. 2, February 2010, pp. 466-478.

The values of the honeycomb core geometry shown in Table 4.1 correspond to an expanded sheet of Hexcel Composites Aluminum 5052-H39 Hexweb [61] has a 0.125 inch cell size and a foil thickness of 0.0015 inches. Each cell has walls which are the same height

Table 4.1. Honeycomb Physical Geometry Values for the Current Validation Study

Honeycomb Parameters	*Value*	*Description*
h	1.833×10^{-3} m	height of cell wall
l	1.833×10^{-3} m	length of cell wall
Θ	30^{o}	angle of inclined cell wall
t_l	3.81×10^{-5}m	inclined cell wall thickness
t_h	7.62×10^{-5}m	vertical cell wall thickness

and length, with the inclined sections at 30^{o} inclination with respect to the *x*-axis in Figure 4.7. The double wall thickness in the "ribbon" direction (*y*-direction above) is because strips of foil are adhesively bonded and then expanded to create the honeycomb core structure. This process is also outlined in Figure 2.4. The double thickness of the vertical walls provides an added benefit that the honeycomb has higher in-plane and shear stiffness in this direction. This will have a significant effect on the way the model will deform under uniform in-plane crushing.

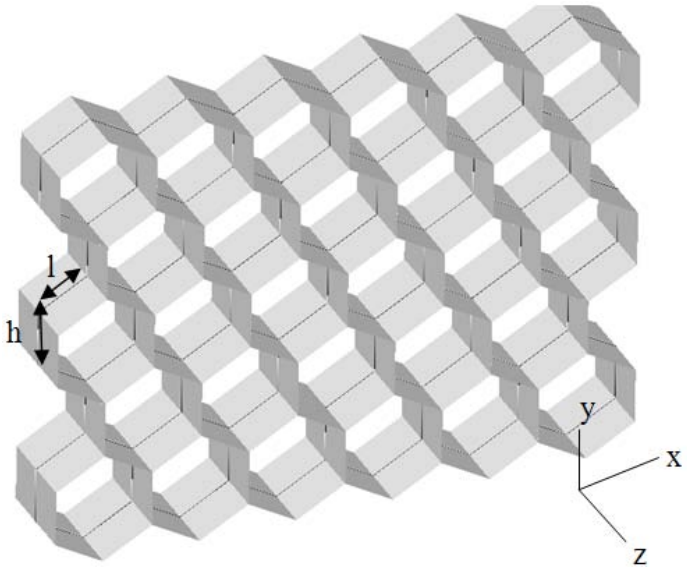

Figure 4.7. A three dimensional rendering of a honeycomb core with associated coordinate system.

4.2.2 Finite Element Model Material Definition

Aluminum alloy 5052, temper H39, is commonly used in aircraft honeycomb applications [62]. The material properties can be found in Table 4.2.

Table 4.2. Aluminum Material Properties

Aluminum5052-H39 Properties	*Value*	*Description*
ρ	2680 kg/m^3	Density
E	68.97GPa	Elastic Modulus
E_y	687.9MPa	Post-Yield Elastic Modulus
σ_y	292MPa	Yield Strength
v	0.33	Poisson Ratio

Aluminum 5052-H39 is a strain hardening material that can be accurately represented by a bi-linear stress-strain curve. Aluminum 5052-H39 bilinear strain hardening material models have been previously used by Papka and Kyriakides[53] and others [52].

Figure 4.8 presents the various equations for stress-strain behavior in the elastic and plastic regimes and correspond to the values shown in Table 4.2. The post-yield modulus was taken in [52] to be 100 times less than the pre-yield modulus based on previous empirically obtained data. Actual plastic strain values used in the ABAQUS/Standard analysis are also tabulated in Table 4.3.

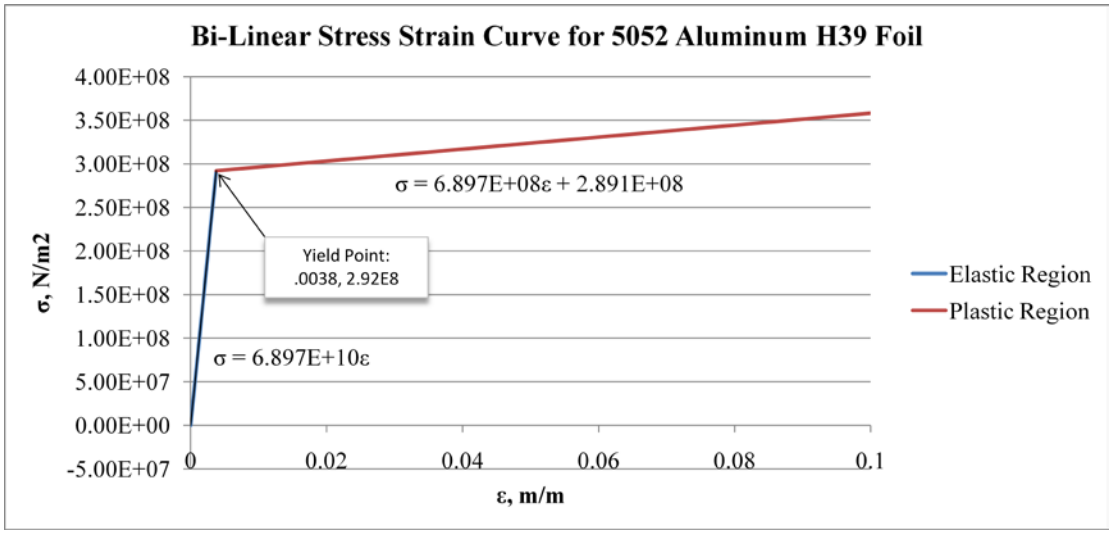

Figure 4.8. Stress Strain curve definition for model.

To properly determine the element type to use in this analysis, a study was conducted to show that a particular beam element would converge and provide an efficient solution when tested under large deformation. A classical test performed in engineering is to subject a cantilever beam to a tip moment and observe that the proper deformations occur under large rotations of the tip node. The beam geometry was kept simple; a square, uniform,

Table 4.3. Actual Values Used in ABAQUS for Material Definition

Stress (Pa)	Plastic Strain
2.92E+08	0
3.61E+08	0.1
4.30E+08	0.2
4.99E+08	0.3
5.68E+08	0.4
6.37E+08	0.5
7.06E+08	0.6
7.74E+08	0.7
8.43E+08	0.8
9.12E+08	0.9
9.81E+08	1

4.2.3 Finite Element Model Plastic Element Investigation

isotropic beam with aspect ratio of 50 (length/width). The exact boundary conditions and load conditions are show below in Figure 4.9. Cantilever beam element (left) with profile rendered and plate element (right) test model setup.

Beam Element Geometry	*Plate Element Geometry*
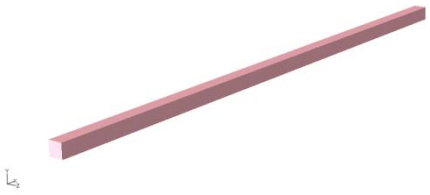	

Figure 4.9. Cantilever beam element (left) with profile rendered and plate element (right) test model setup.

A beam constructed of the same material that would be used in the honeycomb model (Aluminum 5052 H39) was used to construct a simple model, clamped at the root, and a large moment applied at the tip. A dynamic ABAQUS/Standard solution was obtained which converged for a beam modeled as a 2D plate (SR4 quad node), with B21 (2 node linear shear deformable, 6 degrees of freedom) elements, and with B22 (3 node quadratic formulation, 9 DOFs) elements.

The elements chosen to test were each applied to the model, then a tip moment was applied (ramped from zero to $6.5x10^7$ N·m) in ten seconds. Sufficient deformation however occurred after 0.65s, and this is the point in time used for convergence. Inertial effects were ignored, although these would have been equivalent for each model. Each model shown had the same number of DOFs using a varying number of elements in the length direction, an important aspect to consider when comparing convergence. Tip rotation was noted at 0.65s for the different element types. The results are shown in Figure 4.10. All three models agree with one another. When looking at the convergence rate (Table 4.4 and Table 4.5), beam elements perform better. Even after more than ten thousand DOFs, the plate elements did not converge as well as the beam model with only 700 DOFs. Based on convergence testing, beam elements were chosen over plate elements. Because of the small number of DOFs required to converge the model, B21 and B22 elements are possible choices. However due to the large number of contact definitions which are necessary for the honeycomb model and because they are easier to define with ABAQUS if B21 elements are used, B21 elements were selected for the honeycomb uniform in-plane crushing model.

4.2.4 Honeycomb Finite Element Model Assembly and Boundary Conditions

With the proper material definition created, property definitions extending into plastic deformation regime, and also with the proper type of beam elements chosen for the model, the geometry and boundary conditions as well as the mesh convergence were completed for the honeycomb model.

The finite element analysis model was constructed to represent a 5x6 (rows x columns) regular hexagonal honeycomb core using a 2D planar deformable body with a wire base feature, given all the previously defined geometries for honeycomb shape and bilinear material properties for aluminum. Figure 4.11 presents the geometry of the honeycomb core, along with the boundary conditions. Two beam sections and associated rectangular profiles were also defined; one for the vertical walls which have two times the thickness of the inclined walls, and a second section/profile combination was defined for the inclined walls. The mechanical properties for each wall are identical, and it was assumed that the foil comprising the vertical walls are bonded together perfectly (same as [52]). This is a good assumption due to the lower (3 orders of magnitude) stresses which develop in the vertical

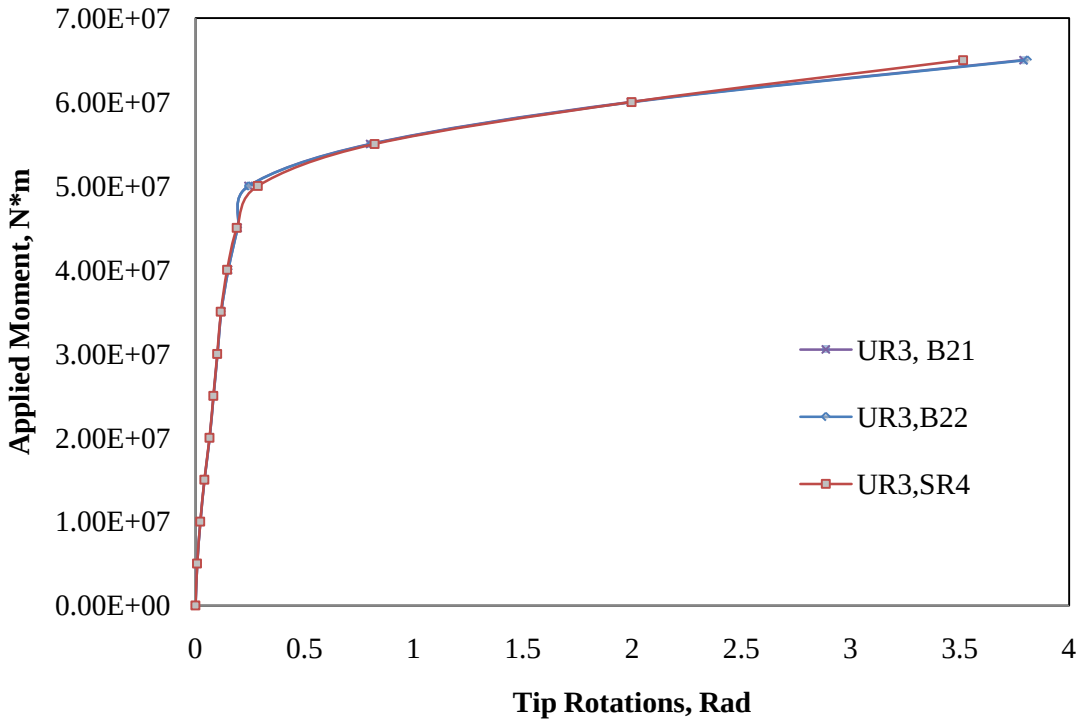

Figure 4.10. Tip rotations on neutral axis of beam vs. applied moment.

Table 4.4. Plate Element Convergence

S4R Elements (Plate Model, w/Symmetry BCs)				
Elements (Length)	***Nodes***	***DOFs***	***End Rotation after 0.65s***	***%Change***
30	62	372	2.70926	
60	183	1098	2.95624	9.12%
120	484	2904	3.60137	21.82%
240	1687	10122	3.87255	7.53%
480	6253	18759	4.12057	6.40%
640	*10897*	*65382*	*4.20826*	*2.13%*

Table 4.5. Beam Element Convergence

B21 Elements (Beam Model)				
Elements	***Nodes***	***DOFs***	***Tip UR3 after 0.65s***	***%Change***
30	31	93	3.47194	n/a
60	61	183	3.8087	9.70%
120	121	363	3.82056	0.31%
240	241	723	3.81495	-0.15%
480	*481*	*1443*	*3.82369*	*0.23%*

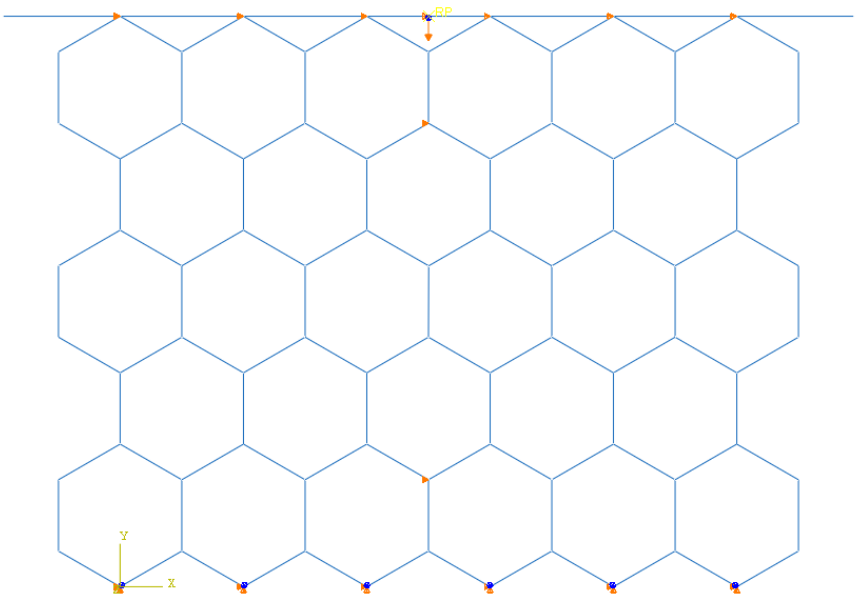

Figure 4.11. Undeformed model with BC shown.

walls during the simulations in comparison to the stresses which develop in the inclined walls at plastic hinge points. The model is converted to plane strain. Unit out of plane thickness of the honeycomb is assumed.

The model was next given a dynamic step, which is meant to simulate a uniform compression loading scenario, where a non-deformable 2D planar rigid body crushes the honeycomb in the negative *y*-direction (see Figure 4.5). This dynamic step runs through 8 seconds, where each 1/10 of a second accounts for 1% global strain, or 1 second is simply 10% strain. Global strain is defined as overall reduction in height (*y*-direction) over the original height of the model.

The duration of the deformation was chosen as the shortest amount of time which would allow for a converging solution, i.e., the stress at a given global strain percentage did not change whether the full deformation occurred over more 8 seconds. This was to ensure that kinetic energy did not contribute to deformation and to ensure a fast solution time. This boundary condition describes the motion of the plane shown in the top of Figure 4.11 in the negative *y*-direction, reducing the honeycomb to 30% of its original height over the duration.

The other boundary conditions chosen were that the 6 nodes at the bottom of the model (Figure 4.11) were fixed in both *x* and *y* degrees of freedom to prevent rigid body motion, while 6 locations at the top were given a no slip boundary condition in the *x* direction against the crush plane. Additionally, two central nodes were fixed in the *x- direction*, one between rows 1 and 2 and another between rows 5 and 6, in order to prevent bending in the transverse direction [53].

So that the model would depart from the linear elastic region of the stress strain curve in a predictable manner, it is beneficial to implement a vertical wall imperfection. It has been shown that the amount of initial imperfection has little effect on the global stress-strain curve during simulation [53] it is only important that it be present. To be consistent with previous work, a 0.2^{o} initial imperfection was used on the central vertical wall in the 3^{rd} row.
It was important to specify contact definitions so that the walls do not penetrate through each other during the crushing simulation. The most common of these is shown in Figure 4.12. An example of a contact definition specified for a cell is shown in row 1, column 6. This definition was prescribed to each cell in the model to ensure that the upper right hand part of each cell deforms in the negative *y*-direction until finally contacting the lower left portion of the cell (30 conditions). In some cases, adjacent walls would contact each other, so additional contact conditions were added (like those shown in the lower left of Figure 4.12. Contact definitions were added iteratively by viewing the model deform until contact was made. If the elements protruded through one another an appropriate contact definition was assigned. In total, 42 conditions were assigned which included the contact of the crushing plane and the top most cells.

Each contact definition was modeled with a pressure overclosure modification, as was done previously [53]. This modification allows pressure on the cell walls to increase exponentially as they near each other later (0.3-0.4 global strain) in the deformation. This

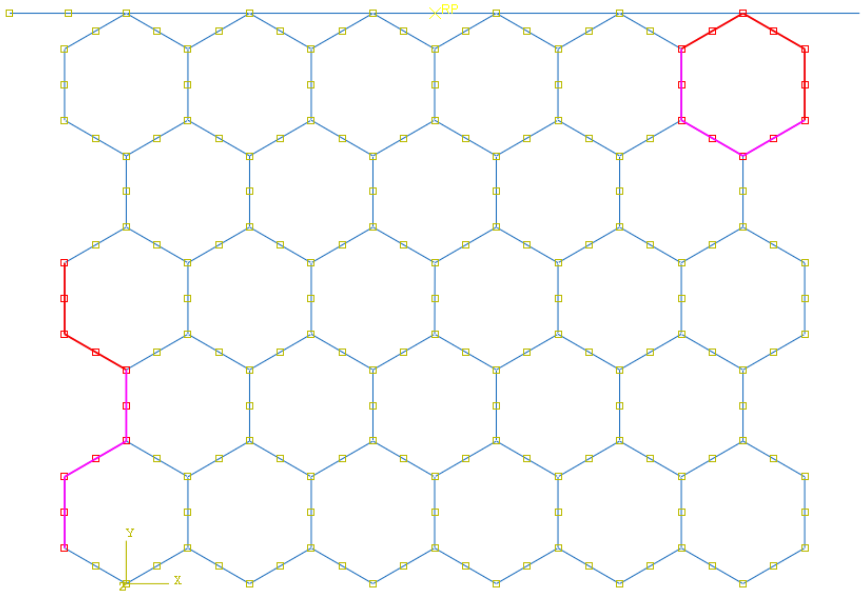

Figure 4.12. Example of contact conditions imposed on the honeycomb model, red nodes cannot penetrate magenta nodes.

also makes a much less noisy final stress-strain curve when compared to a simple friction contact condition, where the cell walls are free to stick to each other and rub, then become free, and repeat. This is shown in Figure 4.13.

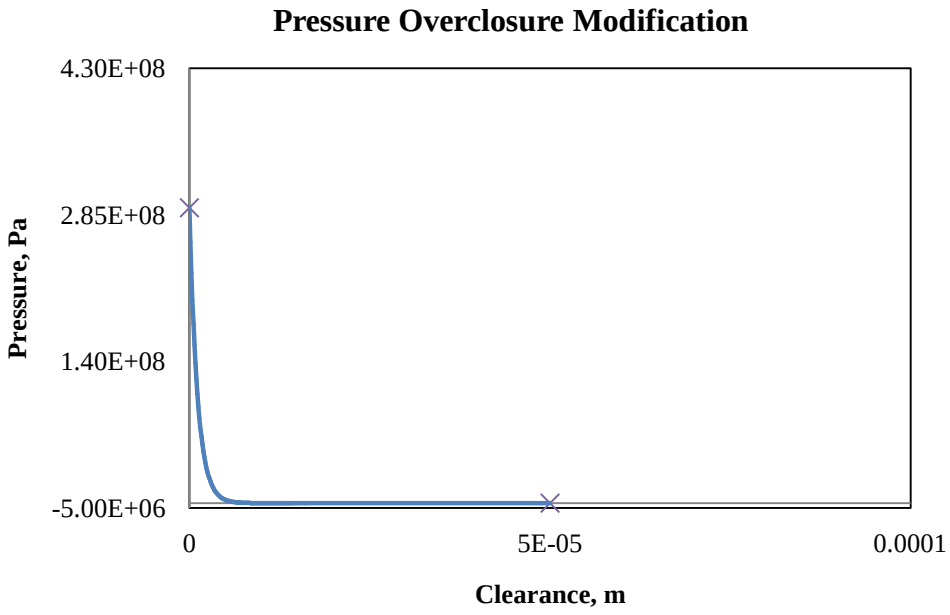

Figure 4.13. Exponential pressure overclosure.

4.3 Finite Element Model: Model Convergence Study

Several different models with a different numbers of elements were run through a convergence analysis at three different points: One at 5% (linearly elastic region), one at 10% (knee region) and one at 50% (densification region), solving for global stress versus these strain values. It was shown that although the vertical walls have much lower stresses thus requiring fewer elements than the inclined walls, it was unnecessary to assemble the model this way for satisfactory results. First, 2, 3 and then 6 B21 elements were assigned to each wall both vertical, and inclined each of which had a simple frictional contact condition. Next, 4 elements were assigned to the vertical walls, and 24 elements were assigned to the inclined walls. This was done in accordance with [52]. This seemed to converge well, but only provided a 1.28% difference when compared to an evenly distributed 12 elements per wall model (last in Table 4.6). Since the evenly distributed model with 12 elements per wall length had 1118 less DOFs than the 4x24xB21 model, but only a 1% difference in solution, it was chosen in favor of a shorter solution time. This gave an overall beam element length of $2.8x10^{-4}$m.

Table 4.6 Convergence of 5x6 Hexagonal Cell Model, Model in Italics & Underlined, Selected

Convergence Study 5x6 Core							
Model Type	***DOF***	***Stress(Pa) at X% Strain***					
		5%	***% Δ***	***20%***	***% Δ***	***50%***	***% Δ***
2xB21	552	4.22E+06		4.50E+06		7.46E+06	
3xB21	867	3.60E+06	14.69%	3.47E+06	22.89%	5.53E+06	25.87%
6xB21	2127	3.22E+06	10.56%	3.17E+06	8.65%	3.39E+06	38.70%
4x24xB21 (pressOver)	5502	3.13E+06	2.80%	3.23E+06	1.89%	3.65E+06	5.49%
12xB21 (pressOver)	*4384*	*3.09E+06*	*1.28%*	*3.17E+06*	*1.86%*	*3.46E+06*	*5.21%*

4.4 Finite Element Model Validation: A Qualitative Comparison of Deformation and Stress-Strain

It is important to show that the current model simulations match those of previous work. This validates our finite element model and can therefore be used to study alternate methods of core crushing. To do this, the current model simulations are compared in both a

quantitative and qualitative fashion by comparing both the deformation patterns and stress curves over various values of strain.

The current simulation provides nearly the identical stress-strain curve shapes as previously published studies [52, 53, and 63].

Despite the difference in number of cells (5x6 cells in our study vs. 9x6 cells in the work of Papka and Kyriakides [53]), the state of deformation are found to be very similar at different global strains (Figure 4.14 and Figure 4.15 [53]), from 0% on to 70%. As soon as the central vertical wall bifurcates in the clockwise direction (about 13% strain) due to the prescribed 0.2^o imperfection in that region, the entire central region collapses with the vertical walls remaining virtually un-deformed except for overall translation. Then inclined walls hinge near the point where they join with the vertical walls. This is more apparent when visualized in Figure 4.16.

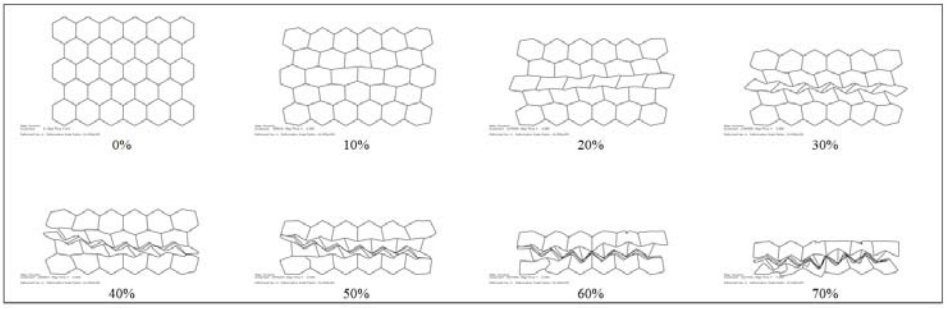

Figure 4.14. Current simulations of regular 5x6 cell honeycomb core.

4.5 FINITE ELEMENT MODEL VALIDATION: A DATA COMPARISON

It is also important to compare the stress-strain curve shapes and ensure that the model is converged. Both of these goals are accomplished in Figure 4.17. Stress was calculated by measuring the reaction forces in the bottom nodes at the fixed boundary conditions (labeled in Figure 4.11), summing them, and dividing by the effective area. The effective area is simply the area of honeycomb core contacting the support which in this case was the out of plane depth (one) multiplied by the vertical wall thickness t_l, multiplied by the number of cells contacting the support (six), yielding an effective area of $0.0004572m^2$. This is seen in equation 4.12).

$$A_{eff} = (unit\ depth)\ t_l(\#\ of\ cells\ at\ contact) \tag{4.12}$$

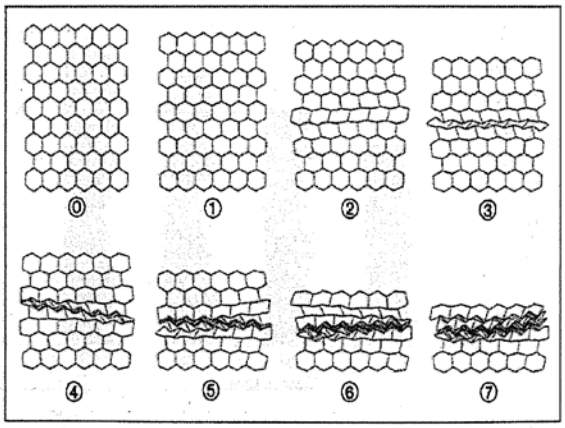

Figure 4.15. Papka and Kyriakides's results for 9x6, 1994. Source: Papka, S. D., and Kyriakides, S., "In-Plane, Compressive Response and Crushing of Honeycomb," *Journal of Mechanics and Physics of Solids*, Vol. 42, No. 10, 1994, pp.1499-1532.

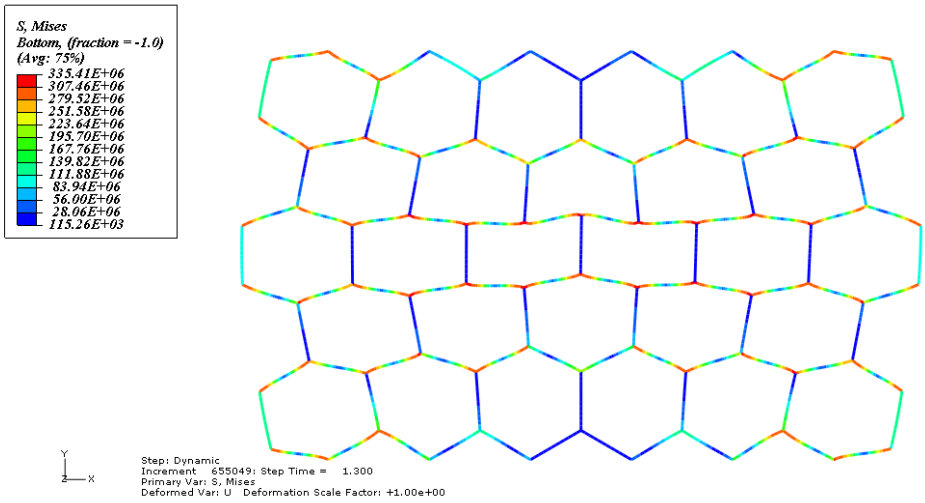

Figure 4.16. Contour, Von Mises stresses large near "hinging" (red) points, 13% strain.

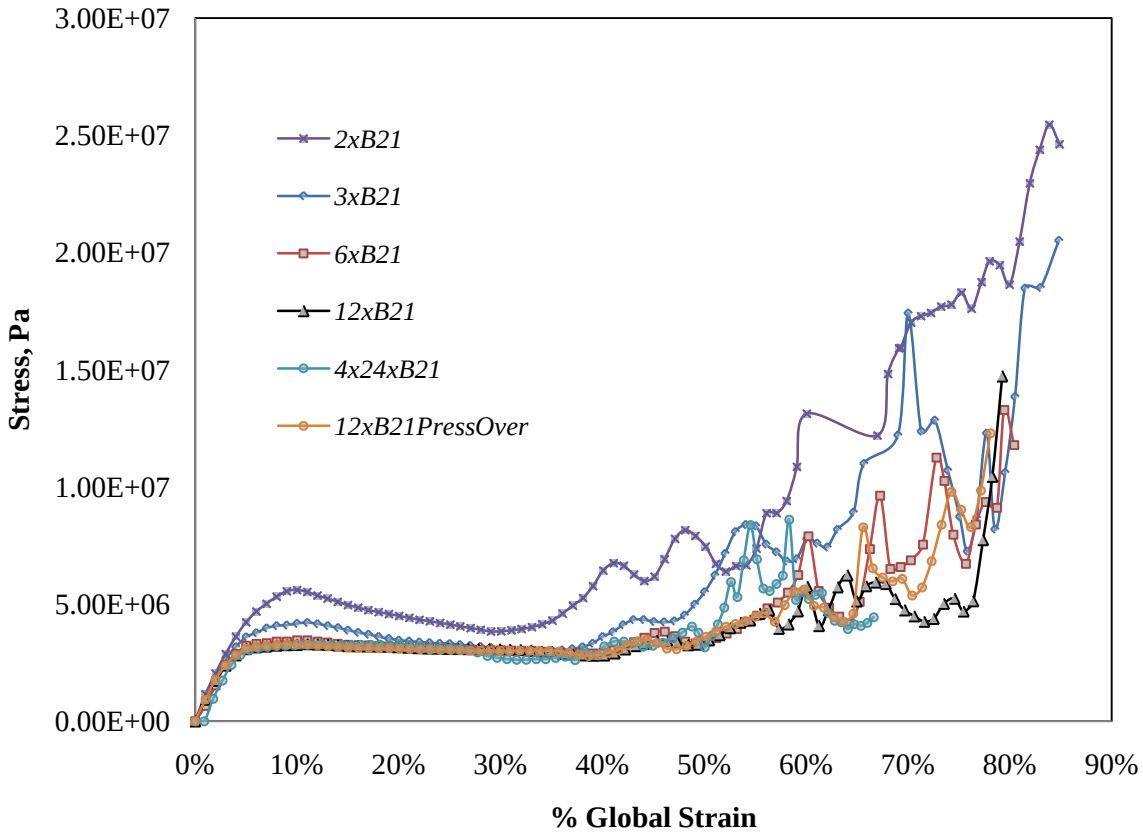

Figure 4.17. Stress-strain curve from current simulations on 5x6 honeycomb core, showing various meshes and pressure overclosure modification effect.

Comparing this with Figure 4.18 [4] shows that the magnitudes of the stresses are quite different due to the cell geometry differences (compare dimensions in Figure 4.19 [52] to those of current simulations in Table 4.1). Also note that [52] used a single cell to understand the stress-strain relationship of the entire core, whereas Figure 4.17 represents a 5x6 core of cells. This is evident during the densification phase when contact is made (40-50% in the converged pressure overclosure model in Figure 4.17). Due to multiple, separate contacts over the course of the deformation, the stress will jump slightly when a contact is made. The pressure overclosure modification mitigates this slightly, but when compared to a single cell, a multi-cell core will always have a more noisy stress strain curve after densification.

Qualitative comparison of the result from this study with [4] for a 5x6 honeycomb cell model shows excellent agreement (Figure 4.18). Quantitatively the results vary due to the different cell sizes between the model in this work versus the model in [4], but key aspects are intact,

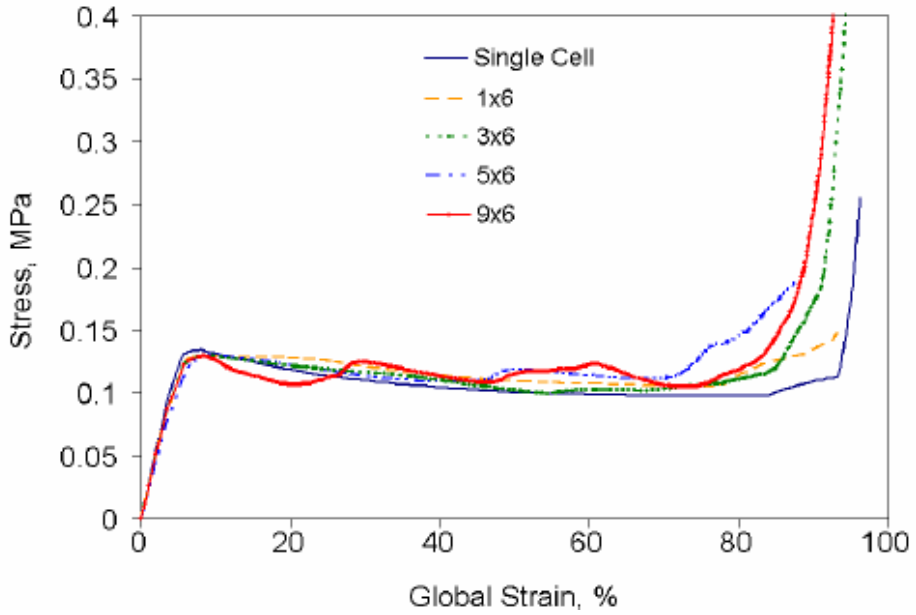

Figure 4.18. Stress curves for uniform in-plane crushing of honeycomb cells obtained from the work of Atli-Veltin. Source: Atli-Veltin, B., "Effect of Geometric Parameters on the In-Plane Crushing Behavior of Honeycombs and Honeycombs with Facesheets," Ph.D. Dissertation, Dept. of Aerospace Engineering, Pennsylvania State Univ., University Park, PA, 2009.

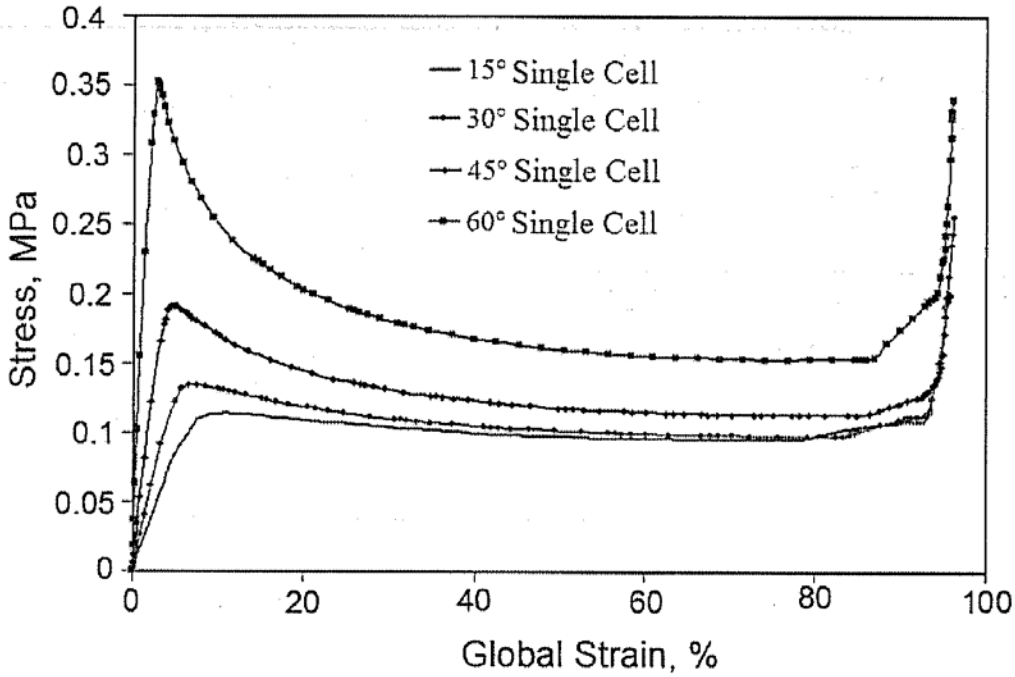

Figure 4.19. Atli-Veltin and Gandhi results for single cell, h = l = 5.5mm, th = 2*tl = 290mm. Source: Atli-Veltin, B., and Gandhi, F., "Effect of Cell Geometry on Energy Absorption of Honeycombs Under In-Plane Compression," *AIAA Journal*, Vol. 48, No. 2, February 2010, pp. 466-478.

for example the densification region, and the slight increases in stress when cells begin to collapse and interact with one another (compare Figure 4.17 to Figure 4.18).

Also interesting to note is the reaction forces at each support node viewed over the course of the deformation. For the 12 element per side final model, the reaction force in the support nodes are shown in Figure 4.20. The reaction force numbering shown is from left to right if viewing the support nodes of Figure 4.11, 1 being the most left support and 6 being the most right. The outer supports experience double the reaction force than the inner supports, and therefore double the stress. This causes the entire structure to focus deformation on the central vertical wall, which ultimately instigates its rotation and collapse the 3rd cell row together as one unit. A densification band appears, the beginnings of which are seen in Figure 4.16.

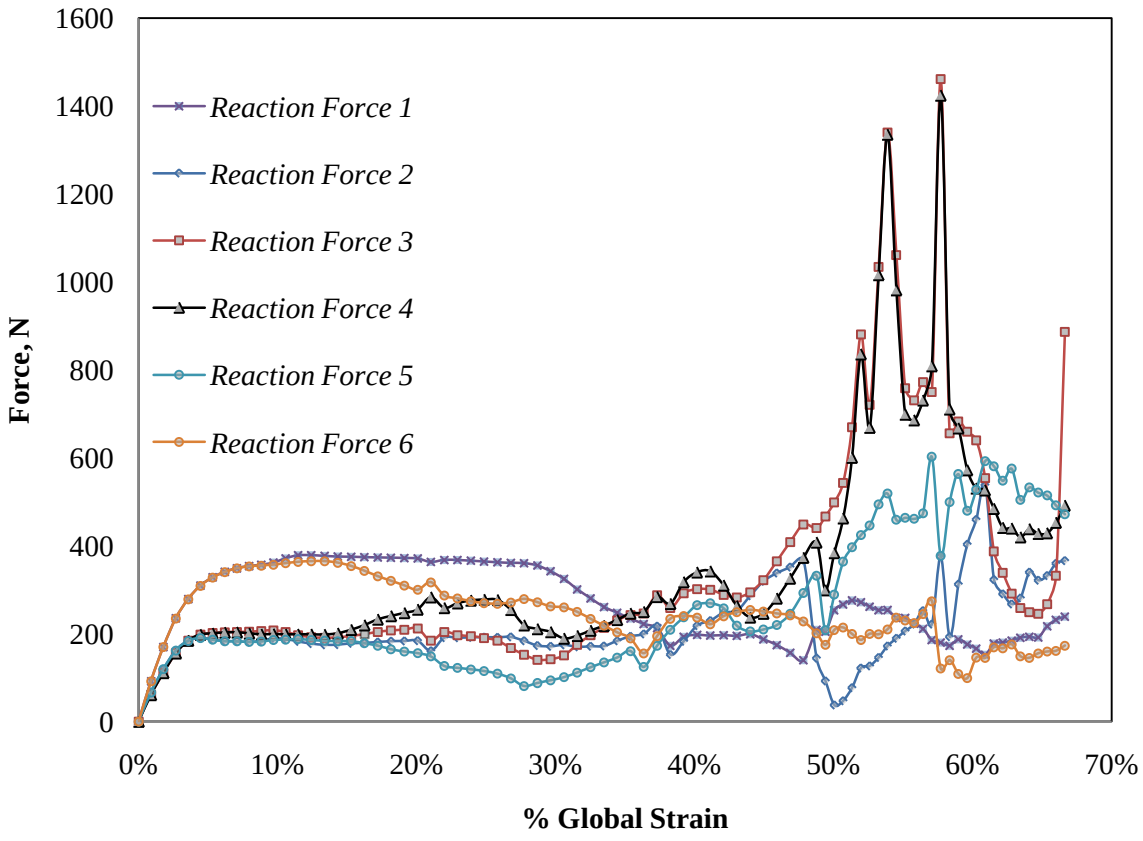

Figure 4.20. Nodal reaction force at supports in global y direction vs. global strain.

4.6 IMPERFECTION SENSITIVITY ON MULTI-CELLULAR HONEYCOMB

Aluminum honeycomb cores are typically wrought with imperfections. This is confirmed in [52] and can have a significant effect on the knee region of the stress-global strain curve shown in Figure 4.20 (5-10% global strain). Imperfections hinder a structures ability to resist buckling and can therefore affect the result of in-plane crushing simulations.

The studies in [52] and [63] merely add a 1-2^{o} imperfection to the central row of cells to initiate plastic crushing. In this study a full eigenvalue buckling problem was performed and the buckling mode shapes obtained . In the past, [59] has done full simulations of honeycomb expansion and has then applied these to the perfect model and validated via experimentation. Rather than perform such extensive calculations the buckling mode shapes are used as geometric imperfections. Typically buckling mode shapes are the worst possible geometric imperfection for buckling. The mode shapes are determined in an analysis below. This is to determine how significant imperfections are to the deformation seen in the honeycomb during in-plane crushing.

To determine the eigenvalues (for bifurcation buckling) of the structure shown in Figure 4.21, an Euler buckling step in ABAQUS [64] was used. The analysis was done using exactly the same model with the previously discussed converged mesh with B21 elements.

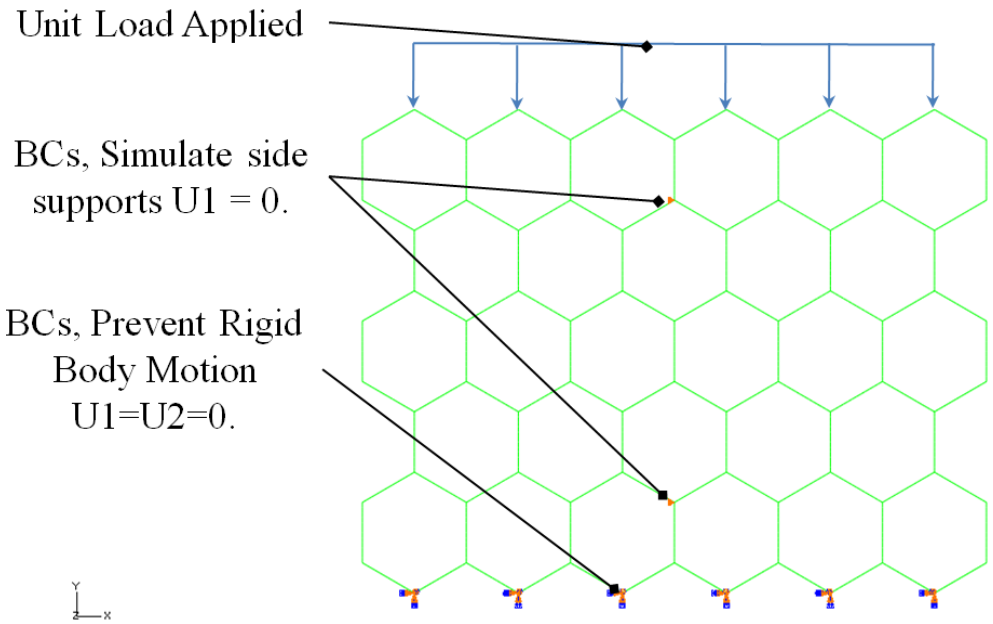

Figure 4.21. Eigenvalue buckling analysis of a 5x6 honeycomb with boundary conditions.

After the bifurcation buckling analysis the buckling mode shapes (eigenvectors) were extracted. These are shown in Table 4.7. Each mode shape's displacements are then individually scaled to 4% of the thickness of the aluminum foil (38.1μm), and subsequently in an investigation added to the perfect model geometry as an imperfection.

To determine which mode shape superimposed on the perfect model would cause the worst case imperfection, an analysis was done where each of the first four buckling modes were individually added to the perfect honeycomb structure, and crushed to 30% global strain. The effective stress (same stresses as discussed in Figure 4.17) is plotted against the global strain values and shown in Figure 4.22.

As expected the first buckling resulted in the largest role in reduction of the peak value of global stresses during in-plane crushing. This is further explained by viewing a honeycomb being crushed in-plane and noticing global strain values compared to the angles of the vertical walls. In the perfect honeycomb model, the walls remain nearly vertical up to 13% global strain, which is evident by the high peak stress produced by the perfect model in Figure 4.22. However when the first buckling mode is scaled and added to the model as an imperfection, this peak is reduced and visually this is because the vertical walls in the 3rd row of the model have buckled and are not longer 90^{o} vertical. This is illustrated in Table 4.8.

Typically a honeycomb has been expanded from strips of aluminum foil and handled by manufacturing process workers. For this reason it would also have randomized imperfections and therefore the first three buckling modes are chosen to superimpose on the final model, rather than only the first mode. The final model used on this and all models hereafter is shown below in Figure 4.23.

Table 4.7. List of Eigenvalues and Mode Shapes for 5x6 Honeycomb Structure

Eigenvalue Buckling Analysis		
Mode Number	***Eigenvalue (Buckling Load, N)***	***Mode Shape***
0	Na	
1	633.49	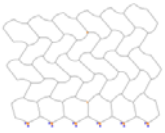
2	773.28	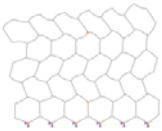
3	867.19	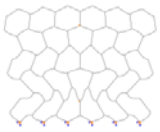
4	945.80	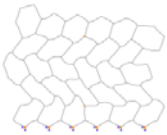
5	986.13	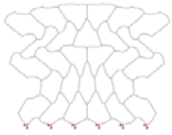
6	1075.6	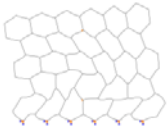
7	1087.1	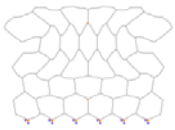
8	1201.0	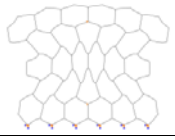
9	1463.0	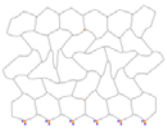
10	1570.1	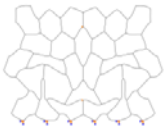

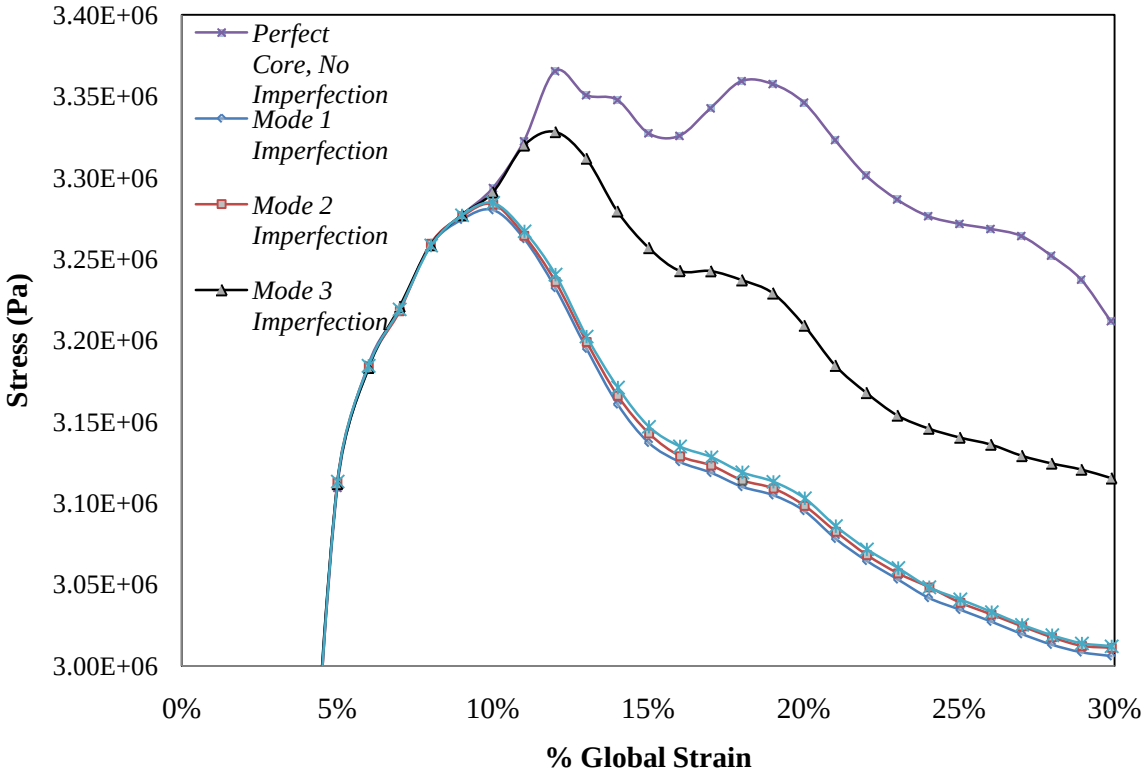

Figure 4.22. Effect of buckling mode shape superposition on perfect geometry model, imperfection sensitivity analysis.

Table4.8. Geometrically Different Result for Buckling Mode Added as Imperfection

Crushing with Perfect Honeycomb Core, Global Strain = 13%
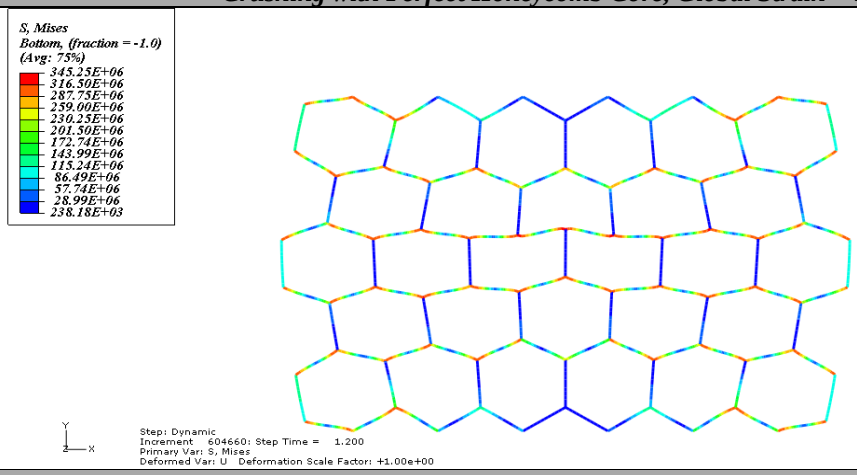
Crushing with Imperfect Honeycomb Mode 1 x 0.001Global Strain = 13%
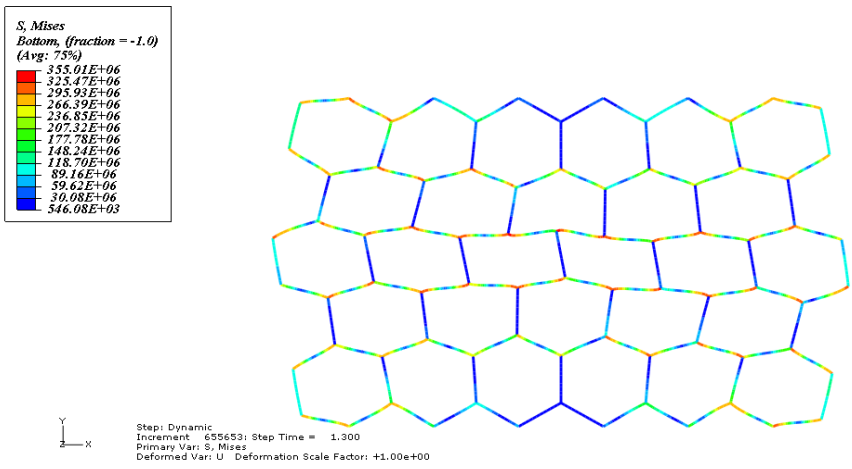

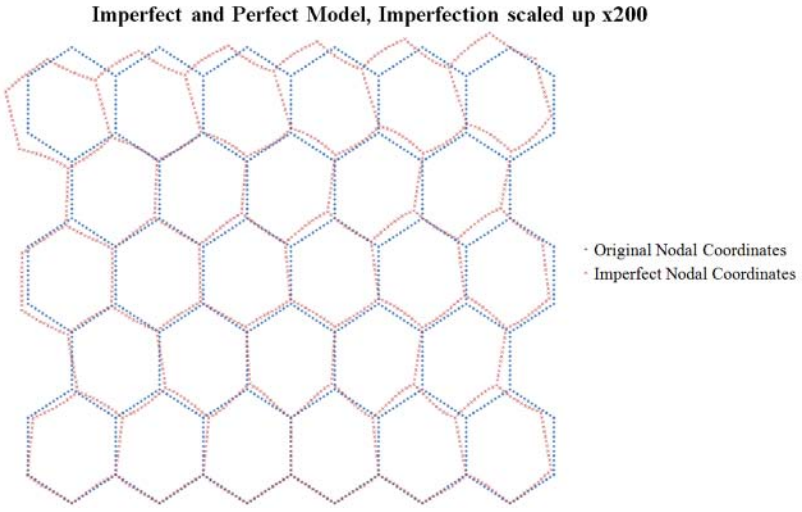

Figure 4.23. Final imperfection used in all subsequent models.

CHAPTER 5

ROLLER CRUSHING OF HONEYCOMB

The final part of this effort is to demonstrate that by using a rolling operation, more gradual densifications of the core along the edge can be achieved. The motivation for investigating this comes from observing the variation of stress in a 2D elastic half space continuum loaded by a circular disk contact (Figure 5.1). The radial and tangential stress under the point of contact develop are inversely proportional to the radial distance away from the point of contact. The rolling of sandwich honeycomb has several differences. First, the honeycomb material is anisotropic. It cannot be considered a continuum unless the roller diameter is many times larger than the honeycomb cell size. Second, for roller crushing we need to induce deformations that are large and beyond the linear elastic regime. This creates non-linearities which could change the stress field when compared to the continuum body in Figure 5.1. Our goal is to investigate the densification of honeycomb cores due to the localized loading from a roller contact.

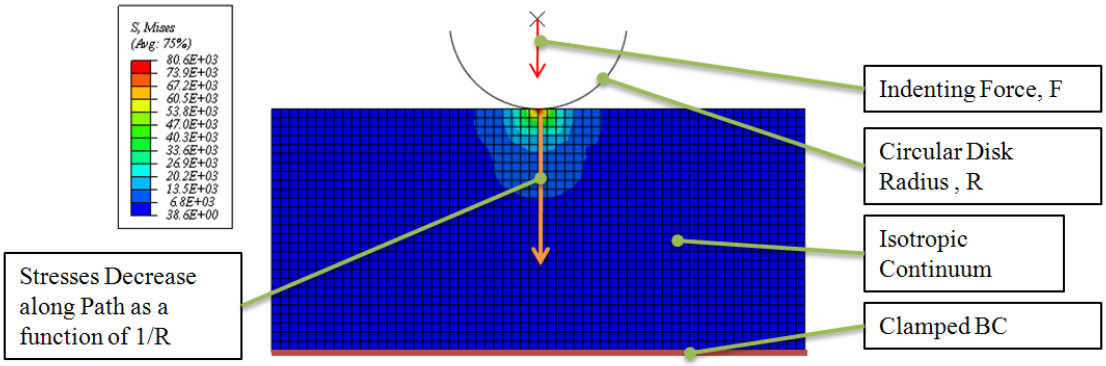

Figure 5.1. Example of contact between circular indenter and flat continuum medium in classical elasticity with resulting stress distribution.

5.1 ROLLING MODEL: MODEL SETUP

The finite element model for the honeycomb core is used to investigate the crushing with a roller is the finite element model discussed section 4.2 of this work, with a few modifications. Here the model itself is presented.

The beam element honeycomb model is nearly the same as before, except for modification of contact definitions. Contact definitions had to be modified to prevent the cell walls from penetrating one another during the rolling simulation. These conditions for contact are different than before because the honeycomb deformation under rolling causes cell walls to contact one another differently than under uniform in-plane crushing. The rigid body boundary conditions, wall support boundary conditions, degrees of freedom, element mesh, and pressure overclosure modification are all the same as previously described.

The roller is allowed to roll counter clockwise and translate at the same rate (no slip) over the top of the honeycomb core from right to left in a dynamic analysis (see Figure 5.2). Rolling is done in a 2D plane strain ABAQUS non-linear dynamic step where an analytically rigid surface is used to model the roller. The rolling speed, v_x, was set at 1 inch per second, to minimize any inertial effects. Any speed slower than this gave little difference in global stresses or in nodal deformation. The angular speed, ω, of the roller was set such that at the point of contact between the roller and the honeycomb the *x*-component of radial velocity in the direction of the rolling process was equal and opposite the translational velocity in the same direction. Since they are equal, the *x*-component of radial velocity and the translational velocity are both labeled v_x in Figure 5.2. This procedure is similar to plate rolling verification problems in [64] and is shown in detail below.

The contact between the roller and foil material is a penalty contact with a coefficient of friction equal to 0.2. The contact between the honeycomb with itself is set as described previously in section 4.2.3 of this work. Also, with the exception of the uniform applied unit load, the boundary conditions for the honeycomb in this model are identical to Figure 4.21. The only prescribed boundary conditions for motion not equal to zero on the roller are the translational velocity (v_x) and angular velocity ω. v_y, shown in Figure 5.2 is simply the vertical component of the radial velocity V_r; it is set by defining ω and Θ and is not directly prescribed.

5.2 Investigation of Effect of Geometric Imperfection on Densification Due to Rolling

The results from the investigation of the effect of geometric imperfection on densification obtained by rolling is presented and discussed. The 5x6 cell honeycomb structure finite element model is used.

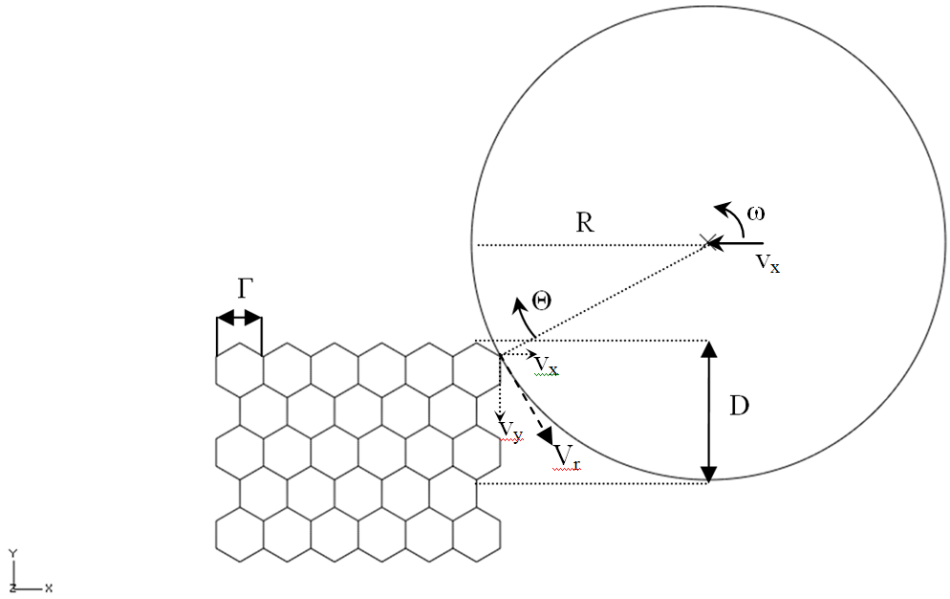

Figure 5.2. Set up and parameterization of roller crushing model.

To determine the effect of geometric imperfection the buckling mode shapes are scaled and added to the initial geometry (Figure 4.23). The model of perfect and imperfect honeycomb cores are rolled to achieve a global strain of 27% using a crush depth (D) of 1.5Γ and roller radius (R) of 3Γ where Γ is the cell size (Γ=3.175mm). The resulting cell deformations of the perfect and imperfect honeycombs are shown in Table 5.1.

Comparison of the plastically deformed final shape of the honeycomb cell (Table 5.1) suggest that geometric imperfections are not a significant factor in densification due to rolling as it was for the uniform crushing investigation in the previous chapter. This is due to the localized nature of the stress induced by the roller type contact and the presence of a shear stress component which was not introduced with uniform in-plane crushing simulations. To make simulations more realistic the imperfection was included in all rolling cases.

5.3 Single Pass Rolling, Effect of Roller Diameter and Crush Depth Variation

The graded core densifications obtained are a function of crush depth and roller diameter (refer to Figure 5.2). To understand the effects of varying these parameters a design matrix of combinations of roller radius and crush depth (Table 5.2) was constructed and each case is investigated.

Table 5.1. Deformation of Honeycomb Cores with and without Added Imperfection Due to Rolling (D=1.5Γ, R = 3Γ)

Rolling with Perfect Honeycomb Core, Global Strain = 27%

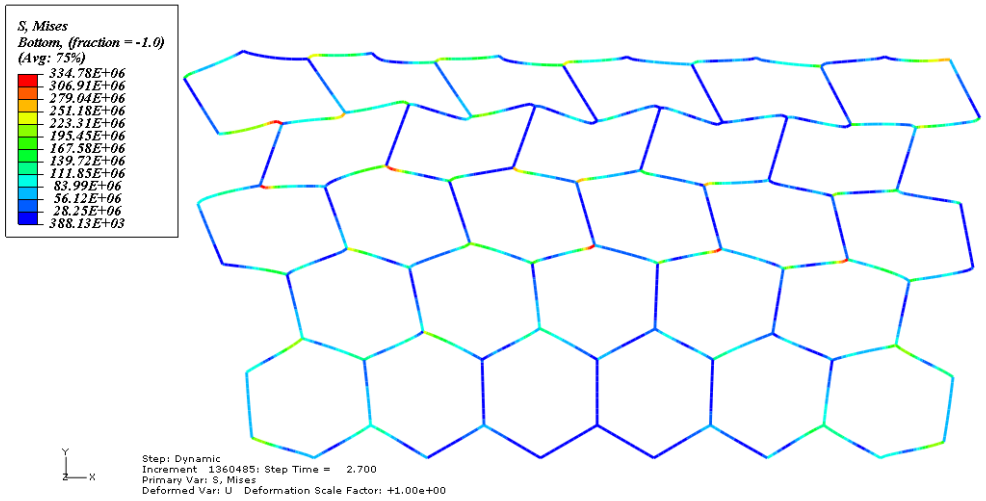

Rolling with Imperfect Honeycomb Mode 1,2,3 x0.001, , Global Strain = 27%

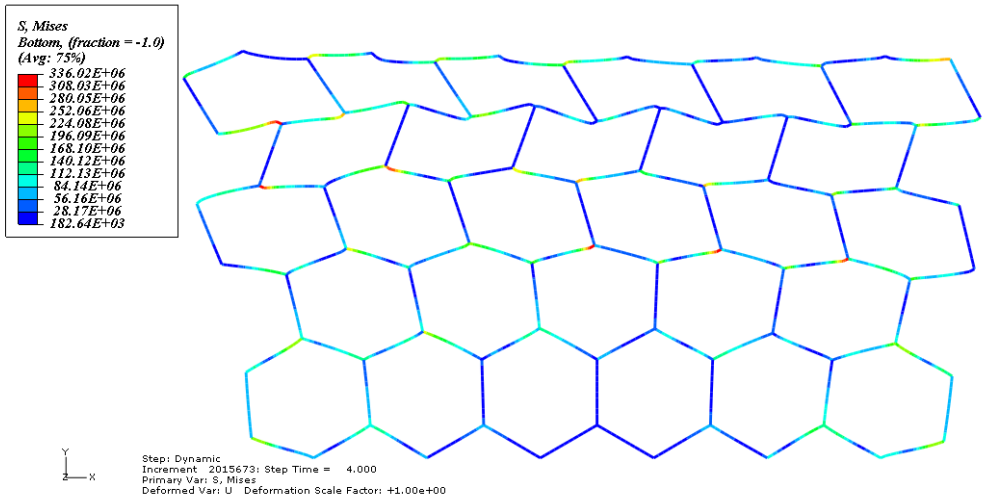

Table 5.2. Design Space for Single Pass Rolling Analysis of 5x6 Honeycomb Structure

Single Pass Test Matrix		***Roller Radius***			
		R = 1.5Γ	***R = 2.5Γ***	***R=5Γ***	***R=10Γ***
Rolling Depth	***D = 1Γ***	Case 1	Case 2	Case 3	Case 7
	D = 3Γ	Case 4	Case 5	Case 6	Case 8

The deformed shape of the honeycomb cores at various stages of the rolling for the eight test cases is shown below in Table 5.3. The crushing deformations indicate a correlation between a defined parameter Θ (see Figure 5.2) and the effect of localized crushing. While Θ does not have a direct relationship between the core density variation itself, it does provide some insight on whether a larger or smaller radius roller should be used on the first pass on the honeycomb and at what depth one might begin the process. It was found that any angle Θ which was smaller (including zero and negative values) than 45^o would produce undesirable localized crushing in the region where the roller first made contact with the material. This is evident in case 4, 5, 1, 6, and 2. At below 45^o, the roller is simply folding a localized portion of the material's plastic hinges, rather than uniformly crushing individual cells. For case 4, where Θ is the smallest, the aluminum foil actually begins to fail in tension and element distortion begins to occur.

When Θ is more than 45^o, a uniform and predictable crushing pattern emerges as in cases 3 and 7, This is not the only requirement. In case 8, the angle is more than 45^o, but the crush depth is 3Γ. In this case the densification does not start at the edge as is desired. The goal in the first pass was to get a densified core along the rolled edge. With densification occurring along the edge it is possible to then subject the honeycomb core to a series of rolling operations (multi-pass rolling) to achieve a continuously graded core density.

Since the final deformation from rolling in case 3 and 7 resulted in a uniform grading and since they are nearly identical, case 3 from above is chosen for a final investigation involving multipass rolling. This multi-pass rolling will stem from the previous deformation, where the parameter D will continue to increase with the roller radius R fixed, to determine the best combination of three passes to yield varying core densifications.

5.4 MULTI-PASS ROLLING, EFFECT OF DEPTH RATE

The multi-pass rolling uses the deformed nodal coordinates of the output of one rolling operation as the input for the next rolling operation, with different roller boundary conditions. Also, the depth D (refer to Figure 5.2) is considered a parameter and combinations of depth rates are examined.

Table 5.3. Result of Single-Pass Roller Crushing Experiment, Parameters R and D Vary

Result of Single-Pass In-Plane Rolling of Honeycomb Core						
Case #	***Θ (deg)***	***Model Setup (X = 0)***	***Normalized Roller Path X***			
			.25	***.5***	***.75***	***1***
4	-47.0		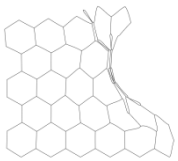		*Element Distortion (tearing)*	*Element Distortion (tearing)*
5	-2.3		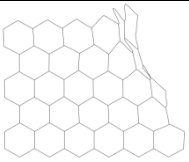			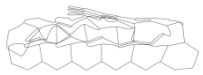
1	25.0	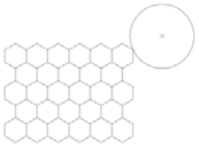				
6	28.7	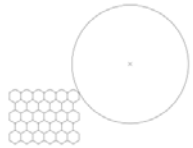			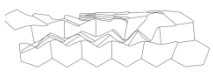	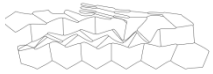
2	40.8	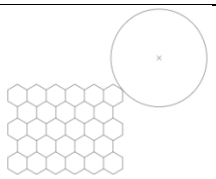			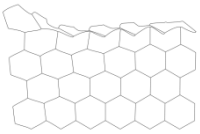	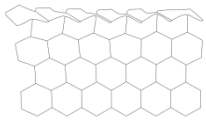
8	47.7	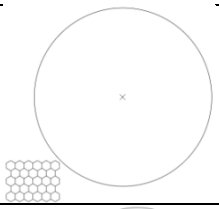				
3	55.8	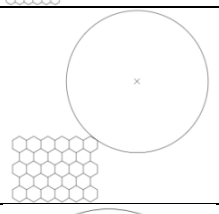	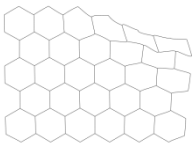		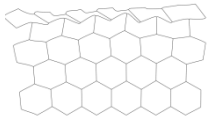	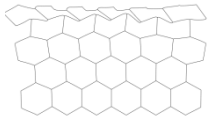
7	66.0	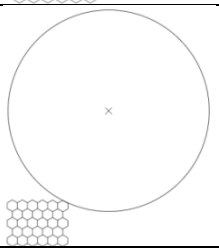	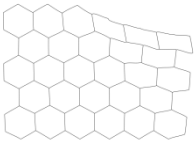	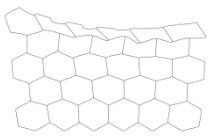	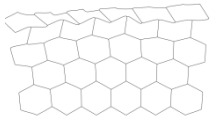	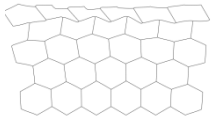

A test matrix for different number of passes and crush depths is shown in Table 5.4. The case ID numbers are continued on from the previous part of the chapter to avoid confusion between sections. The overall depth (D) of the model (5Γ) limits the total amount of total passes and the variety of depth rate. Previously case 3 in Table 5.3 was chosen as the most desirable of the original 8 cases, with a roller radius of 5Γ. The output of case 3 is the same as pass 1 in both cases 9 and 10 in Table 5.5. From there on testing on case 9 and 10 diverge, using different depth rates.

Table 5.4. Multiple Pass Test Matrix, Roller Radius Held Constant Throughout

Multiple Pass Test Matrix		***Roller Radius R = 5Γ***			
		Pass 1	***Pass 2***	***Pass 3***	***Pass 4***
Rolling Depth	***D = 1Γ***	Case 9/Case 10			
	D = 1.5Γ		Case 9		
	D = 2Γ		Case 10	Case 9	
	D = 2.5Γ				Case 9
	D = 3Γ			Case 10	

The progressive crushing of the honeycomb core after each pass for case 9 and case 10 is shown in Table 5.5. In case 9, the depth rate is set (after Pass 1) at 0.5Γ per pass. Note that the depth is defined from the original height of the model, regardless of the deformation which results in each pass. Here, as D increases to 1.5Γ in pass 2, the vertical walls in row 2 begin to fold and buckle. As the depth increases in pass 3 to 2Γ the inclined walls on the upper half of row three begin to fold downward gradually and a gradation begins to emerge. The quantitative apparent densities of the gradations have not yet been analyzed, but visually this looks appealing. It is necessary to obtain a core which gradually decreases in density from the point of roller contact to the far field (negative *y*-direction in Figure 4.21) in order to mimic the sort of gradations which are presented in chapter 3.

In case 10, the depth rate is set to 1Γ per pass. This higher depth rate compared to case 9 does not seem to change the deformation until after a crush depth of 2Γ is reached. In fact, the deformation is nearly identical from pass 3 of case 9 to pass 2 in case 10, both of which have reached a depth of 2Γ. This indicates that a crush rate of 1Γ per pass works well up until a depth of 2Γ. After this a more gradual crushing should be considered or a different radius roller should then be employed to continue further densification (investigated next). Also note that only 3 passes could be performed, after which this particular core becomes nearly fully dense.

Table 5.5. Visual Result of Multi-Pass Rolling with Varying Depth Rates

Result of Multi-Pass In-Plane Rolling of Honeycomb Core			
Case #	***Pass #***	***Depth, D***	***Result***
Case 9	Initial Model Setup	na	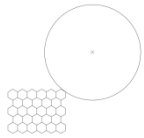
	Pass 1	1Γ	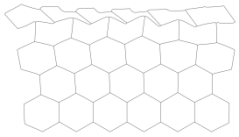
	Pass 2	1.5Γ	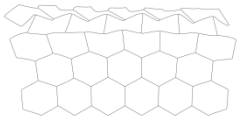
	Pass 3	2Γ	
	Pass 4	2.5Γ	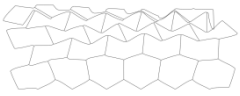
Case 10	Model Setup	na	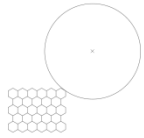
	Pass 1	1Γ	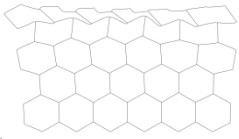
	Pass 2	2Γ	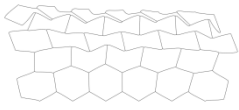
	Pass 3	3Γ	

5.5 FINISHING PASS EFFECT OF VARYING ROLLER RADIUS

To further investigate all possible methods of core densification, the result of Case 9, (see Table 5.5) was chosen as the base state for the roller radius study. This case was chosen as the basis because it already has a core which has increasing density in one direction, but there are still nearly undisturbed cells near the bottom of the model. The inclined walls of these cells have not buckled yet and still deform and buckle after Pass 3. This is essentially an extended case study for Case 9, where the rolling depth is being increased from 2Γ (Case 9, Pass 3) to 2.5Γ (Case 9, Pass 4) using different radii rollers (Case 9 used roller radii equal 5Γ).

Roller radii which were greater than and also smaller than that of Case 9, Pass 3 (which had a roller radius of 5Γ) were chosen as 2Γ, 3Γ, 4Γ, 6Γ, and 7Γ. The test matrix for this experiment is shown below in Table 5.6.

Table 5.6. Roller Variation Test Matrix, Rolling Depth Held Constant Throughout.

Roller Radius Variation Test Matrix: Extended Study of Case 9		***Roller Radius***					
		R = 2Γ	***R = 3Γ***	***R = 4Γ***	***R = 5Γ***	***R = 6Γ***	***R = 7Γ***
Rolling Depth	***D = 2.5Γ***	Case 13	Case 12	Case 11	Case 9	Case 14	Case 15

The result from varying the roller radius has much less effect on the overall deformation of the honeycomb than the effect of changing the crushing depth. However, it is proven here quantitatively using the change in a central cell wall angle (row 4, column 3) that changing the roller radius changes the amount of deformation and the variation of stress in the negative *y*-direction. The cell wall angle in question here is deemed *β*, and is shown below in Figure 5.3. Because the vertical wall directly above the cell containing β is no longer vertical, a trend directly related to roller size and β emerges which is based the amount of *y*-direction strain in that cell. This is studied by taking the angle between 3 nodes.

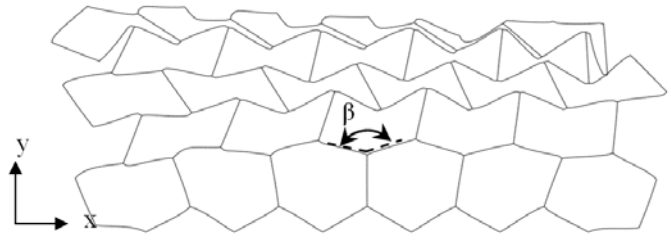

Figure 5.3. Deformed model: example measurement of cell wall angle β, row 4, col. 3.

The result is what was expected by looking at the classical elasticity indentation case, that increasing the roller size causes an increase in measured angle β after the pass is complete. This indicates that the extent of the local stress region in the honeycomb can be varied by varying the roller size and that many different core gradations can be achieved using this technique. Furthermore it is learned that large changes in core gradation can be accomplished by varying to a degree (around 2Γ depths) the crush depth, and that finer adjustments in the core gradation can be made by varying the roller size. Increasing the roller size increases the depth to which the higher stresses reach into the honeycomb in the *y*-direction and vice versa. The visual result of the study is in Table 5.7 and Table 5.8, while the numerical result of the change in cell wall angle versus roller radius is contained in Table 5.9 and Figure 5.4. Note that in Table 5.9, β for an un-deformed honeycomb core is not exactly 120^o due to the added buckling mode imperfection.

5.6 MOVING AVERAGE APPARENT DENSITY CALCULATIONS

Due to the complex cell geometries which are generated by plastic rolling techniques discussed here, it is very difficult to gauge the overall in-plane material properties and how they vary in each direction. Previous work done in [18] shows that there are functional relationships between apparent density of cellular honeycomb and their elastic moduli in both in-plane and out of plane directions. However [18] does not consider the elastic moduli gradient in the plane, only the overall achieved elastic moduli. Here, to understand how the material properties might vary after rolling deformation a moving average of apparent density is used rather than overall apparent density.

Apparent density is used typically in the cellular structure industry as a measure of density in porous solids. For a regular hexagonal honeycomb [18] presents the expression for apparent density as:

$$\rho = \frac{t\sum_{i=0}^{n} l_i}{L_x L_y} \tag{5.1}$$

where t is the foil thickness, l_i is the length of each cell wall, L_x and L_y are the overall lengths of the honeycomb walls with unit thickness out of plane (z direction) assumed and n is the number of cell walls. It appears, although it is not directly mentioned in [18], that each

Table 5.7. Visual Result of Varying the Roller Radius while Keeping the Crush Depth the Same

Result of Finishing Pass, Varying Roller Radius, Final Crush Depth = 2.5Γ				
Case	***Roller Radius***	***β (Deg)***	***Initial Setup***	***Result***
15	7Γ	142.4	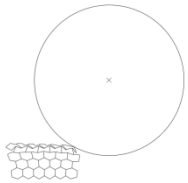	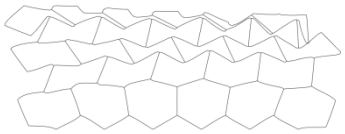
14	6Γ	140.9	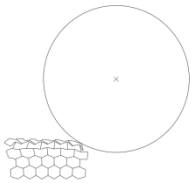	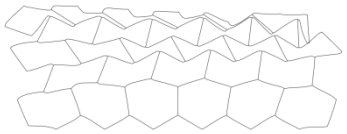
9	5Γ	140.4	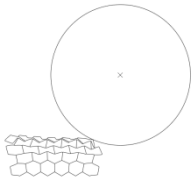	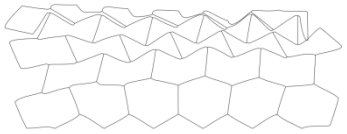
11	4Γ	131.1	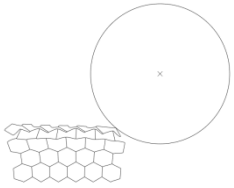	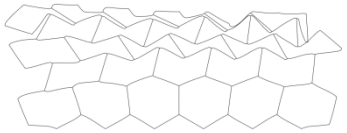
12	3Γ	127.8	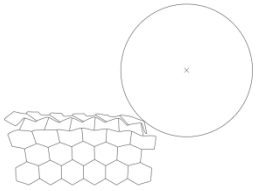	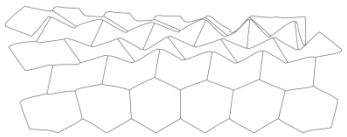
13	2Γ	122.8	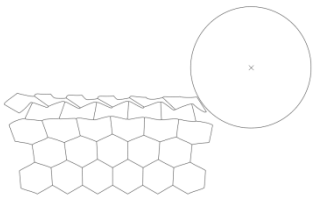	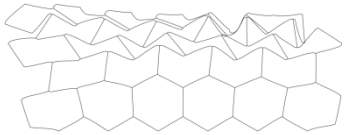

Table 5.8. Detail of Visual Result for Xases 13 and 15

Result of Finishing Pass, Detail Comparison of Cases 13 and 15				
Case	***Roller Radius***	***β (Deg)***	***Initial Setup***	***Result***
13	2Γ	122.8	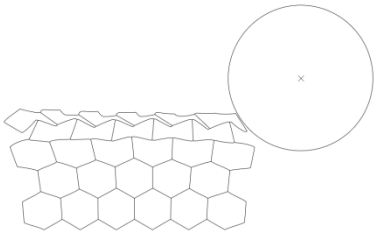	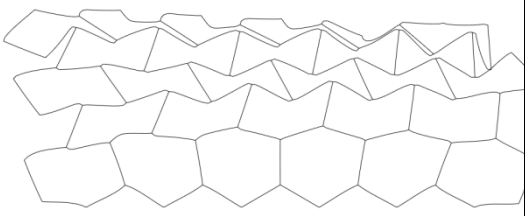
15	7Γ	142.4	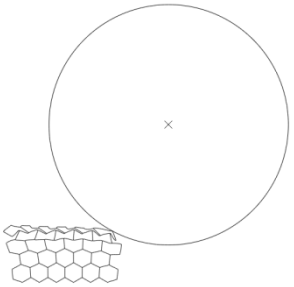	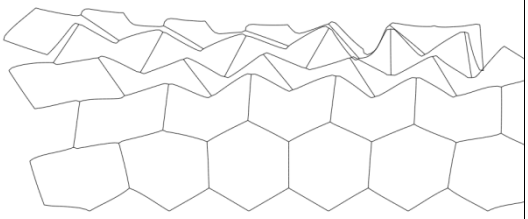

Table 5.9. Effect of Variation of Roller Radius on the Depth of the Stress Field as Quantified by the Change in Angle of a Honeycomb Cell Internal Wall Angle (Original Value Before Deformation β = 118.9^{o})

Roller Radius (Γ)	*β(deg)*	*% Change from original value*
2	122.8	+1.57%
3	127.8	+5.71%
4	131.1	+8.44%
5	140.4	+16.13%
6	140.9	+16.54%
7	142.4	+17.78%

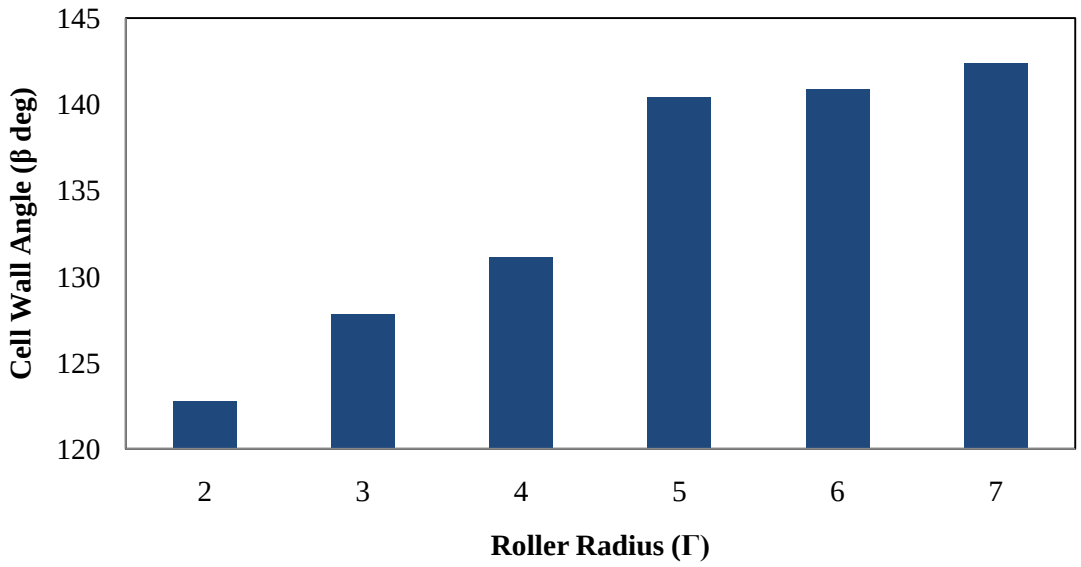

Figure 5.4. Graphical increase of angle beta as roller radius is increased, indicates further penetration of higher principal stresses into the negative y-direction.

wall is assumed to be of the same thickness. This is not true, generally speaking since vertical walls are double thickness due to manufacturing process. To calculate an apparent density at specific locations about the *y*-direction in the model, a similar formula is developed employing a moving average window technique.

To understand the variation of apparent density in the *y*-direction of the model (again, refer to Figure 5.4 for orientations) the apparent density is calculated for a window of the honeycomb model. The window is shown in Figure 5.5 as cyan and magenta lines. MATLAB [65] software was used to write a script to perform these calculations by importing the centroid coordinates of each element after deformation from the previous cases in the ABAQUS rolling simulations. For each window location, the apparent density is calculated as

$$\rho_{apparent} = \frac{\sum_{i=0}^{n}(l_i t_i)}{L_{x,window} L_{y,window}} \tag{5.2}$$

or , the sum of the elements contained in the window divided by total area of the window, where $L_{y,window}$ is defined as 10 times an element length (where the elements are each 0.153mm), $L_{x,window}$ is the overall width of the model, and n is the total number of elements contained in the window. The MATLAB script is run iteratively, such that the window is

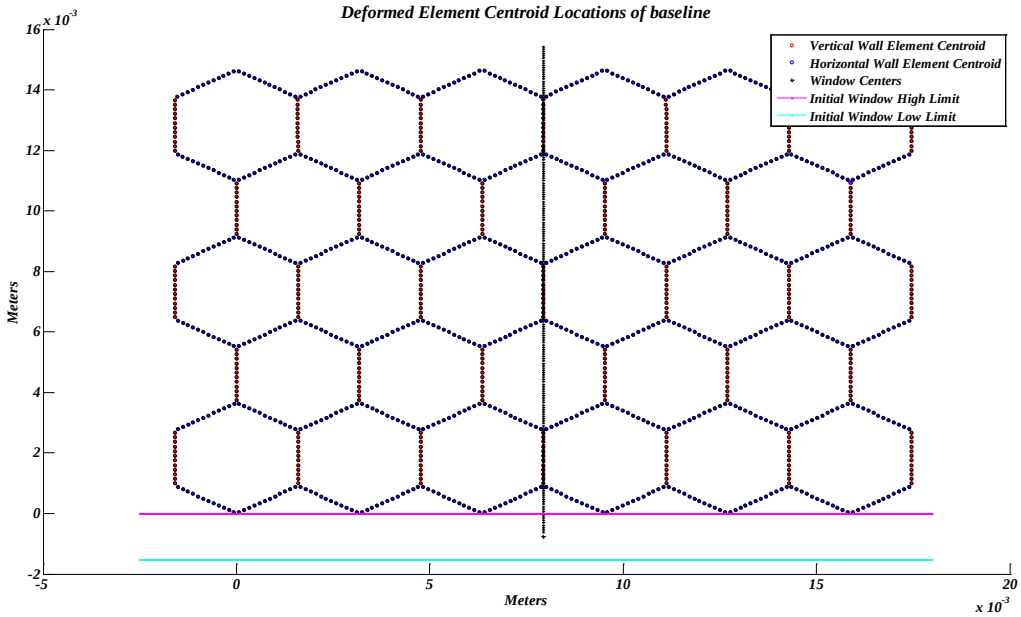

Figure 5.5. Setup of windowed apparent density calculations, undeformed honeycomb case.

first defined as shown in Figure 5.5. Next the apparent density as in equation 5.2 is calculated,and summed over all the elements contained in the window. Then the window moves by the window step size in the positive y direction (set as 0.5 times the element length), and again the apparent density is calculated for the new set of elements contained by the window and stored in the next element of the vector. This calculation continues in a while loop which iterates the window center location (shown plotted as + marks in Figure 5.5) until the apparent density calculated for the window is zero (when the window lower limit has passed the very top of the model, and no elements are contained in the window). To begin the while loop, the apparent density is set to a very small value greater than zero and many orders of magnitude lower than the apparent density values. Each honeycomb case is examined (16 in total); 15 separate rolling cases as well as a baseline case where the honeycomb is not deformed and the apparent density vs. window location is plotted below in Table 5.10. In the baseline case, we see that the apparent density pattern is very regular as expected.

Typically a homogenization of a mirco-structure should use a scale length over which one or more repeating cell patterns of the non-homogeneous microstructure is included. Here it can be seen the window height is smaller than the honeycomb cell size. This therefore

Table 5.10. Apparent Density Plots for Each Case in this Work, Including a Baseline Case with No Honeycomb Deformation

Apparent Density Calculations Summary of All Cases	
Case	***Apparent Density Plots Along the Positive Y Direction***
Baseline (no deformation)	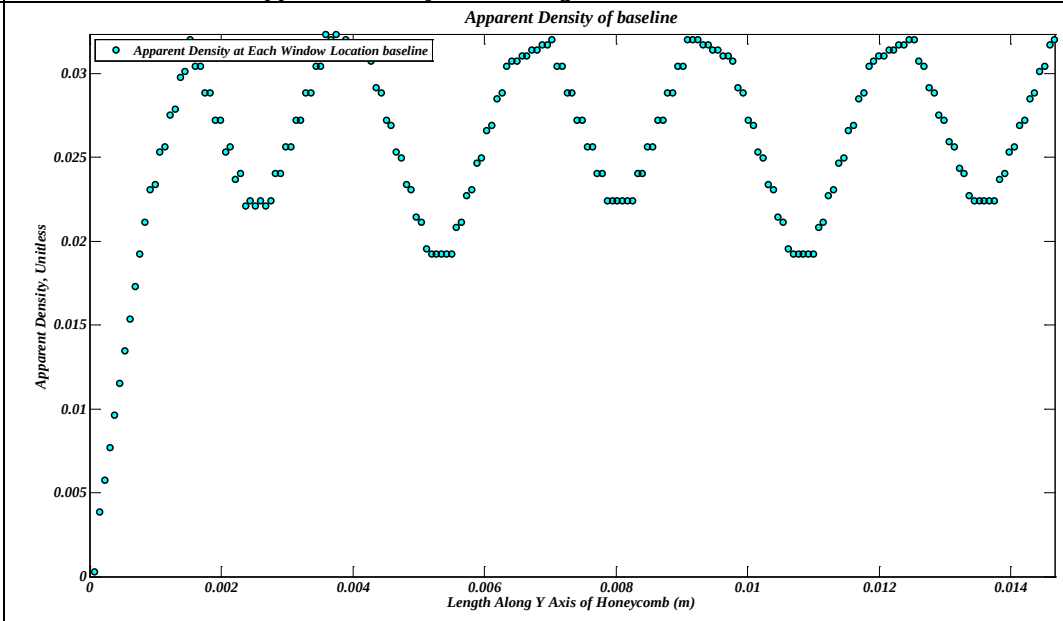
Case 1	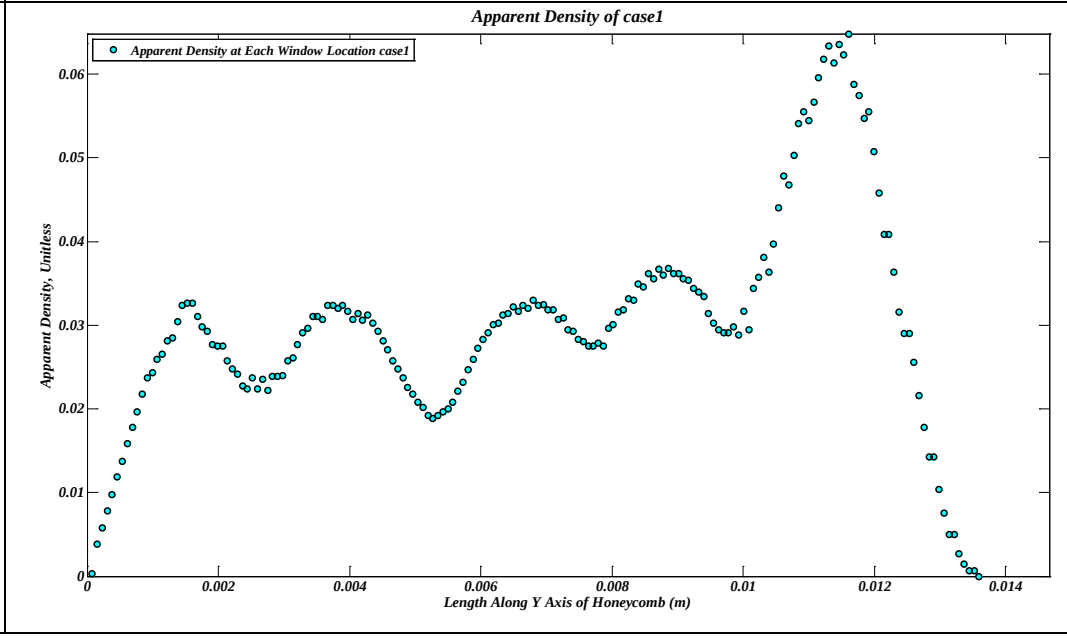

(table continues)

Table 5.10. (continued)

Case 2	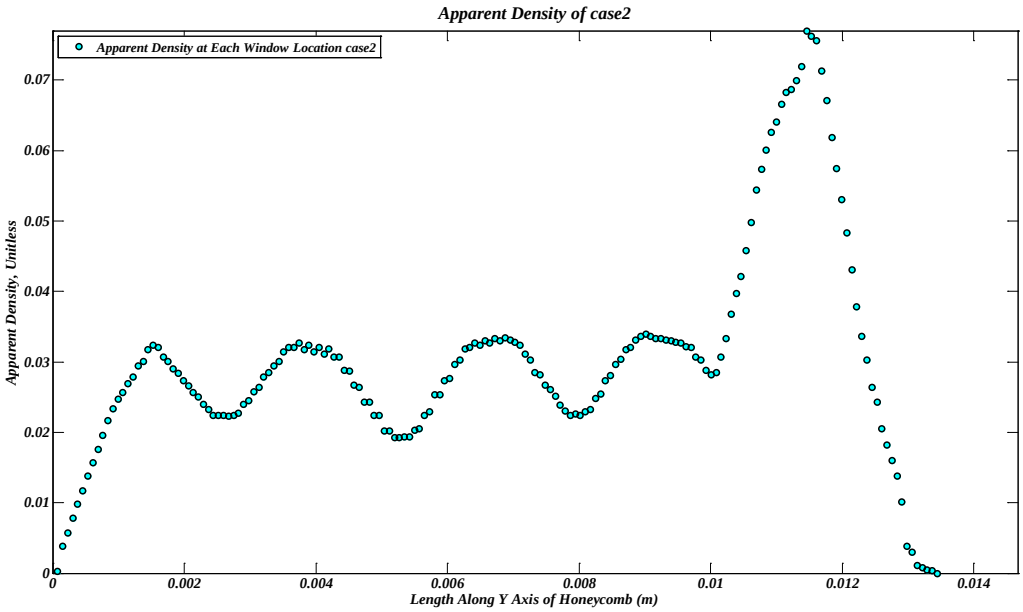
Case 3	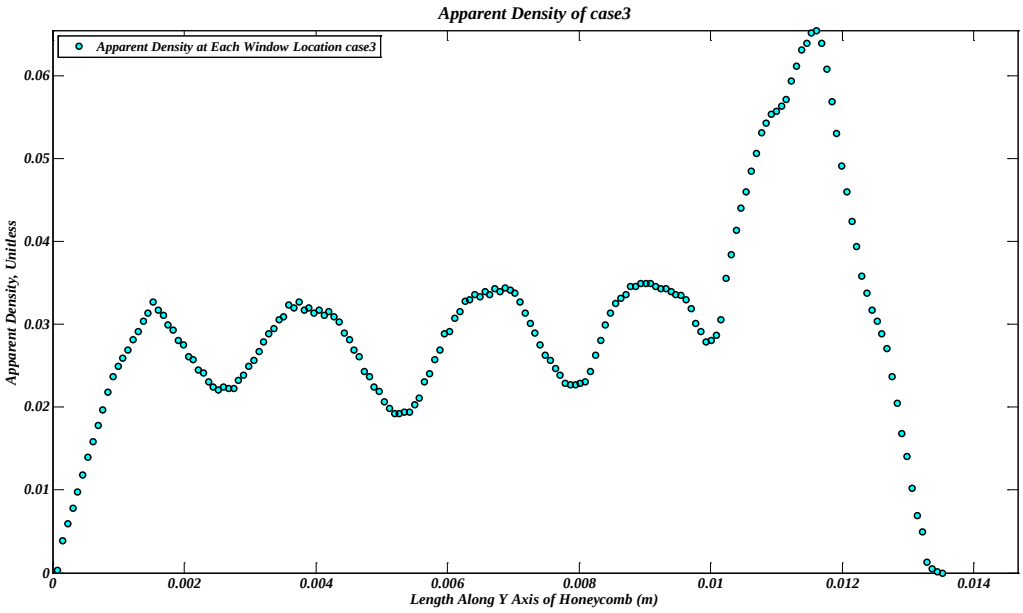

(table continues)

Table 5.10. (continued)

Case 4	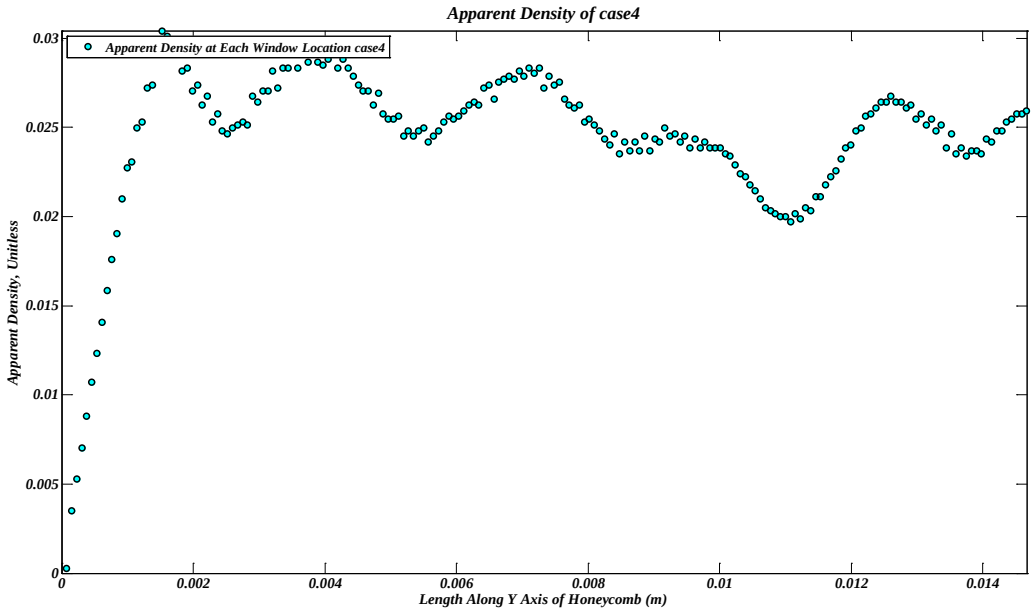
Case 5	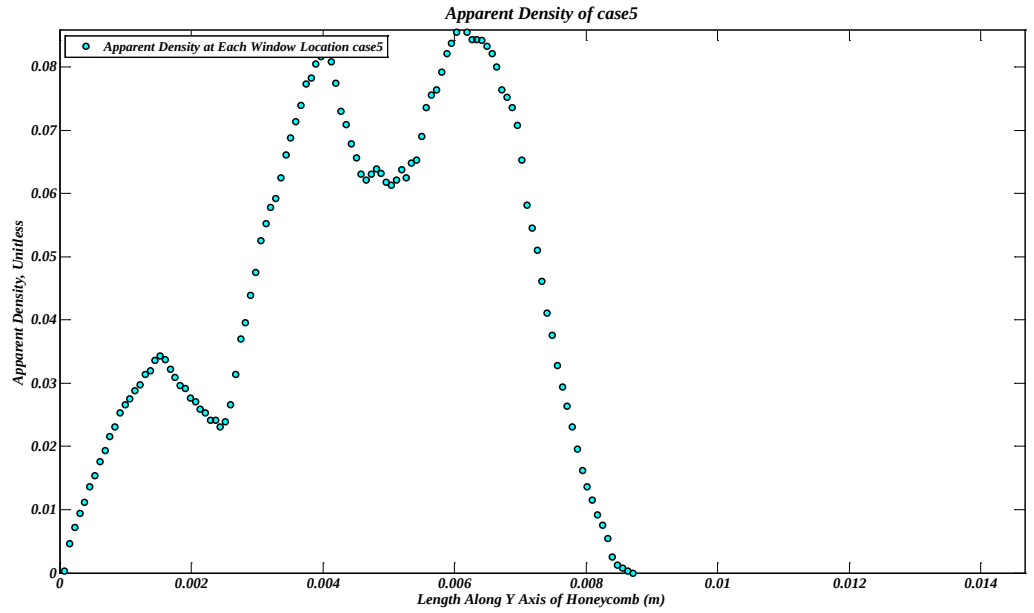

(table continues)

Table 5.10. (continued)

Case 6	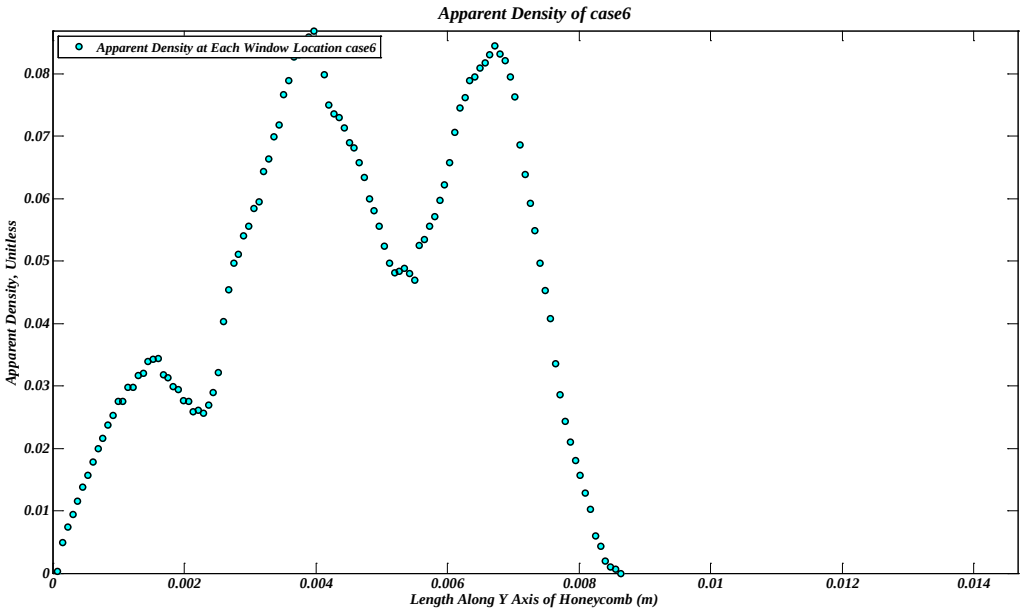
Case 7	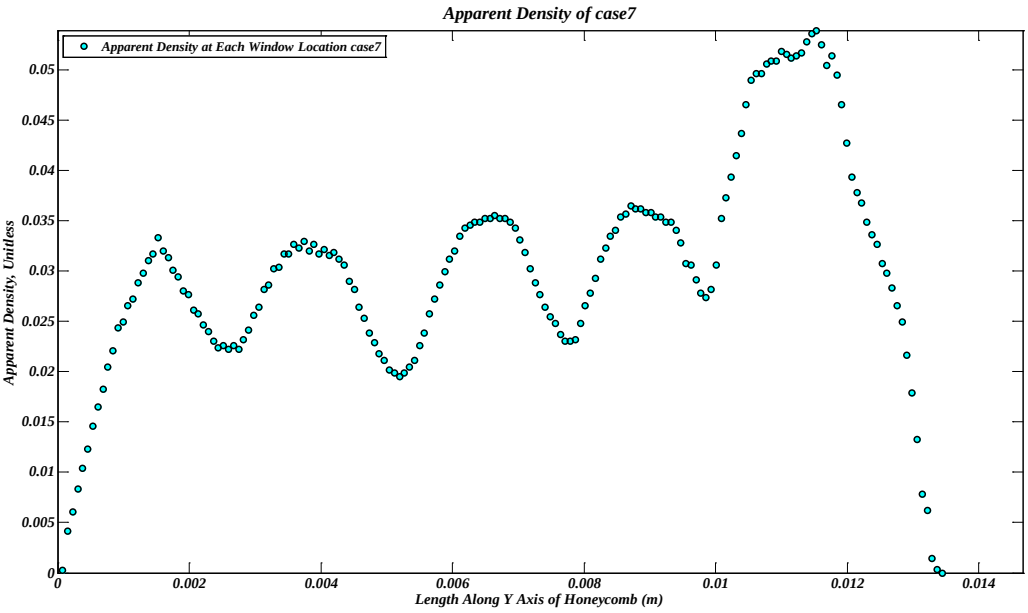

(table continues)

Table 5.10. (continued)

Case 8	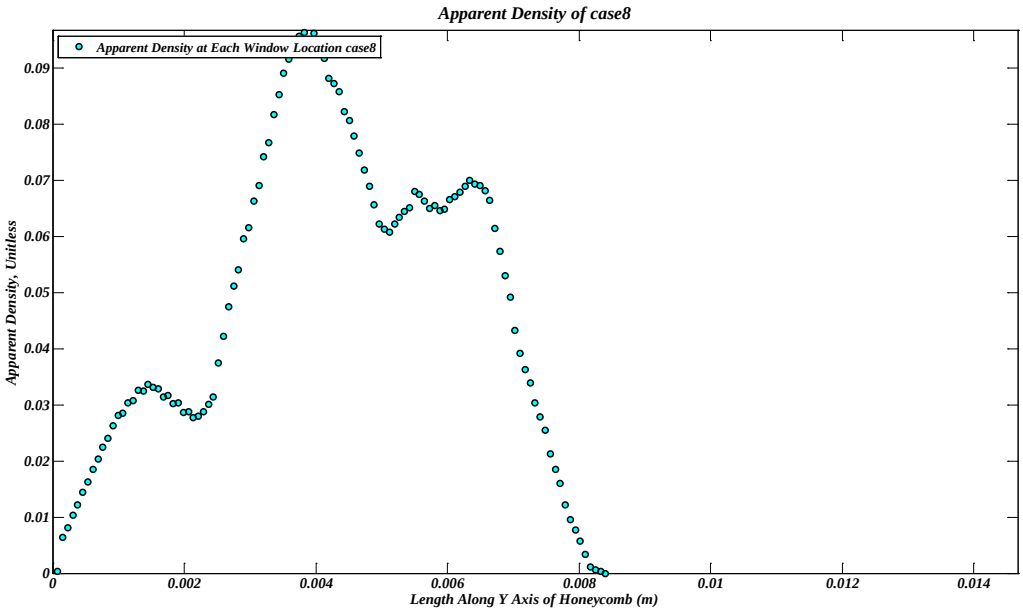
Case 9	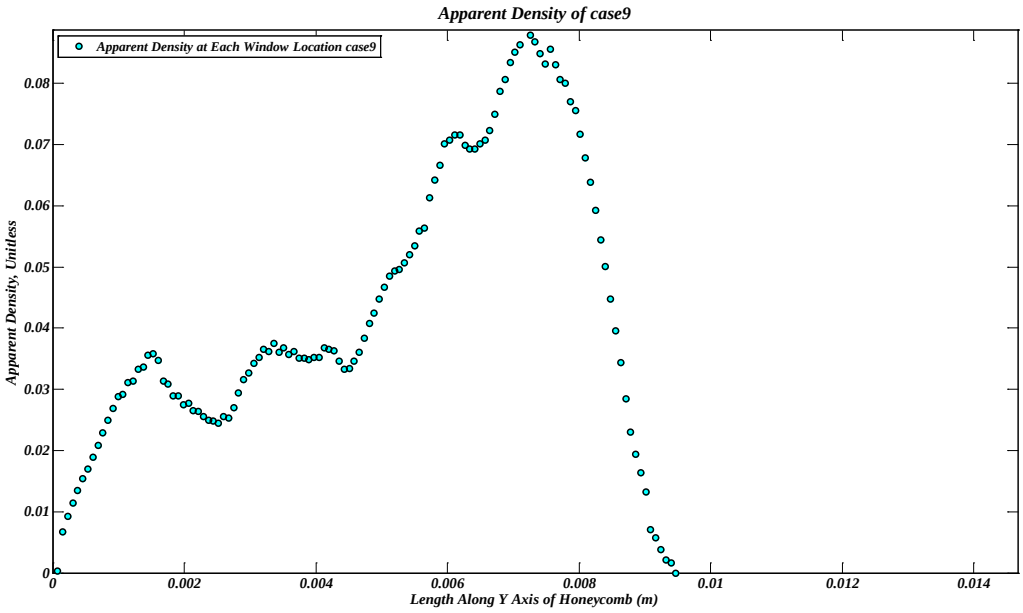

(table continues)

Table 5.10. (continued)

Case 10	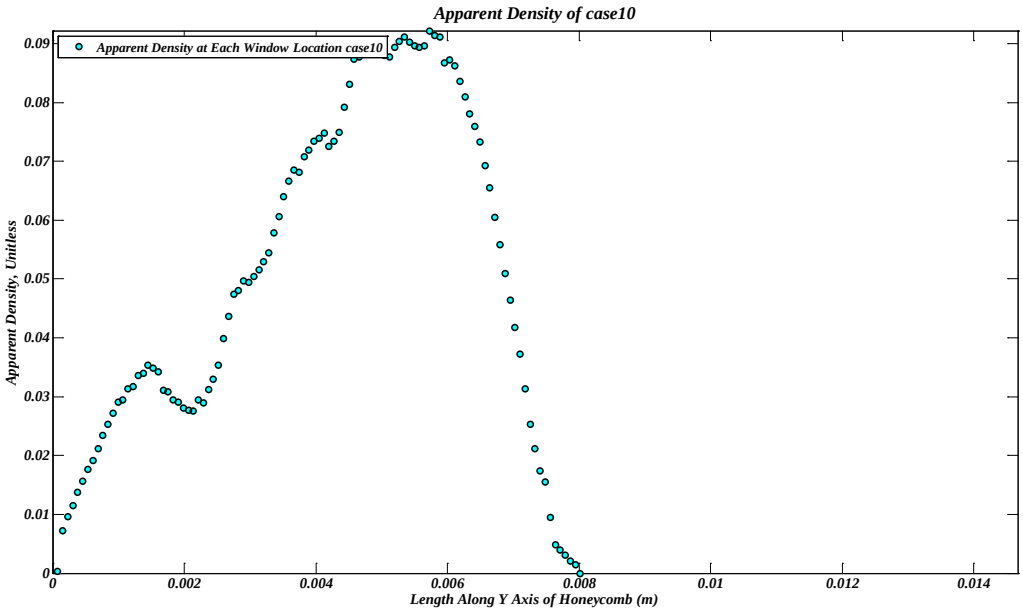
Case 11	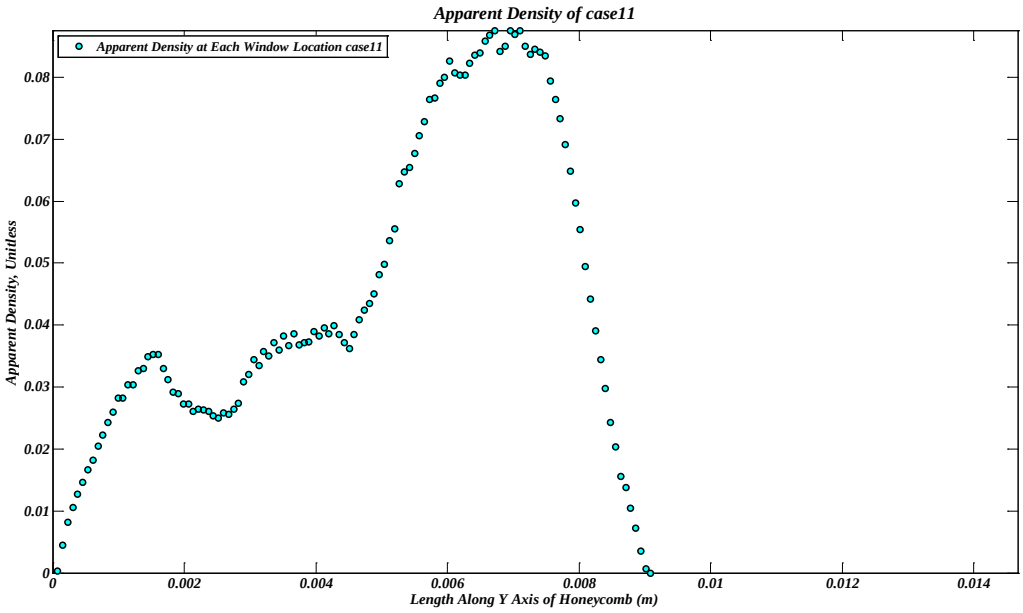

(table continues)

Table 5.10. (continued)

Case 12	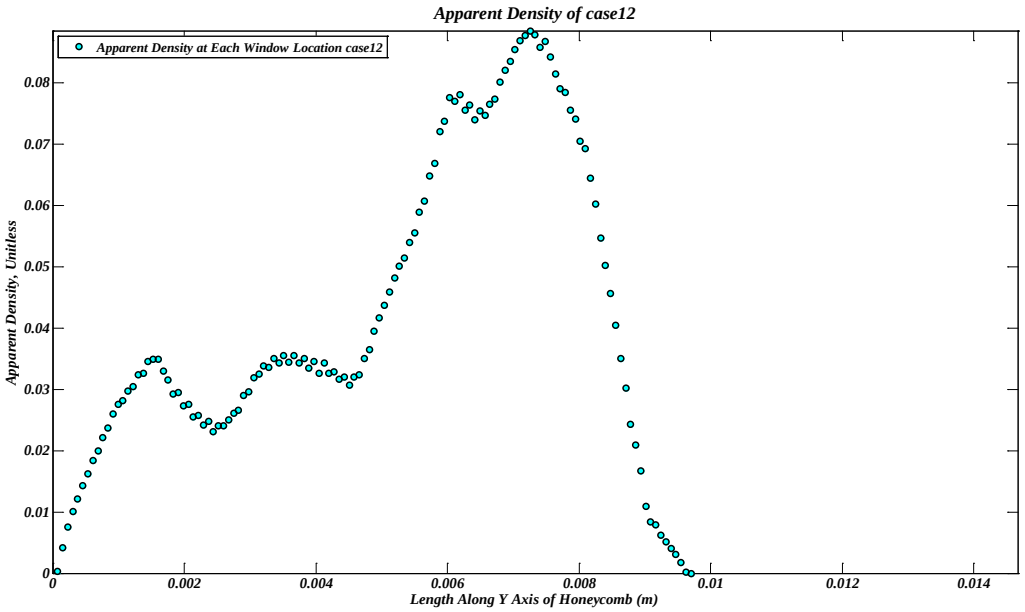
Case 13	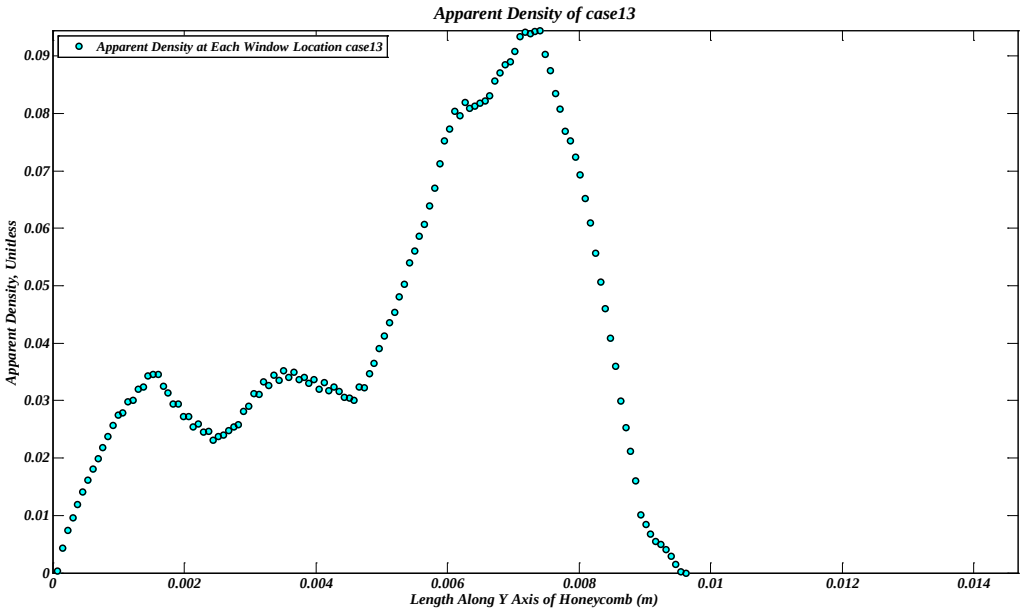

(table continues)

Table 5.10. (continued)

Case 14	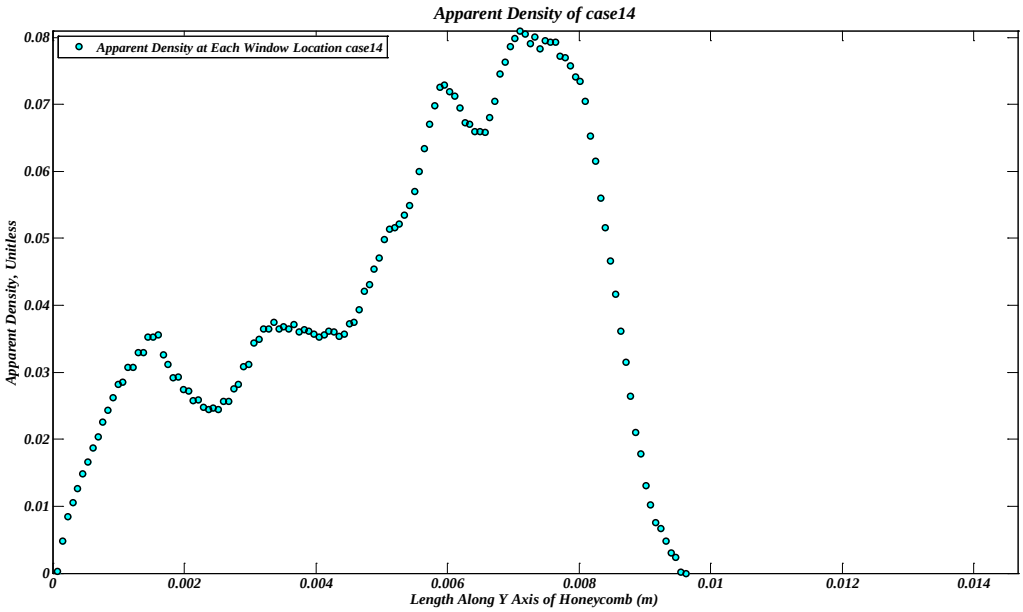
Case 15	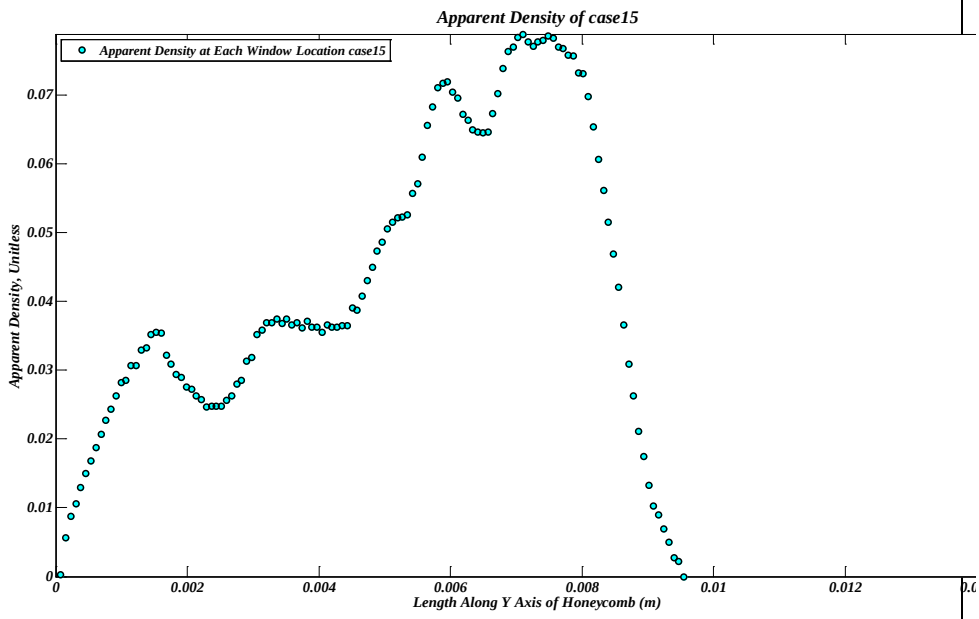

does not give a uniform density for the non-deformed honeycomb core. However, the smaller size chosen gives better information for the densified cores as well as allows the comparison of the densified honeycombs to the initial geometry whereas the typical size chosen for the homogenization of a microstructure would not reveal these details. The apparent densities calculated in the baseline model are less than 0.1 by an order of magnitude, and even the most densified case has a maximum value around 0.092. For a perfect cellular honeycomb [18] shows that the apparent density has a linear relationship with the increase in overall elastic modulus, and thus by taking the apparent density in specific locations along a desired path one provides insight into the material properties in the path direction. Ideally one would like to see a core which has a gradually increasing apparent density, and therefore a gradually increasing elastic modulus.

The results in [18] were however found for perfect, undeformed honeycomb cells, and the only effect on apparent density that was studied were different cell sizes, and not deformed cells. Therefore exact material properties of deformed cells cannot be deduced directly from apparent density in the work presented here. Measuring the apparent density using a window provides a direction for further research needed to determine the exact material properties of each case.

In the baseline case a nearly uniform apparent density around 0.025 is found, a unit-less measurement. It begins at zero, where the window is completely below the model, and increases as the vertical walls are taken into account. As inclined walls come into the window, the apparent density increases as they pass into the window upper limit, and decreases when inclined cell walls pass beneath the window lower limit. This is explained by noticing that there are 6 peaks in the baseline case, where there are 6 rows of inclined walls in the honeycomb model. As inclined walls flatten out under deformation in subsequent cases, peaks in apparent density become higher, and attain maximum value when the angle β mentioned in the previous section approaches 180^{o}.

Case 1,2,3, and 7 each have a peak at the right side of the apparent density plot indicating that only the end of the honeycomb nearest the roller has become densified, which indeed is the case. Cases which became nearly fully dense exhibit a much shorter plot in the *x*-direction and have only one solid peak, like cases 6 and 8.

The multiple pass roller cases, each with a constant roller radius, however with different depth rates, gave the most continuously increasing apparent density. Case 10 especially, with a depth rate of 1Γ per pass yielded an apparent density gradient of 10.5/m. If this were a regular hexagonal structure, its y direction young's modulus would be expected to increase to 10.5 times the original un-densified value after 1m.

CHAPTER 6

CONCLUSIONS

A literature review found that there was an unresolved issue in rampdown closures of structural sandwiches. It also found that there was a research void in the investigation of functionally graded materials that might be able to improve the performance of these commonly used sandwich closures in the aerospace industry.

Finite element analyses of a sandwich beam rampdown closure with functionally graded materials were performed. The results show it was possible to partially equalize the stress gradient caused by the material mismatch at the interface of the core and facesheets by using a graded core. The use of a graded core also resulted in a decrease in the stress gradient across the facesheet-core boundary. The interface shear and normal stresses along the facesheet-core junction show a small increase. However, since the densification along the edge provides an increase in strength this can still lead to an increase in failure margin.

Once it was shown using a material functionally graded along the ramp closure direction was beneficial in alleviating typical stress gradients from material mismatches that can lead to delamination, a finite element model investigation was performed. It showed that regular hexagonal aluminum honeycombs could be densified to achieve various in-plane core gradations using a rolling operation. A method to calculate the apparent densities of the densified core was demonstrated. This honeycomb model was validated against previous work done on in-plane uniform crushing, and subsequent imperfection analyses were also done.

There are several areas which need further work to make functionally graded honeycombs a reality for use in the aerospace industry. It is necessary to develop finite element homogenization methods that can compute the elastic moduli of graded honeycombs. Although previous literature suggests that apparent density and in-plane overall elastic moduli are related, this is not the same as knowing the actual material properties at each in-plane point of a functionally graded honeycomb.

Also, it is necessary to build a model that can estimate the interface bonding strength (peel and shear) as a function of densification. Typically the bond strength is a function of the area of the bond along the honeycomb cell and the fillet width and depth. It is believed that increasing the number of fillets per unit surface area due to densification [37] will have a positive effect on the prevention of delamination.

REFERENCES

[1] Peters. S. T., *Handbook of Composites*, 2nd ed., Chapman & Hall, New York, 1998, Chap. 12.

[2] Collier, C., Yarrington, P., and Pickenheim, M., "Analysis Methods used on the NASA Composite Crew Module (CCM)," 49th AIAA/ASME/ASCE/AHS/ASC Structures, Structural Dynamics and Materials Conference, AIAA Hampton, VA, 2008, pp. 2008-2251.

[3] Cronkhite, J. D., and Berry,V .L., "Crashworthy Airframe Design Concepts Fabrication and Testing," NASA Contractor Report, No. 3603, Fort Worth, TX, 1982.

[4] Atli-Veltin, B., "Effect of Geometric Parameters on the In-Plane Crushing Behavior of Honeycombs and Honeycombs with Facesheets," Ph.D. Dissertation, Dept. of Aerospace Engineering, Pennsylvania State Univ., University Park, PA, 2009.

[5] Albat, A. M., "Thermal Residual Stresses in Bonded Composite Repairs on Cracked Metal Structures," Ph.D. Dissertation, Dept. of Mechanical Engineering, Univ. of British Colombia, Vancouver, Canada, 1998.

[6] US Department of Defense Handbook, "Composite Materials Handbook Volume 3, Polymer Matrix Composites Materials Usage, Design and Analysis," MIL-HDBK-17-3F, Vol. 3, June 2002.

[7] Willden, K. S., Harris, C. G., Flynn, B. W., Gessel, M. G., Scholz, D. B., Stawski, S., and Winston, V., "Advanced Technology Composite Fuselage-Manufacturing," NASA Contractor Report, no. 4735, 1999.

[8] Paul, D., Kelly, L., and Venkayya V., "Evolution of U.S. Military Aircraft Structures Technology," *AIAA Journal*, Vol. 39, No. 1, 2002, pp. 18-29.

[9] Vinson, J. R., *The Behavior of Sandwich Structures of Isotropic and Composite Materials*, Technomic Publishing Company, Lancaster, PA, 1999, Chap. 1.

[10] Romanoff, J., and Varsta, P., "Bending Response of Web-Core Sandwich Beams," *Composite Structures*, Vol. 73, 2006, pp. 478-487.

[11] O'Brien, T. K., and Paris, I. L., "Exploratory Investigation of Failure Mechanisms in Transition Regions between Solid Laminates and X-cor® Truss Sandwich," *Composite Structures*, Vol. 57, 2002, pp. 189-204.

[12] Resetar, S. A., Rogers, J. C., and Hess, R. W., "Advanced Airframe Structural Materials, A Primer and Cost Estimating Methodology", USAF, Air Force Resource and Financial Issues, R-4016-AF, Santa Monica, CA, 1991.

[13] Davalos, J. F., Qiao, P., Xu, X. F., Robinson, J., and Barth, K. E., "Modeling and Characterization of Fiber-Reinforced Plastic Honeycomb Sandwich Panels for Highway Bridge Applications," *Composite Structures*, Vol. 52, 2001, pp. 441-452.

[14] Aminanda, Y., Castanié, B., Barrau, J. J., and Thevenet, P., "Experimental Analysis and Modeling of the Crushing of Honeycomb Cores," *Applied Composite Materials*, Vol. 12, 2005, pp. 213-227.

[15] Doyoyo, M., and Mohr, D., "Microstructural Response of Aluminum Honeycomb to Combined Out-of-Plane Loading," *Mechanics of Materials*, Vol. 35, 2003, pp. 865-876.

[16] Aktay, L., Johnson, A. F., and Kröplin, B. H., "Numerical Modeling of Honeycomb Core Crush Behavior," *Engineering Fracture Mechanics*, Vol. 75, 2008, pp. 2616-2630.

[17] MatWeb, "Aluminum 5052-H19 Foil," *Material Property Data* [online data], http://www.matweb.com/search/datasheet.aspx?matguid=a400cb1757a440e98540468b1b2b24a2&n=1&ckck=1 [retrieved 21 March 2001]

[18] Ajdari, A., "Mechanical Behavior of Cellular Structures: A Finite Element Study," M.S. Thesis, Dept. of Mechanical and Industrial Engineering, Northeastern Univ., Boston, MA, 2008.

[19] Kassapoglou, C., "Stress Determination and Core Failure Analysis in Sandwich Rampdown Structures under Bending Loads," *Key Engineering Materials*, Vols. 121-122, 1996, pp. 307-326.

[20] Bruhn, E. F., *Sandwich Construction and Design, Analysis and Design of Flight Vehicle Structures*, Tristate Offset Company, Cincinnati, OH, 1965, Chap. 12.

[21] Hirose, Y., Nishitani, M., Ochi, S., Fukumoto, K., Kawasaki T., and Hojo, M., "Proposal of Suppression of Delamination for the Foam Core Sandwich Panel Joint with Filler," *Advanced Composite Materials*, Vol. 15, No. 3, 2006, pp. 319-339.

[22] Clark, S. D., Shenoi, R. A., and Allen, H. G., "Modeling the Fatigue Behavior of Sandwich Beams Under Monotonic, 2-Step and Block-Loading Regimes," *Composites Science and Technology*, Vol. 59, 1999, pp. 471-486.

[23] Agastra, P., Samborsky, D. D., and Mandell, J. F., "Fatigue Resistance of Fiberglass Laminates at Thick Material Transitions," AIAA SDM Wind Energy Special Session, AIAA, Bozeman, MT., 2009, pp. 2009-2411.

[24] Burman, M., "Fatigue Crack Initiation and Propagation in Sandwich Structures," Ph.D. Dissertation, Dept. of Aeronautics, Division of Lightweight Structures, Royal Institute of Technology, Stockholm, Sweden, 1998.

[25] Hazizan, M. A., and Cantwell, W. J., "The Low Velocity Impact Response of an Aluminum Honeycomb Sandwich Structure," *Composites: Part B*, Vol. 34, 2003, pp. 679-687.

[26] Abbadi, A., Koutsawa, Y., Carmasol, A., Belouettar, S., and Azari, Z., "Experimental and Numerical Characterization of Honeycomb Sandwich Composite Panels," *Simulation Modeling Practice and Theory*, Vol. 17, 2009, pp. 1533-1547.

[27] Chen, A., and Davalos, J. F., "A Solution Including Skin Effect for Stiffness and Stress Field of Sandwich Honeycomb Core," *International Journal of Solids and Structures*, Vol. 42, 2005, pp. 2711-2739.

[28] El-Sayed, S., and Sridharan, S., "Cohesive Layer Models for Predicting Delamination Growth and Crack Kinking in Sandwich Structures," *International Journal of Fracture*, Vol. 117, 2002, pp. 63-84.

[29] Sharma, N., Gibson, R. F., and Ayorinde, E. O., "Fatigue of Foam and Honeycomb Core Composite Sandwich Structures: A Tutorial," *Journal of Sandwich Structures and Materials*, Vol. 8, July 2006, pp. 263-319.

[30] Rizov, V., Shipsha, A., and Zenkert, D., "Indentation Study of Foam Core Sandwich Composite Panels," *Composite Structures*, Vol. 69, 2005, pp.95-102.

[31] Zhang, J., and Ashby, M. F., "The Out-of-Plane Properties of Honeycombs," *International Journal of Mechanical Sciences*, Vol. 34, No. 6, 1992, pp. 475-489.

[32] Kassapoglou, C., *Design and Analysis of Composite Structures: With Applications to Aerospace Structures*, John Wiley & Sons, Ltd, London, 2010, Chap.10.

[33] McGovern, J., "Novel Analytical Methods for Sandwich Core Termination Features," Navy SBIR 2009.2 – Topic N092-098, NAVAIR, 2009.

[34] O Callaghan, P., and Venkataraman, S., "Review of Analysis Models for Sandwich Panel End Closure Stress and Fatigue Failure Predictions," Dept of Aerospace Engineering, San Diego State Univ., San Diego, CA, 2005 (unpublished).

[35] Thomsen, O. T., Rits, W., Eaton, D. C. G., and Brown, S., "Ply Drop-Off Effects in CFRP/Honeycomb Sandwich Panels-Theory," *Composites Science and Technology*, Vol. 56, November 1995, pp. 407-422.

[36] Castanié, B., Barrau, J. J., Jaouen, J. P., and Rivallant, S., "Combined Shear/Compression Structural Testing of Asymmetric Sandwich Structures," *Experimental Mechanics*, Vol. 44, No. 5, October 2004, pp. 461-472.

[37] Okada, R., and Kortschot, M. T., "The Role of the Resin Fillet in the Delamination of Honeycomb Sandwich Structures," *Composite Science and Technology*, Vol. 62, 2002, pp. 1811-1819.

[38] Evertz, R. L., "Investigation of Core Closeouts in Fiber-Reinforced Sandwich Laminates," M.S. Thesis, Dept. of Mechanical Engineering, Montana State Univ., Bozeman, MT, 2000.

[39] Peled, D., and Frostig, Y., "High-Order Bending of Sandwich Beams with Transversely Flexible Core and Nonparallel Skins," *Journal of Engineering Mechanics-ASCE*, Vol. 120, No. 6, June 1994, pp.1255-1269.

[40] Frostig, Y., Thomsen, O. T., and Mortensen, F., "Analysis of Adhesive-Bonded Joints, Square-End, and Spew Fillet- High Order Theory Approach," *Journal of Engineering Mechanics*, November 1999, pp. 1298-1307.

[41] Thomsen, O. T., and Vinson, J. R., "Modeling of Tapered Sandwich panels Using a High-Order Sandwich Theory Formulation," *AIAA Journal*, Vol. 40, No. 9, September 2002, pp. 1867-1875

[42] Kuczma, S. K., and Vizzini, A. J., "Failure of Sandwich to Laminate Tapered Composite Structures," *AIAA Journal*, Vol. 37, No. 2, February 1999, pp. 227-231.

[43] Pavio, J., and Hyde, D., "Effects of Coefficient of Thermal Expansion Mismatch on Solder Attached GaAs MMICs," *Microwave Symposium Digest*, Vol. 3, July 1991, pp.1075-1078.

[44] Sankar, B. V., "An Elasticity Solution for Functionally Graded Beams," *Composites Science and Technology*, Vol. 61, 2001, pp. 689-696.

[45] Venkataraman, S., and Sankar, B., "Elasticity Solution for Stresses in a Sandwich Beam with a Functionally Graded Core," *AIAA Journal*, Vol. 41., No. 12, 2001, pp. 2501-2505.

[46] Eternadi, E., Khatibi, A., and Takaffoli, M., "3D Finite Element Simulation of Sandwich Panels with a Functionally Graded Core Subjected to Low Velocity Impact," *Composite Structures*, Vol. 89, 2009, pp. 28-34.

[47] Kirugulige, M. S., Kitey, R., and Tippur, H. V., "Dynamic Fracture Behavior of Model Sandwich Structures with Functionally Graded Core: A Feasibility Study," *Composites Science and Technology*, Vol. 65, 2005, pp. 1052-1068.

[48] Jakobsen, J., Andreasen, J. H., and Thomsen, O. T., "Crack Deflection by Core Junctions in Sandwich Structures," *Engineering Fracture Mechanics*, Vol. 76, 2009, pp. 2135-2146.

[49] Bozhevolnaya, E., and Thomsen, O.T., "Structurally Graded Core Junctions in Sandwich Beams: Quasi Static Loading Conditions," Composite Structures, Vol. 70, pp.1-11, 2005.

[50] Whitty, J. P. M, Nazare, F., and Alderson, A., "Modeling the Effects of Density Variations on the In-Plane Poisson's Ratios and Young's Moduli of Periodic Conventional and Re-Entrant Honeycombs – Part 1: Rib Thickness Variations," *Cellular Polymers*, Vol. 21, No. 2, 2002, pp. 69-98.

[51] Zhang, J., and Ashby, M. F., "Buckling of Honeycombs Under in-Plane Biaxial Stresses," *International Journal of Mechanical Sciences*, Vol.34, No. 6, 1992, pp. 491-509.

[52] Atli-Veltin, B., and Gandhi, F., "Effect of Cell Geometry on Energy Absorption of Honeycombs Under In-Plane Compression," *AIAA Journal*, Vol. 48, No. 2, February 2010, pp. 466-478.

[53] Papka, S. D., and Kyriakides, S., "In-Plane, Compressive Response and Crushing of Honeycomb," *Journal of Mechanics and Physics of Solids*, Vol. 42, No. 10, 1994, pp.1499-1532.

[54] Hexcel Composites, "HexWeb™ Honeycomb Sandwich Design Technology," Publication No. AGU 075b, Stamford, CT, 2000.

[55] Ozturk, F., Toros, S., and Kilic, S., "Evaluation of Tensile Properties of 5052 Type Aluminum-Magnesium Alloy at Warm Temperatures," *Archives of Materials Science and Engineering*, Vol. 34, No. 2, December 2008, pp. 95-98.

[56] Gibson, L. J., and Ashby, M. F., *Cellular Solids: Structure and Properties*, Pergamon Press, Oxford, 1988.

[57] Roberts, A. P., and Garboczi,E .J., "Elastic Moduli of Model Random Three-Dimensional Closed-Cell Cellular Solids," *Acta Materialia*, Vol. 49, 2000, pp.189-197.

[58] Biner, S. B., "Thermo-Elastic Analysis of Functionally Graded Materials using Voronoi Elements," *Materials Science and Engineering*, Vol. A315, 2001, pp.136-146

[59] Papka, S. D., and Kyriakides, S., "Experiments and Full-Scale Numerical Simulations of in-Plane Crushing of a Honeycomb," *Acta Materialia*, Vol. 46, No. 8, 1998, pp. 2765-2776.

[60] Chen, W. F., and Lui, E. M., *Structural Stability, Theory and Implementation*, Prentice-Hall Inc., Upper Saddle River, NJ, 1987.

[61] Hexcel Composites, "HexWeb™ Honeycomb Attributes and Properties, A comprehensive guide to standard Hexcel honeycomb materials, configurations, and mechanical properties," *Honeycomb Data Sheets* [online data], http://www.hexcel.com/Resources/Honeycomb-Data-Sheets [retrieved 21 March 2011].

[62] Hatch, J. E., *Aluminum, Properties and Physical Metallurgy*, 2nd ed., American Society for Metals, Russell Township OH, 1984, Chap. 9.

[63] Hönig, A., and Stronge, W. J., "In-Plane Dynamic Crushing of Honeycomb, Part I: Crush Band Initiation and Wave Trapping," *International Journal of Mechanical Sciences*, Vol. 44, 2002, pp. 1665-1696.

[64] ABAQUS version 6.5 User's Manual, Dassault Systèmes Simulia Corporation, Providence, RI, 2010.

[65] MATLAB Version r2010b, MathWorks, Natick, MA, 2010.